METHANE FLUXES IN HUMAN-DOMINATED ECOSYSTEMS: FROM PASTURES TO CITIES

A Dissertation

Presented to the Faculty of the Graduate School

of Cornell University

In Partial Fulfillment of the Requirements for the Degree of

Doctor of Philosophy

by

Samuel Dyer Chamberlain

May 2016

METHANE FLUXES IN HUMAN-DOMINATED ECOSYSTEMS: FROM PASTURES TO CITIES

Samuel Dyer Chamberlain, Ph.D.
Cornell University 2016

The biosphere regulates Earth's climate through the exchange of greenhouse gases between ecosystems and the atmosphere. Human activities have altered terrestrial ecosystems to a substantial degree, with consequence to greenhouse gas exchange rates and climate. Anthropogenic impacts to ecosystem methane (CH_4) fluxes are poorly understood and require further study, as CH_4 emissions are growing and the causes are uncertain. This dissertation explores CH_4 fluxes from subtropical cattle pastures and cities to better understand greenhouse gas exchange in human-dominated ecosystems. These disparate systems are globally relevant because pastures are the most common, and cities are the fastest growing, land use.

Chapter One describes CH_4 fluxes from subtropical cattle pastures in south Florida using a variety of observational approaches. We found that highly variable emissions from the flooded landscape were the dominant CH_4 source and, unexpectedly, cattle-emitted CH_4 was a minor component of ecosystem emissions. Chapter Two further investigates the hydrologic controls of pasture CH_4 fluxes using eddy covariance measurements and laboratory manipulations. We found that flooding of a thin horizon of surface organic soil drove pasture CH_4 fluxes, suggesting that small changes in pasture water table dynamics could induce large

changes in emissions. Chapter Three assesses the impact of water management, and consequent CH_4 emissions, on pasture greenhouse gas budgets by combining eddy covariance observations with analysis of water retention data from south Florida pastures. Subtropical pastures were net CO_2 sinks, but strong greenhouse gas sources when accounting for CH_4 emissions, and water retention practices are likely responsible for only a minor component of pasture and regional greenhouse gas emissions. Chapter Four assesses the impact of natural gas use on greenhouse gas emissions from Ithaca, New York, using mobile surveys and atmospheric monitoring of CO_2 and CH_4 concentrations and isotopes. Pipeline CH_4 leakage rates in Ithaca were low, likely due to a well-maintained pipeline system, but we observed clear signs of natural gas leakage and combustion from the atmospheric monitoring site. This result, combined with spatial analysis, demonstrates a natural gas heat and electricity cogeneration plant is a significant emissions source in Ithaca. In all, this dissertation demonstrates that human-dominated ecosystems play an important role in terrestrial CH_4 exchange and that management choices influence ecosystem greenhouse gas emissions.

BIOGRAPHICAL SKETCH

Sam Chamberlain was born in Cambridge, Massachusetts in 1985. He grew up in Hanover, New Hampshire and later Stanford, California, where he developed an interest in science and the environment exploring eastern forests and western redwood groves. Sam attended Reed College in Portland, Oregon from 2003 to 2008. At Reed, Sam majored in Biology and completed a senior thesis with David Dalton assessing remediation strategies for a diatomite strip mine in central Oregon. He then spent one year working at the Lawrence Berkeley National Laboratory with Mark Conrad tracking the success of remediation efforts for nuclear waste sites in Hanford, Washington. Sam moved around the west for the next couple years, dabbling in alternate career paths such as snowboard instruction, wine making, button making, and aquaculture science. He later had the opportunity to do research at Stanford with his father, Page Chamberlain, using stable isotope records to explore how grassland expansion could induce global hydrologic change. Working on this project showed Sam how creative, fun, and profound science could be. Since 2011, Sam has been working towards his Ph.D. in Ecology and Evolutionary Biology at Cornell University with Jed Sparks. His research at Cornell explores greenhouse gas exchange in human-dominated ecosystems. The following dissertation is the culmination of this work.

ACKNOWLEDGMENTS

I would first like to thank my advisor, Jed Sparks, for his mentorship, support, and encouragement over the last 5 years. Through the ups and downs, Jed has always been very supportive of my choices while offering patient advice and perspective. I would also like to thank my committee members, Peter Groffman and Todd Walter, for their advice, feedback, and continued enthusiasm throughout this process. My progress would have moved at a snail's pace without help from Kim Sparks, whose technical support in the field and lab were indispensible. All the Sparks lab members also deserve thanks, as they were a constant source of constructive feedback on grants, presentations, and manuscripts.

I also thank my collaborators at the MacArthur Agro-ecology Research Station, specifically Betsey Boughton, Earl Keel, and Julia Maki, who provided support in the field and graciously hosted me on my visits to the ranch. My collaborators at the University of Illinois Champaign-Urbana, Nuria Gomez-Casanovas, Evan DeLucia, and Carl Bernacchi, were also a huge help in this work. Our flux tower measurements would not have been possible without help from these collaborators in Florida and Illinois. I also thank Tony Ingraffea for help with my urban research and being good company on methane leak mapping surveys.

This work was supported by a variety of funding sources, including the Department of Ecology and Evolutionary Biology, Cornell's Cross-scale Biogeochemistry and Climate Program, NSF IGERT Traineeship Program, Atkinson Center for a Sustainable Future, Andrew W. Mellon Foundation, and Cornell Sigma Xi. I also thank the staff of EEB, notably John Pollack, Carol Damn, and the accounting department.

I thank my family for their never-ending love and support. Growing up around scientists and being exposed to the lifestyle from an young age undoubtedly lead me to where I am today, and I'm thankful for the experiences my family gave me. My friends here in Ithaca and elsewhere also kept me afloat through this process, and I thank them all for their support. I would certainly not be here writing these acknowledgements if not for my partner, Sue. Thank you for being my best friend and always being there for me.

TABLE OF CONTENTS

CHAPTER 1

UNDERLYING ECOSYSTEM EMISSIONS EXCEED CATTLE-EMITTED METHANE FROM SUBTROPICAL LOWLAND PASTURES

Published as:

Chamberlain SD, Boughton EH, Sparks JP (2015) Underlying ecosystem emissions exceed cattle-emitted methane from subtropical lowland pastures. *Ecosystems*, 8: 933–945.

ABSTRACT

Cattle are a major methane (CH_4) source from pasture ecosystems, however the underlying landscape can be a significant and unaccounted source of CH_4. In general, landscape CH_4 emissions are poorly quantified, vary widely across time and space, and are easily underestimated if emission hotspots or episodic fluxes are overlooked. In this study, CH_4 emissions from subtropical lowland pastures were quantified using static chambers, eddy covariance, and mobile spectrometer surveys. Landscape emissions were the dominant CH_4 source, and cattle were responsible for 19-30% of annual emissions. The entire ecosystem emitted 33.84 ± 2.25 g CH_4 m^{-2} yr^{-1} as estimated by eddy covariance measured fluxes. Landscape emissions were highly variable, and seasonal flooding drove high magnitude emissions from the underlying landscape. Large CH_4 emissions were observed from wetlands and, to a lesser extent, the entire landscape during the wet season. In contrast, during the dry season there were no appreciable landscape CH_4 emissions, though canals, which cover only 1.7% of the total land area, were responsible for 97.7% of dry season emissions. Ecosystem CH_4 fluxes, measured by eddy covariance, varied seasonally and positively correlated to water table depth, soil and air temperature, and topsoil water content. The results presented here are the first to use mobile spectrometers to map biogenic CH_4 emissions at the landscape scale, and strongly suggest that the underlying landscape is a strong CH_4 source that must be considered in addition to cattle emissions.

INTRODUCTION

Pastures are globally widespread and play an important role in greenhouse gas exchange and terrestrial carbon (C) storage. Pastures and rangelands cover ~22% of global ice-free surface

and remove ~0.2 Pg C yr^{-1} from the atmosphere (Ramankutty et al., 2008; Follett and Reed, 2010). These ecosystems are also major sources of methane (CH_4), a greenhouse gas with a warming potential ~25 times higher than carbon dioxide (CO_2) over a 100 year time horizon (Forster et al., 2007). Pasture CH_4 sources are biogenic, and include cattle, saturated soils, and open water, where Archaea produce CH_4 under low-redox anaerobic conditions (Conrad, 2007). Cattle and wetland emissions are important components of the global CH_4 budget, and emit roughly 80 Tg CH_4 yr^{-1} and 105 Tg CH_4 yr^{-1} to the atmosphere respectively (Bridgham et al., 2006; Lassey, 2007). Pasture CO_2 uptake is particularly high in tropical and subtropical regions and may offset CH_4 emissions from grazing cattle (Conant and Paustian, 2002; Soussana et al., 2010). However, CO_2 and CH_4 exchanges in these environments are rarely evaluated simultaneously.

To date, observations of pasture greenhouse gas exchange have focused primarily on temperate upland or peatland pastures. Cattle emissions are generally considered the dominant component of these pasture CH_4 budgets, and can be estimated with some degree of certainty using emission factors and cattle stocking data (Nieveen et al., 2005; Allard et al., 2007; Lassey 2007; Teh et al., 2011; United States Environmental Protection Agency, 2012). However, lowland pastures may exhibit considerable CH_4 emissions from the seasonally flooded landscape in addition to direct cattle emissions. Methane fluxes from seasonally flooded ecosystems are globally significant and highly uncertain (Melack et al., 2004; Kirschke et al., 2013). These landscape emissions tend to vary across time and space, are commonly driven by landform ‘hotspots’ or episodic fluxes, and are often difficult to estimate without direct measurement (Schrier-Uijl et al., 2010a; Teh et al., 2011).

Large areas of lowland pasture are located within the northern Everglades watershed of south Florida. Pasture development in the region was facilitated by large-scale drainage efforts that allowed year-round settlement of a once seasonally flooded ecosystem (Bohlen et al., 2009). Unlike peatlands found in the Everglades to the south, the northern Everglades watershed is characterized by sandy mineral soils. The pre-drainage landscape was primarily dry and wet prairie containing a mosaic of embedded depressional wetlands, and sheet flow during the wet season would flood both prairie and wetlands. The watershed was heavily drained between 1940 and 1970 for flood control and cattle ranching (Swain et al., 2013), and within the watershed today, improved pasture is the dominant land-use and covers more than 35% of the total land area (Hiscock et al., 2003). Improved pastures are actively managed, fertilized, and planted with introduced forage for livestock.

The northern Everglades watershed retains many pre-drainage characteristics. Though drainage and water management has reduced seasonal flooding, depressional wetlands and ditches routinely flood during the wet season, and entire pastures flood during heavy wet seasons (Bohlen and Gathumbi, 2007; Bohlen and Villapando, 2011). Flooded pastures may be responsible for high magnitude CH_4 emissions that vary across time and space, yet the magnitude of these fluxes remains unknown.

Pasture and other natural and managed ecosystem CH_4 fluxes are commonly quantified by eddy covariance, static chamber techniques, or a combination of the two (Allard et al., 2007; Rinne et al., 2007; Kroon et al., 2010; Dengel et al., 2011; Herbst et al., 2011; Teh et al., 2011; Baldocchi et al., 2012; Hatala et al., 2012; Wang et al., 2012; Nicolini et al., 2013; Olson et al., 2013; Matthes et al., 2014). Combining these methods allows for a more holistic understanding of variable ecosystem CH_4 fluxes. However, emission hotspots are

often a significant component of ecosystem greenhouse gas budgets (Groffman et al., 2009; Schrier-Uijl et al., 2010a; Teh et al., 2011), and important hotspots may be overlooked depending on sampling effort, chamber placement, and tower placement. To address this issue, this study mapped CH_4 concentrations spatially to ensure a complete consideration of hotpot emissions using a mobile wavelength-scanned cavity ringdown spectrometer (WS-CRDS).

The goals of this work were to: 1) quantify the spatial and temporal variability of landscape fluxes from subtropical pastures, 2) determine the controls of these fluxes, and 3) compare the magnitude of underlying landscape fluxes to that of cattle grazing the landscape. To quantify these potentially variable fluxes, we used chambers to measure fluxes from dominant landforms across season and determined the response of pasture CH_4 fluxes to large episodic rain events, eddy covariance to measure seasonal variability of ecosystem CH_4 fluxes, and mobile WS-CRDS surveys to map CH_4 concentrations during dry and wet seasons. To our knowledge, this is the first study to use WS-CRDS mobile surveys to map biogenic CH_4 emissions at the landscape-scale. We expected emissions to be highly variable across time and space, and expected large emissions to be driven by wet season flooding of low-lying landforms. We also expected that emission from the underlying landscape would approach the magnitude of emissions from cattle stocked within the pasture. This study quantifies variable ecosystem fluxes from subtropical pastures, provides a comparison between landscape and cattle-emitted CH_4, and estimates an overall CH_4 budget for subtropical lowland pastures in south Florida.

METHODS

Study Site

All measurements were made between 2012 and 2014 within a single improved pasture (Griffin Park pasture; 92.1 ha) at the MacArthur Agro-Ecology Research Center (MAERC), a 4290-ha commercial cattle ranch and ecological field station (a division of Archbold Biological Station; N 27.1632004, W 81.187302). The Griffin Park pasture contains three depressional wetlands, cabbage palm hammocks, a network of drainage ditches, and regularly inundated canals. The pasture is planted with Bahia grass (*Paspalum notatum*), an introduced forage species, and is rotationally grazed by cattle. Cattle were grazed at a moderate density (~1.6 cow ha^{-1}) recommended for south Florida pastures (Hersom, 2002). Herbicide and fertilizer has not been applied to the pasture since 2006-08 and 2007-04, respectively. Soils are primarily poorly drained spodosols. The area averages 1300mm of rain per year, 75% of which falls in the summer wet season (Gathumbi et al., 2005).

Eddy Covariance Measures

An eddy covariance tower within the pasture (N 27.1632004, W 81.187302) measured continuous fluxes of heat, energy, water vapor, CO_2, and CH_4. This tower is integrated within a five-tower array at MAERC measuring ecosystem fluxes from multiple land uses. A three-dimensional sonic anemometer measured wind speed and direction (CSAT3, Campbell Scientific Inc., Logan, UT, USA) and open-path infrared gas analyzers measured H_2O, CO_2, and CH_4 concentrations (LI-7500A and LI-7700, Licor Inc., Lincoln, NE, USA). All instrumentation was installed 2.6 m above the ground surface and interfaced with a LI-7550 data logging system (Licor Inc, Lincoln, NE, USA). All data were collected at 10 Hz and

transferred by modem for processing and analysis. Water table depth (m below surface) was monitored at the tower with a CS451 pressure transducer (Campbell Scientific Inc., Logan, UT, USA). Soil volumetric water content (VWC; $m^3\ m^{-3}$) was measured at 5, 10, 20 cm below land surface with CS-616 water content reflectometers (Campbell Scientific Inc., Logan, UT, USA). Soil and air temperatures (°C) were also measured at 5, 10, 20 cm below land surface with copper-constantan thermocouples. All auxiliary measures were reported at 30 min intervals and logged to a CR3000 datalogger (Campbell Scientific Inc., Logan, UT, USA) time synced to the LI-7550.

All fluxes were computed as the covariance of vertical wind velocity and gas concentration over 30-minute intervals. Raw data were screened for spikes, amplitude resolution, drop-outs, absolute value limits, and skewness and kurtosis with tests described in Vickers and Mahrt (1997) and designated default in EddyPro 4.2 (Licor Inc., Lincoln, NE, USA). We applied double rotation tilt corrections to align anemometer measurements with respect to mean wind streamlines, and used block averaging to calculate mean wind speed and gas concentrations over the 30-minute flux interval. Time lags between measured variables were corrected using the covariance maximization method. The Webb, Pearman, and Leuning corrections for density fluctuations were applied according to Webb et al. (1980), fully analytic spectral corrections were applied according to Moncrieff et al. (1997), and data quality was flagged according to Foken et al. (2005). Quality flags range from 1 (best) to 9 (worst), and fluxes were rejected for flags > 5. We estimated the tower footprint according to Hsieh et al., (2000). All of the above corrections and data processing were completed in EddyPro 4.2 (Licor Inc., Lincoln, NE, USA). We used friction velocity (μ^*) filtering to remove all nighttime fluxes collected during periods of low turbulence ($\mu^* < 0.14\ m\ s^{-1}$)

following methods in Aubinet et al., (2012). Overall, 53% of all half-hourly fluxes were removed from the long-term dataset according to quality flag and μ*-threshold criteria.

Mobile WS-CRDS Surveys

To quantify spatial heterogeneity of CH_4 emissions from the pasture, real-time CH_4 concentrations were measured with a mobile WS-CRDS (G2201-*i*, Picarro Inc., Sunnyvale, CA, USA) installed in an off-road vehicle (Ranger, Polaris Industries, Medina, MN, USA). This technique has been used to survey CH_4 leaks from refineries, industry, cities, and natural gas infrastructure (Shorter et al., 1996; Farrell et al., 2013; Leifer et al., 2013; Phillips et al., 2013; Jackson et al., 2014). Air samples were drawn through perforations in ¼" Teflon tubing attached to the vehicle's front bumper (~0.5 m above ground surface) covered with PTFE membrane filters. We used the Picarro Invesigator mobile system (Picarro Inc., Sunnyvale, CA, USA) in the wet season, and a self-designed custom system in the dry season. For both configurations, a 12V battery bank supplied power and GPS recorded location at 1-second intervals. The Investigator system merged location data with G2201-*i* output with Picarro P3 software (Picarro Inc., Sunnyvale, CA, USA), while the custom system recorded GPS location (GPS18x, Garmin Ltd., Olathe, KS, USA) in a separate file and then WS-CRDS and GPS data files were merged post-survey. Time lags between GPS location and CH_4 measurements due to sample tubing length (~3.7 m) were corrected by measuring the time delay between gas standard injections at the bumper inlet and G2201-*i* response. GPS location was then matched with delay-corrected CH_4 concentration measurements during data processing. The G2201-*i* was calibrated with known standards of CH_4 in air (Air Liquide, Philadelphia, PA, USA).

We surveyed north to south transects to evenly sample the pasture and all major landforms, and conducted surveys at night when atmospheric turbulence was low. Gas concentrations at the land surface are generally higher at night due to decreased wind speed and increased atmospheric stability, and mobile surveys of CH_4 plumes are commonly conducted at night for this reason (Shorter et al., 1996; Farrell et al., 2013; Leifer et al., 2013). The same transect was followed on four nights during the wet season (2013-08-23, 2013-08-25, 2013-09-01, 2013-09-02) and four nights during the dry season (2014-03-26, 2014-03-30, 2014-04-01, 2014-04-03). Data were visualized by kriging CH_4 concentrations across a coordinate grid (see *Statistical Analysis and Geostatistical Mapping* below). Emission maps were then compared to LIDAR remote sensing imagery of the pasture obtained from the MacArthur Agro-ecology Research Center (http://www.archbold-station.org/html/datapub/data/spatialdata.html).

Chamber Flux Measures

All chamber fluxes were measured between June 2012 and July 2014. Within each year, fluxes were measured in both dry and wet seasons. Wet season (May-October) fluxes were measured August-September 2013 and June-July 2014. Dry season (November-April) fluxes were measured February-March 2013 and March-April 2014. All chamber measurements took place within the pasture containing the eddy covariance tower. Landform fluxes were measured from improved pasture, palm hammocks, ditches, canals, and depressional wetlands. Three chamber collars were installed 3 m from one another within each landform and sampled concurrently. Chamber fluxes from each landform were measured biweekly. Soil collars were inserted 3 cm into the ground and enclosed a 0.065 m^2 area. When the water level

was too deep to insert collars (> 3 cm above ground surface), fluxes were measured from the water surface using three floating chambers. Floating chambers enclosed a 0.037 m^2 area and 6.71 L volume. Soil and floating chambers were pressure vented to the atmosphere. Soil chambers were installed five days prior to initial sampling to minimize the impact of disturbance on measured fluxes.

Chamber headspaces were closed for 30 min, and four gas samples were withdrawn using a 60 ml syringe at 30 sec, 10 min, 20 min, and 30 min after closure. Gas samples were transferred to 22 ml pre-evacuated gas vials sealed with Geo-Microbial Technologies septa (Geo-Microbial Technologies Inc., Ochleata, OK, USA). All samples were analyzed for CO_2 and CH_4 concentration on a Picarro G2201-*i* analyzer equipped with a Picarro SSIM2 Small Sample Isotope Module (Picarro Inc., Sunnyvale, CA, USA). The G2201-*i* and SSIM2 were calibrated with known standards of CH_4 in air (Air Liquide, Philadelphia, PA, USA). All samples were analyzed within 3 months of collection. Methane travel standards (10 ppm) detected no leakage between collection and analysis. Chamber fluxes were calculated by applying a linear regression to concentrations over time ($P < 0.05$), fluxes that did not meet the regression criteria were omitted from analyses. Exceptions were made when CH_4 concentration varied less than 0.2 ppm throughout the closure period. In this case, fluxes that did not meet the $P < 0.05$ linear regression criteria were set to zero. For floating chambers, ebullition fluxes were analyzed separately and were assumed to occur when CH_4 concentration abruptly and non-linearly rose during chamber closure. Ebullition fluxes were calculated as the total concentration increase over the 30 min closure period.

Soil temperature (°C), volumetric water content (VWC; m^3 m^{-3}), and water table depth (m below surface) was monitored at the time of chamber measurement. Soil temperatures

were measured every 30 min at 5 cm depth with buried HOBO Pendant data loggers (Onset Co., Bourne, MA). Volumetric water content (0 – 5 cm) was measured using a handheld TDR probe (ML2, Delta-T Devices Ltd. Cambridge, UK) and reported as the average of four measurements taken directly outside of the chamber base. Water table depth (m below surface) was measured from an augered well at each chamber site. For each floating chamber we measured water temperature (°C) at 30 min intervals with HOBO Pendant data loggers (Onset Co., Bourne, MA).

Stimulated Large Rain Event

Large rain events were defined as > 2 inches of rain occurring over a 48-hour period. From 1969-2012, rain events fitting these criteria have occurred in the northern Everglades watershed approximately four days per year (Florida Climate Center, 2013). Two simulated rain events were conducted in February 2012. We simulated large rain events in the dry season to quantify the effect of episodic rains on pasture CH_4 fluxes. We applied two inches of water over a 0.5 m by 1.5 m marked area containing three equidistant soil chambers. Water was spread evenly across the entire area over the span of 10 minutes using a large plastic tub with perforated holes in the base. Chamber fluxes were then measured at -1, 0.25, 1.5, 3.5, 6, 12, and 24 hours after water addition using the methods described above.

Methane Budget and Cattle Emission Estimates

Annual CH_4 budgets were estimated using three strategies: 1) scaling from spatially weighted landform fluxes, 2) eddy covariance and 3) total cattle emissions estimated by Tier 2 IPCC guidelines. All budgets were calculated from 2013-05-01 to 2014-04-30. This time period was

chosen to cover one annual wet-dry cycle. For the chamber-based budget, we estimated the areal extent of each landform in GoogleEarth Pro (Google Inc., Mountain View, CA, USA) weighing the contribution of each landform flux by percent land cover of the entire pasture. Wet season fluxes were applied from 2013-05-01 to 2013-10-31, and dry season fluxes were applied from 2013-11-01 to 2014-04-30. Only fluxes measured within the one-year time frame were applied with the exception of wet season hammock fluxes. For wet season hammock fluxes, we applied values measured in wet season 2014 because no hammock fluxes were measured during the wet season in 2013.

The annual eddy covariance budget was calculated as the sum of 365 daily mean CH_4 fluxes. Daily fluxes were estimated following methods outlined in Rinne et al. (2007). For days with data coverage greater than 33%, daily fluxes were calculated as the mean of all half-hourly measurements scaled over the 24-hour day. Diurnal variation in half-hourly fluxes was not observed in either season, and we therefore did not introduce systematic bias to daily estimates by scaling daily datasets with > 33% coverage. Days with less than 33% coverage were gap filled by linear interpolation. Fourteen percent of days in the year were gap filled, and the longest gap filled was nine days.

Total cattle emissions were estimated for the Griffin Park pasture using IPCC Tier 2 emission factors generated from cattle management data supplied by MAERC and suggested input data for Florida beef cattle (IPCC, 2006; EPA, 2014). Emission factors were estimated for both direct CH_4 emissions from enteric fermentation and CH_4 emissions from manure deposited on pasture. Cattle emission estimates were generated using herd size, average weight, percent of cows pregnant, and forage information for herds grazing the Griffin Park pasture from 2013-05-01 to 2014-04-30. Using IPCC Tier 2 guidelines, we estimated gross

energy intake (MJ day^{-1}) and consequent emission factors (kg CH_4 $animal^{-1}$ yr^{-1}) for two subcategories of cattle grazing the pasture: 1) mature non-pregnant cows and 2) mature pregnant cows. These categories were chosen based on the availability of sufficient cattle management data. A complete discussion of the Tier 2 estimation process is further outlined within the Appendix. Manure and enteric fermentation CH_4 budgets were calculated at a daily time scale accounting for herd size and the percentage of herd pregnant within the pasture. Cattle emission estimates were then divided by the total area of the Griffin Park pasture (92.1 ha) to yield comparable units of g CH_4 m^{-2} yr^{-1}.

Cattle management data were also used to bound the potential contribution of enteric fermentation emissions to the eddy covariance measured fluxes assuming cattle were: 1) equally dispersed across the entire pasture (by dividing daily enteric fermentation emissions by the entire pasture area), or 2) all located within the tower footprint area (by dividing daily enteric fermentation emissions by the annual mean 90% tower footprint area). These estimates are presented in Figure 1.1 and were used to place general bounds on the potential contribution of enteric fermentation-emitted CH_4 to net ecosystem fluxes. Footprint area was estimated by calculating the 90% footprint fetch and lateral spread using models outlined in Hsieh et al. (2000) and Detto et al. (2006), respectively. The footprint area was averaged across the entire measurement period so that potential cattle emissions reflected changes in stocking density, rather than day-to-day variability in footprint area. The estimated footprint area (fetch = 541 m, lateral spread = 177 m, area = 75207 m^2) encompassed 8% of the total pasture area. These theoretical cattle enteric fermentation emission bounds are referred to throughout as ‘potential cattle emissions’.

Statistical Analysis and Geostatistical Mapping

All spatial survey data were kriged in R 3.0.1 using the "sp" and "gstat" packages (R Core Team, 2013). Pasture CH_4 concentrations were interpolated across a 2 m x 2 m two-dimensional coordinate grid (460 x 590 grid cells) using ordinary kriging. A semivariogram was produced from measured concentrations and kriged concentrations were predicted using the exponential model:

$$\gamma(\mathrm{h}) = C_0 + C_1 \cdot \left[1 - e^{-\left(\frac{\mathrm{h}}{a}\right)}\right] \text{ when } |\mathrm{h}| > 0$$

Where h is the distance between locations, γ(h) is the predicted semivariance at a distance h, C_0 is the nugget, $C_0 + C_1$ is the sill, and a is the range.

We used Kruskal-Wallis non-parameteric ANOVA to evaluate whether landform CH_4 fluxes exhibited significant spatial and temporal variability, Mann-Whitney U tests to determine whether landform fluxes varied seasonally, and Tukey's HSD analyses to determine significant mean differences for comparisons between environmental variables and fluxes in the simulated rain treatment. Linear regression was used to determine significant relationships between environmental variables, landform fluxes, and daily-averaged ecosystem fluxes. Methane fluxes were log transformed to meet assumptions of normality. All regressions of eddy covariance fluxes to environmental variables were conducted on daily averaged values due to high levels of random error in half-hourly fluxes.

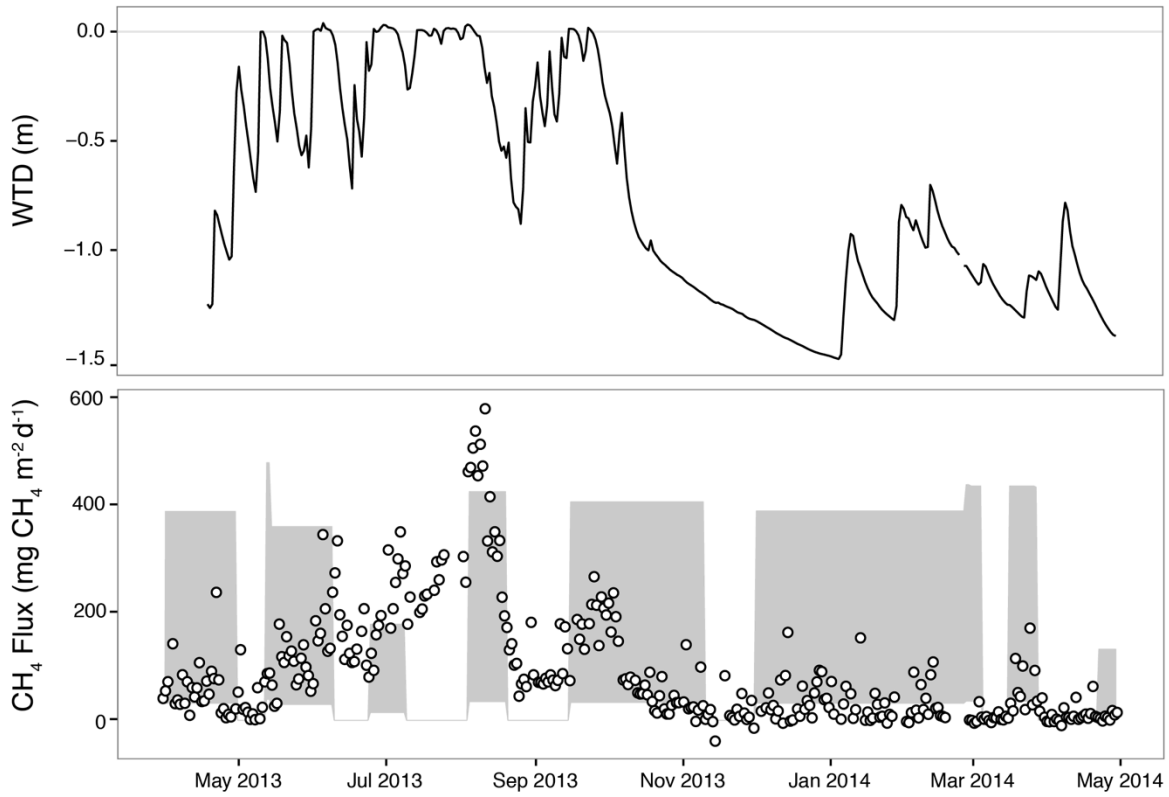

Figure 1.1 Water table depth (WTD; top panel) and daily mean CH_4 fluxes (bottom panel) measured by eddy covariance. The shaded area on the bottom panel represents the potential range of cattle-emitted CH_4 throughout the measurement period. The 90% flux footprint area was averaged over the entire measurement period to normalize potential cattle emissions, and was calculated according to models in Hsieh et al. (2000) and Detto et al. (2006).

RESULTS

Ecosystem CH_4 fluxes, measured by eddy covariance, were high from the pastures. Emissions peaked during the wet season (May – October) when the water table rapidly approached the land surface and flooded the pasture (Figure 1.1). At the onset of the dry season (November – April), the water table retreated from the land surface to ~1 m below surface and CH_4 emissions reduced to near zero fluxes concurrently. Positive emission spikes were observed throughout the dry season (Figure 1.1). Cattle were rotationally grazed at a moderate stocking density (~1.6 cows/ha) throughout the pasture during the measurement period and likely contributed to observed ecosystem fluxes. Potential cattle emissions (enteric fermentation

only) are represented in Figure 1.1 as the grey shaded range on the bottom panel. Upper bounds of the shaded range assume all cattle within the pasture were located within the mean tower footprint area (~8% of total pasture area), and the lower bounds assume all cattle were equally dispersed throughout the pasture. Potential cattle emissions are zero when no cattle were stocked within the pasture. Comparing measured fluxes to potential cattle emission estimates suggest that cattle may be responsible for observed dry season emission spikes when cattle graze within the tower footprint (Figure 1.1). During the wet season, ecosystem fluxes generally exceeded potential cattle emissions and persisted in the absence of cattle, strongly suggesting soil and water CH_4 sources (Figure 1.1).

Ecosystem CH_4 fluxes were positively correlated to fluctuations in the water table ($r^2 = 0.49$, $P < 0.0001$), topsoil water content ($r^2 = 0.54$, $P < 0.0001$), and soil temperature ($r^2 = 0.46$, $P < 0.0001$). Water table depth and topsoil water content were highly co-linear ($r^2 = 0.94$; $P < 0.0001$). No other related environmental variables displayed correlation coefficients greater than 0.90. The daytime 90% tower fetch averaged 286 m over the entire measurement period and encompassed improved pasture, ditches, and some depressional wetlands (Figure 1.2).

Large variability was observed in the spatial structure and magnitude of CH_4 plumes between dry and wet seasons (Figure 1.2). Interpolated concentration maps were compared to LIDAR imagery from the site to identify CH_4 emission sources across the pastures. Darker zones on the LIDAR imagery are lower topographically and correspond to depressional wetlands, ditches, and canals within the pasture landscape (Figure 1.2a). Methane concentration plumes were largest above depressional wetlands during the wet season (Figure 1.2b), and background pasture CH_4 concentrations were up to 33% higher in the wet season

when compared to the dry season (Figure 1.2b, 1.2c). No cattle were present in the pasture during these surveys. These results suggest that wetlands were a dominant CH_4 source and the entire pasture landscape was producing CH_4 during the wet season. Observed wet season CH_4 concentrations ranged from 1.92 – 2.42 ppm to maximum concentrations of 3.95 – 6.90 ppm across all wet season surveys. Dry season concentrations were relatively uniform and near atmospheric background across the pasture (Figure 1.2c), suggesting that the pasture landscape was not producing significant levels of CH_4 during the dry season. Without cattle present, dry season CH_4 concentrations ranged from 1.78 – 1.87 ppm to a maximum 2.06 ppm.

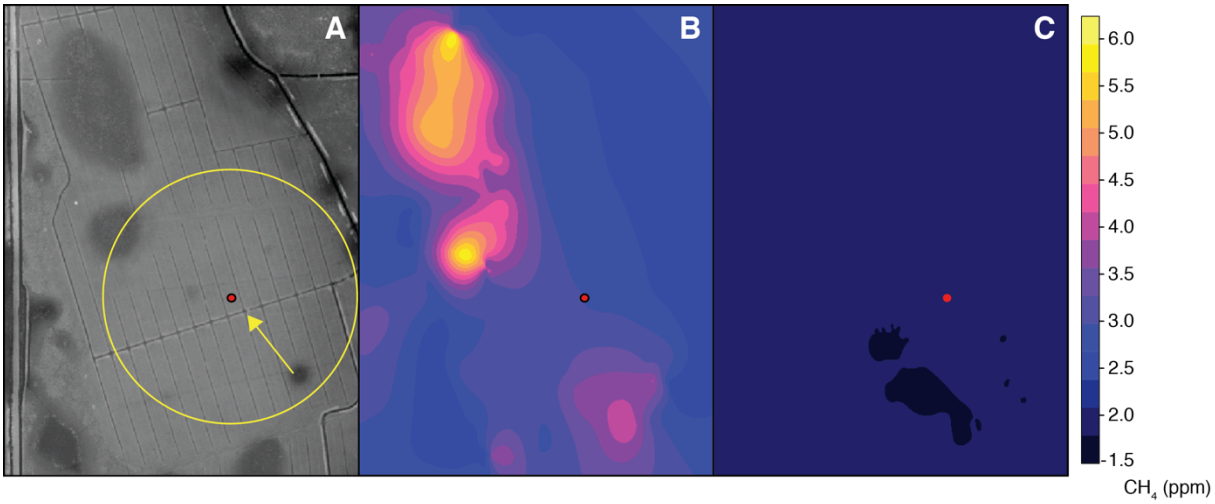

Figure 1.2 LIDAR imagery (a) and kriged CH_4 concentrations above pasture in wet (b) and dry (c) seasons. Darker zones on LIDAR map are areas of lower surface elevation and correspond to depressional wetlands, ditches, and canals. The dot on panels a, b, and c mark the location of the eddy covariance tower. The circle and arrow on panel a represents the mean annual 90% daytime tower footprint (286 m) and predominant wind direction, respectively.

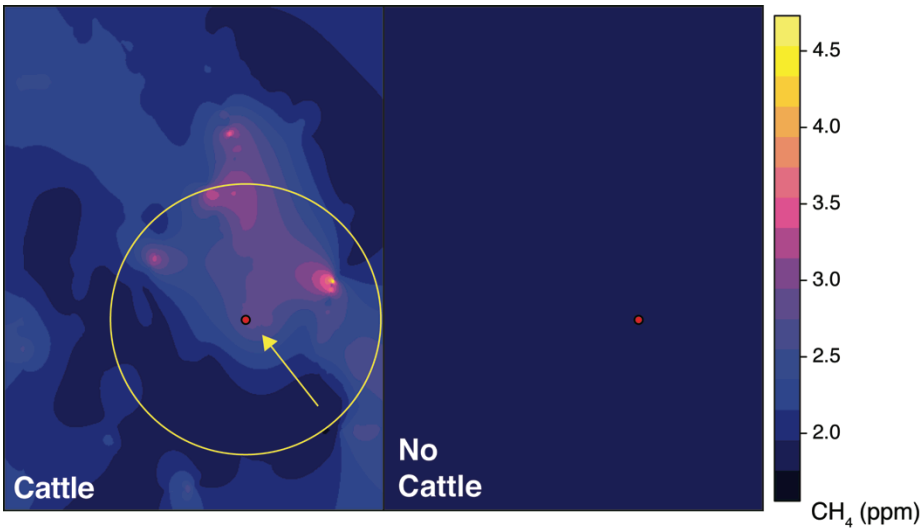

Figure 1.3 Kriged CH_4 concentrations above dry season pasture with (A) and without (B) grazing cattle. Increased CH_4 concentrations in the pasture with grazing cattle correspond to the location of cattle herds; 186 cattle were present in A. The dot on panels A and B mark the location of the eddy covariance tower. The circle and arrow on panel A represents the mean annual 90% daytime tower footprint (286 m) and predominant wind direction, respectively.

Cattle produced observable CH_4 concentration plumes when herds were grazing the pasture (Figure 1.3). Cattle-derived plumes approached the magnitude of wet season wetland plumes (Figure 1.2b), though cattle emissions were irregularly structured due to the transient and point source nature of cattle-emitted CH_4 (Figure 1.3a). Cattle CH_4 plumes fell within the tower footprint (Figure 1.3a), also suggesting that cattle may be responsible for observed ecosystem emission spikes (Figure 1.1). Cattle were present in two of four dry season surveys and no wet season surveys. With cattle present, dry season CH_4 concentrations ranged from 1.83 – 1.84 ppm to a maximum 2.17 – 4.53 ppm, considerably larger than the range of observed concentrations in dry season surveys when no cattle were present.

Methane fluxes from major landforms displayed high spatial and temporal variability (Figure 1.4; Table 1.1). Fluxes varied among landforms during the dry season (Kruskal-Wallis, $P < 0.0001$), wet season (Kruskal-Wallis, $P < 0.0001$), and independent of season (Kruskal-Wallis, $P < 0.0001$; see Table 1.1 for post-hoc comparisons).

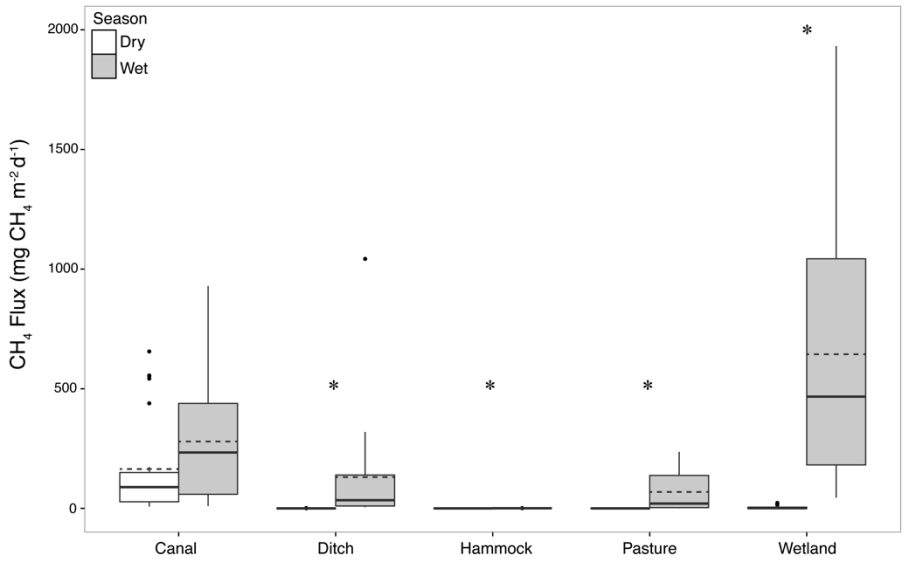

Figure 1.4 Wet and dry season CH_4 fluxes (mg CH_4 m^{-2} d^{-1}) from major pasture landforms. Solid lines are medians, dashed lines are means, boxes are the interquartile range (IQR), and whiskers are ± 1.5 IQR. Asterisks denote significant differences in CH_4 flux between seasons for each landform (Mann-Whitney U, $P < 0.05$).

Volumetric water content, soil temperature, and water table depth all varied across landforms (Kruskal-Wallis, $P < 0.005$). During the dry season, emissions from canals (166.97 ± 42.44 mg CH_4 m^{-2} d^{-1}, n=24) and wetlands (2.79 ± 0.95 mg CH_4 m^{-2} d^{-1}, n=36) dominated the total flux, and negligible fluxes were observed from the remaining landforms. Ditches emitted 0.08 ± 0.07 mg CH_4 m^{-2} d^{-1} (n=23), and minor CH_4 uptake was observed in hammocks (-0.42 ± 0.09 mg CH_4 m^{-2} d^{-1}, n=10) and pastures (-0.27 ± 0.04 mg CH_4 m^{-2} d^{-1}, n=34). In contrast, during the wet season all landforms emitted CH_4. Canals (280.35 ± 64.70 mg CH_4 m^{-2} d^{-1}, n=17), ditches (267.22 ± 150.88 mg CH_4 m^{-2} d^{-1}, n=18), hammocks (0.52 ± 0.11 mg CH_4 m^{-2} $d^{-}1$, n=9), pastures (67.46 ± 13.99 mg CH_4 m^{-2} d^{-1}, n=28), and wetlands (692.72 ± 110.10 mg CH_4 m^{-2} d^{-1}, n=32) all generated positive fluxes (Figure 1.4; Table 1.1).

Fluxes from ditches (Mann-Whitney U, $P < 0.0001$), hammocks (Mann-Whitney U, $P = 0.0003$), pastures (Mann-Whitney U, $P < 0.0001$), and wetlands (Mann-Whitney U, $P < 0.0001$) varied among seasons. Canal fluxes did not vary seasonally and were the only

landform flooded year round (Figure 1.4). For all landforms, fluxes were higher from open water (Kruskal-Wallis, $P < 0.0001$). Ebullitive fluxes from open water were the highest emissions recorded, which comprised 7% of all reported fluxes.

Table 1.1 Landform area (ha), percent cover, and fluxes of CH_4 (mg CH_4 m^{-2} d^{-1}) in subtropical lowland pastures. Standard errors reported for all landform fluxes. Letters indicate significant differences between mean fluxes (Tukey's HSD, $P < 0.05$).

Landform	Area	% Cover	Dry Season	Wet Season	Annual
Canal	1.55	1.7%	166.97 ± 42.44 *a*	280.35 ± 64.70 *a*	213.98 ± 37.13 *ab*
Ditch	3.68	4.0%	0.08 ± 0.07 *b*	267.22 ± 150.88 *a*	117.36 ± 68.46 *a*
Hammock	8.48	9.2%	-0.42 ± 0.09 *b*	0.52 ± 0.11 *a*	0.02 ± 0.13 *a*
Pasture	68.3	74.2%	-0.27 ± 0.04 *b*	67.46 ± 13.99 *a*	30.32 ± 7.60 *a*
Wetland	10.06	10.9%	2.79 ± 0.95 *b*	692.72 ± 110.10 *b*	327.46 ± 66.40 *b*

Experimental watering resulted in pulse CH_4 emissions (Figure 1.5). Fifteen minutes after the simulated rain event, CH_4 fluxes increased from -0.008 ± 0.002 mg CH_4 m^{-2} hr^{-1} to 0.236 ± 0.052 mg CH_4 m^{-2} hr^{-1} (Tukey's HSD, $P < 0.0001$), and topsoil water content increased from 0.039 ± 0.004 m^3 m^{-3} to 0.267 ± 0.032 m^3 m^{-3} (Tukey's HSD, $P < 0.0001$). Within 1.5 hours of simulated rain, CH_4 fluxes returned to near zero (0.013 ± 0.005 mg m^{-2} hr^{-1}) and were not higher than pre-treatment fluxes. All remaining time points up to 24 hours did not vary from pre-treatment fluxes (Figure 1.5). Over the course of simulated rain treatments, CH_4 fluxes positively correlated to topsoil water content ($r^2 = 0.26$, $P = 0.0005$).

Overall, the pastures emitted between 33.84 ± 2.25 g CH_4 m^{-2} yr^{-1} and 36.76 ± 6.57 g CH_4 m^{-2} yr^{-1}, as estimated by eddy covariance and spatially weighted chamber fluxes, respectively. Enteric fermentation emission factors were estimated to be 58.9 ± 9.1 kg CH_4 $animal^{-1}$ yr^{-1} and 63.9 ± 9.8 kg CH_4 $animal^{-1}$ yr^{-1} for non-pregnant and pregnant cows, respectively. Manure emission factors were estimated to be 2.0 ± 0.3 kg CH_4 $animal^{-1}$ yr^{-1} and

2.2 ± 0.3 kg CH_4 $animal^{-1}$ yr^{-1} for non-pregnant and pregnant cows, respectively. These emission factors are similar to Tier 1 emission factors reported by the IPCC (2006). Cattle grazing the pasture produced an estimated 8.0 ± 1.2 g CH_4 m^{-2} yr^{-1} from enteric fermentation and 0.3 ± 0.1 g CH_4 m^{-2} yr^{-1} from deposited manure.

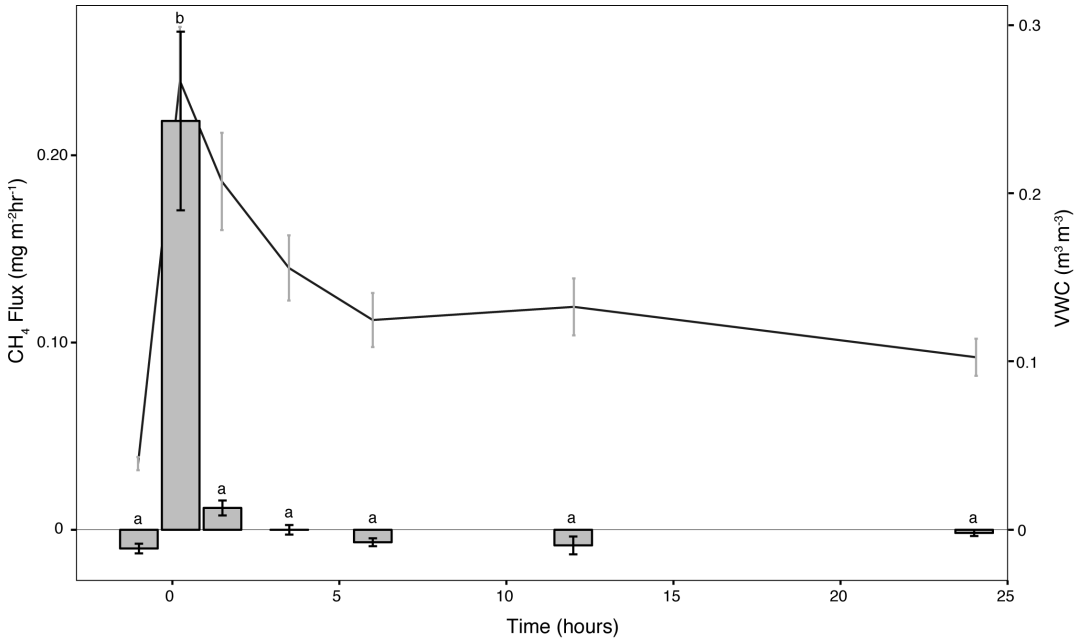

Figure 1.5 Methane fluxes (bar; mg m^{-2} hr^{-1}) and topsoil (0-5 cm depth) volumetric water content (line; m^3 m^{-3}) following simulated rain event. Mean and standard error are presented for both fluxes and topsoil water content. The rain event occurred at time zero, and letters above CH_4 flux values indicate significant differences between fluxes (Tukey's HSD < 0.05).

DISCUSSION

This study demonstrates that underlying landscape emissions are the dominate component of ecosystem pasture emissions, and cattle are responsible for ~19-30% of annual CH_4 emissions. The majority of cattle-emitted CH_4 was produced by enteric fermentation, and emissions from manure comprised only 2-6% of total cattle emissions. These results suggest that cattle are not the dominant CH_4 emission source in subtropical lowland pastures, and ecosystem emissions are instead driven by large fluxes from the flooded landscape. As

expected, landscape emissions were highly variable across time and space (Figure 1.1, 1.2, 1.4) and were driven strongly by seasonal flooding and landform hotspots. Wetlands were the dominant CH_4 source, cover 10.9% of the pasture area, and were responsible for 53.5% of the total wet season flux. Canals were dry season emission hotspots, and emitted 97.7% of dry season CH_4 while covering only 1.7% of the landscape (Table 1.1). The results presented here highlight the importance of accounting for all potential emission sources, rather than assuming cattle are the dominant CH_4 emission source in pasture ecosystems. Such assumptions are generally valid in upland or well-drained ecosystems, but landscape emission sources need to be considered in low-lying flooded environments.

This work also suggests that large rains can stimulate episodic CH_4 emissions from pasture soils (Figure 1.5). However, these emissions are short-lived and small, likely due to the rapid percolation of rainwater through dry sandy soils. The rain-induced emission we observed (0.236 ± 0.052 mg CH_4 m^{-2} hr^{-1}) were low compared to wet season fluxes, and were similar to dry season wetland fluxes (0.116 ± 0.040 mg CH_4 m^{-2} hr^{-1}). Given the frequency of large rain events (4 per year; Florida Climate Center, 2013), the short duration of rain-induced emissions, and the high magnitude of wet season ecosystem fluxes, it is unlikely that periodic rain-induced emissions are a significant component of pasture CH_4 budgets.

Fluxes from the pastures were high compared to a number of natural and managed ecosystems. Nicolini et al.'s (2013) review of eddy covariance CH_4 studies reported mean fluxes of 2.61 ± 1.25 g CH_4 m^{-2} yr^{-1} for forests (n = 20), 8.98 ± 3.47 g CH_4 m^{-2} yr^{-1} for croplands (n = 6), and 27.13 ± 5.07 g CH_4 m^{-2} yr^{-1} for wetlands (n = 59). The estimates presented here for subtropical pasture emissions are considerably higher than fluxes from other managed grasslands and pastures, and were on the high end of reported wetland fluxes

(Nicolini et al., 2013). Annual pasture CH_4 emissions are larger than estimates from temperate peatland pastures (Hendriks et al., 2010; Schrier-Uijl et al., 2010b; Teh et al., 2011; Baldocchi et al., 2012; Hatala et al., 2012), are similar to estimates from subtropical flooded savannahs and bottomland forests (Otter and Scholes, 2000; Yu et al., 2008), are at the low end of estimates from tropical wetlands and floodplains (Devol et al., 1990; Mitsch et al., 2010; Nahlik and Mitsch, 2011). Annual pasture emissions are also higher than those reported for nearby Everglades' ecosystems, which range from 1.46 to 29.89 g CH_4 m^{-2} yr^{-1}, though pastures fall within the high range of emissions reported for Everglades dwarf red mangroves, swamp forests, and artificial impoundments (Harriss et al., 1988; Bartlett et al., 1989; Whiting et al., 1991). These comparisons indicate that lowland pastures are a strong and unaccounted for CH_4 source in regional greenhouse gas inventories. Pastures are the most common land use in the northern Everglades (Hiscock et al., 2003) and appear to be a major regional source of CH_4 . Large annual emissions from these pastures cannot be attributed to direct cattle emissions, and the estimates presented here remain within the high range of Everglades' wetland budgets if cattle-emitted CH_4 (8.3 g CH_4 m^{-2} yr^{-1}) is removed from the annual budget.

High input of organic matter from cattle waste or recent photosynthate may be responsible for the large emissions we observed compared to nearby Everglades' ecosystems. Flooded manure deposits are potential CH_4 emission hotspots and are unlikely completely captured with current estimation methodologies. Our manure emission estimates were calculated according to IPCC guidelines for manure deposited on open pasture, a predominantly aerobic manure management system. Actual manure emissions are likely higher during periods of flooding when manure is deposited directly in or leached into standing water, however the magnitude and duration of these emissions are difficult to

estimate due to the transient nature of flooding and manure deposition. Additionally, the methanogenic potential of pasture soil likely varies widely between subsurface sandy horizons (>10 cm depth) and surface organic horizons (<10 cm depth), and the magnitude and variability of wet season emissions may be driven by transient flooding of surface organic soils. Quantifying the relative importance of cattle waste versus soil organic matter as substrate for methanogenesis will improve our understanding of the variable and high magnitude fluxes from these pastures.

Preliminary eddy covariance measurements from this tower as well as partner towers in similar ecosystems suggest that pastures in the region are weak net sinks of CO_2, but greenhouse gas sources when CH_4 emissions from the landscape and cattle are included (Gomez-Casanovas, personal communication). Nitrous oxide emissions have yet to be quantified, but given the anoxic nature of the systems during flooding, likely contribute to the pasture greenhouse gas source strength.

Our assessment suggests that improved pastures in this region are a net greenhouse gas source. However, the source or sink strength of the pastures likely varies widely between wet and dry years, and long-term measurements will be necessary to fully understand and estimate average greenhouse gas exchange. This work presents information from a relatively wet year. The region also experiences drought on a regular basis, and in particularly dry years the water table does not reach the land surface (Bohlen and Villapando, 2011). Therefore, it is likely that pasture CH_4 emissions vary widely among years due to fluctuations in the pasture hydroperiod.

Water retention and wetland restoration programs are common throughout this region and alter pasture hydroperiods. Water retention programs aim to reduce phosphorus (P)

loading to the Everglades, and effectively reduce water nutrient levels but also increase pasture flooding (Bohlen and Villapando, 2011). Pastures in the northern Everglades watershed are the primary source of P loading to the Everglades, and ranchers are currently compensated to retain water on pastures through state and federal agencies (Bohlen et al., 2009). The effect of increased pasture flooding on CH_4 emissions is not known, but it is likely that increasing the pasture hydroperiod leads to an extended period of landscape CH_4 emissions. Further research is needed to evaluate the effect of water management practices on greenhouse gas emissions from these pastures.

The results from this study suggest that subtropical lowland pastures are a strong regional source of CH_4, and unlike upland pasture ecosystems, cattle are not the dominant emission source. Landscape emissions varied widely across time and space, and high magnitude emissions were driven by wet season flooding of pastures and low-lying landforms. The annual emission estimates were high compared to Everglades' wetlands and other pastures ecosystems, indicating subtropical pasture ecosystems are potentially large and unaccounted for CH_4 sources in regional greenhouse gas inventories. These results highlight the need for full accounting of potential greenhouse gas fluxes, and demonstrate that cattle may not be the dominant CH_4 source in lowland pasture ecosystems.

ACKNOWLEDGEMENTS

We thank Hilary Swain, Earl Keel, Julia Maki, and the rest of the staff at the MacArthur Agro-ecology Research Center for site access, lodging, transportation, and continued support in the field. We also thank Carl Bernacchi and Nuria Gomez-Casanovas for help with eddy covariance tower setup, maintenance, data transfer, and processing. Archbold Biological

Station and the MacArthur Agro-ecology Research Center provided LIDAR data used in this work. Hilary Swain and Nuria Gomez-Casanovas provided helpful comments and edits to the manuscript. This research was supported by the Cornell University Program in Cross-Scale Biogeochemistry and Climate, Department of Ecology and Evolutionary Biology, Andrew W. Mellon Foundation, Cornell Sigma Xi, and University of Illinois USDA ARS.

REFERENCES

Allard V, Soussana JF, Falcimagne R, Berbigier P, Bonnefond JM, Ceschia E, D'hour P, Hénault C, Laville P, Martin C. 2007. The role of grazing management for the net biome productivity and greenhouse gas budget (CO_2, N_2O and CH_4) of semi-natural grassland. Agriculture, Ecosystems & Environment 121: 47–58.

Aubinet M, Feigenwinter C, Heinesch B, Laffineur Q, Papale D, Reichstein M, Rinne J, Van Gorsel E. 2012. Nighttime flux correction. Aubinet M, Vesala T, Papale D, editors. Eddy covariance a practical guide to measurements and data analysis. New York: Springer. p133–57.

Baldocchi D, Detto M, Sonnentag O, Verfaillie J, Teh YA, Silver W, Kelly NM. 2012. The challenges of measuring methane fluxes and concentrations over a peatland pasture. Agricultural and Forest Meteorology 153: 177–87.

Bartlett DS, Bartlett KB, Hartman JM, Harriss RC, Sebacher DI, Pelletier Travis R, Dow DD, Brannon DP. 1989. Methane emissions from the Florida Everglades: Patterns of variability in a regional wetland ecosystem. Global Biogeochemical Cycles 3: 363–74.

Bohlen PJ, Gathumbi SM. 2007. Nitrogen cycling in seasonal wetlands in subtropical cattle pastures. Soil Science Society of America Journal 71: 1058–65.

Bohlen PJ, Lynch S, Shabman L, Clark M, Shukla S, Swain H. 2009. Paying for environmental services from agricultural lands: an example from the northern Everglades. Frontiers in Ecology and the Environment 7: 46–55.

Bohlen PJ, Villapando OR. 2011. Controlling runoff from subtropical pastures has differential effects on nitrogen and phosphorus loads. Journal of Environmental Quality 40: 989–98.

Bridgham SD, Megonigal JP, Keller JK, Bliss NB, Trettin C. 2006. The carbon balance of North American wetlands. Wetlands 26: 889–916.

Conant RT, Paustian K. 2002. Potential soil carbon sequestration in overgrazed grassland ecosystems. Global Biogeochemical Cycles 16: 90–1–90–9.

Conrad R. 2007. Microbial ecology of methanogens and methanotrophs. Sparks DL, editor. Advances in agronomy. Vol. 96. Advances in agronomy. New York: Elsevier. p1–63.

Dengel S, Levy PE, Grace J, Jones SK, Skiba UM. 2011. Methane emissions from sheep pasture, measured with an open- path eddy covariance system. Global Change Biology 17: 3524–33.

Detto M, Montaldo N, Albertson JD, Mancini M, Katul G. 2006. Soil moisture and vegetation controls on evapotranspiration in a heterogeneous Mediterranean ecosystem on Sardinia, Italy. Water Resources Research 42: W08419.

Devol AH, Richey JE, Forsberg BR, Martinelli LA. 1990. Seasonal dynamics in methane emissions from the Amazon River floodplain to the troposphere. Journal of Geophysical Research: Atmospheres 95: 16417–26.

Environmental Protection Agency (EPA). 2014. Annex 3. Methodological descriptions for additional source or sink categories. Washington DC. p. A125-A384.

Farrell P, Culling D, Leifer I. 2013. Transcontinental methane measurements: Part 1. A mobile surface platform for source investigations. Atmospheric Environment 74: 422–31.

Florida Climate Center (2013) Big rain events in the Southeast. Florida State Univeristy. http://climatecenter.fsu.edu/climate-data-access-tools/big-rain

Foken T, Göockede M, Mauder M, Mahrt L, Amiro B, Munger W. 2005. Post-field data quality control. Lee X, Massman WJ, Law BE, editors. Handbook of micrometeorology. Dordrecht: Kulwer Academic Publishers. p181–208.

Follett RF, Reed DA. 2010. Soil carbon sequestration in grazing lands: societal benefits and policy implications. Rangeland Ecology & Management 63: 4–15.

Forster P, Ramaswamy V, Artaxo P, Berntsen T, Betts R, Fahey D, Haywood J, Lean J, Lowe CD, Myhre G, Nganga J, Prinn R, Raga G, Schulz M, Van Dorland R. 2007. Changes in atmospheric constituents and in radiative forcing. Solomon S, Qin D, Manning M, Chen Z, Marquis M, Averyt KB, Tignor M, Miller HL, editors. Climate change 2007: the physical science basis: contribution of working group 1 to the fourth assessment report of the Intergovernmental Panel on Climate Change. New York: Cambridge University Press. p129–234.

Gathumbi SM, Bohlen PJ, Graetz DA. 2005. Nutrient enrichment of wetland vegetation and sediments in subtropical pastures. Soil Science Society of America Journal 69: 539–48.

Gibbs MJ, Conneely D, Johnson D, Lasse KR, Ulyatt MJ. (2000) CH_4 emissions from enteric fermentation. Penman J, Kruger D, Galbally I, editors. Good practice guidance and uncertainty management in national greenhouse gas inventories. Switzerland: Intergovernmental Panel on Climate Change. p297-320.

Groffman PM, Butterbach-Bahl K, Fulweiler RW, Gold AJ, Morse JL, Stander EK, Tague C, Tonitto C, Vidon P. 2009. Challenges to incorporating spatially and temporally explicit phenomena (hotspots and hot moments) in denitrification models. Biogeochemistry 93: 49–77.

Harriss RC, Sebacher DI, Bartlett KB, Bartlett DS, Crill PM. 1988. Sources of atmospheric methane in the south Florida environment. Global Biogeochemical Cycles 2: 231–43.

Hatala JA, Detto M, Sonnentag O, Deverel SJ, Verfaillie J, Baldocchi DD. 2012. Greenhouse

gas (CO_2, CH_4, H_2O) fluxes from drained and flooded agricultural peatlands in the Sacramento-San Joaquin Delta. Agriculture, Ecosystems & Environment 150: 1–18.

Hendriks D, van Huissteden J, Dolman AJ. 2010. Multi-technique assessment of spatial and temporal variability of methane fluxes in a peat meadow. Agricultural and Forest Meteorology 150: 757–74.

Herbst M, Friborg T, Ringgaard R, Soegaard H. 2011. Interpreting the variations in atmospheric methane fluxes observed above a restored wetland. Agricultural and Forest Meteorology 151: 841–53.

Hersom M. 2002. Pasture stocking density and the relationship to animal performance. University of Florida IFAS Extension AN155.

Hiscock JG, Thourot CS, Zhang J. 2003. Phosphorus budget—Land use relationships for the northern Lake Okeechobee watershed, Florida. Ecological Engineering 21: 63–74.

Hsieh C-I, Katul G, Chi T-W. 2000. An approximate analytical model for footprint estimation of scalar fluxes in thermally stratified atmospheric flows. Advances in Water Resources 23: 765–72.

Intergovernmental Panel on Climate Change (IPCC). 2006. Emissions from livestock and manure management. Eggleston HS, Buendia L, Miwa K, Ngara T, Tanabe K, editors. 2006 IPCC guidelines for national greenhouse gas inventories. Vol. 4. Agricultural, forestry and other land uses. IGES, Japan. p. 10.1-10.87.

Jackson RB, Down A, Phillips NG, Ackley RC, Cook CW, Plata DL, Zhao K. 2014. Natural gas pipeline leaks across Washington, DC. Environmental Science Technology 48: 2051–8.

Kirschke S, Bousquet P, Ciais P, Saunois M, Canadell JG, Dlugokencky EJ, Bergamaschi P, Bergmann D, Blake DR, Bruhwiler L. 2013. Three decades of global methane sources and sinks. Nature Geoscience 6: 813–23.

Kroon PS, Schrier-Uijl AP, Hensen A, Veenendaal EM, Jonker H. 2010. Annual balances of CH_4 and N_2O from a managed fen meadow using eddy covariance flux measurements. European Journal of Soil Science 61: 773–84.

Lassey KR. 2007. Livestock methane emission: from the individual grazing animal through national inventories to the global methane cycle. Agricultural and Forest Meteorology 142: 120–32.

Leifer I, Culling D, Schneising O, Farrell P, Buchwitz M, Burrows JP. 2013. Transcontinental methane measurements: Part 2. Mobile surface investigation of fossil fuel industrial fugitive emissions. Atmospheric Environment 74: 432–41.

Matthes JH, Sturtevant C, Verfaillie J. 2014. Parsing the variability in CH_4 flux at a spatially heterogeneous wetland: Integrating multiple eddy covariance towers with high-resolution flux footprint analysis. Journal of Geophysical Research: Biogeosciences.

Melack JM, Hess LL, Gastil M, Forsberg BR, Hamilton SK, Lima IB, Novo EM. 2004. Regionalization of methane emissions in the Amazon Basin with microwave remote sensing. Global Change Biology 10: 530–44.

Mitsch WJ, Nahlik A, Wolski P, Bernal B, Zhang L, Ramberg L. 2010. Tropical wetlands: seasonal hydrologic pulsing, carbon sequestration, and methane emissions. Wetlands Ecology and Management 18: 573–86.

Moncrieff JB, Massheder JM, De Bruin H, Elbers J, Friborg T, Heusinkveld B, Kabat P, Scott S, Søgaard H, Verhoef A. 1997. A system to measure surface fluxes of momentum, sensible heat, water vapour and carbon dioxide. Journal of Hydrology 188: 589–611.

Nahlik A, Mitsch WJ. 2011. Methane emissions from tropical freshwater wetlands located in different climatic zones of Costa Rica. Global Change Biology 17: 1321–34.

Nicolini G, Castaldi S, Fratini G, Valentini R. 2013. A literature overview of micrometeorological CH_4 and N_2O flux measurements in terrestrial ecosystems. Atmospheric Environment 81: 311–9.

Nieveen JP, Campbell DI, Schipper LA, Blair IJ. 2005. Carbon exchange of grazed pasture on a drained peat soil. Global Change Biology 11: 607–18.

Olson DM, Griffis TJ, Noormets A, Kolka R, Chen J. 2013. Interannual, seasonal, and retrospective analysis of the methane and carbon dioxide budgets of a temperate peatland. Journal of Geophysical Research: Biogeosciences 118: 226–38.

Otter LB, Scholes MC. 2000. Methane sources and sinks in a periodically flooded South African savanna. Global Biogeochemical Cycles 14: 97–111.

Phillips NG, Ackley R, Crosson ER, Down A, Hutyra LR, Brondfield M, Karr JD, Zhao K, Jackson RB. 2013. Mapping urban pipeline leaks: methane leaks across Boston. Environmental Pollution 173: 1–4.

R Core Team. 2013. R: A language and environment for statistical computing. R Foundation for Statistical Computing. Vienna, Austria.

Ramankutty N, Evan AT, Monfreda C, Foley JA. 2008. Farming the planet: 1. Geographic distribution of global agricultural lands in the year 2000. Global Biogeochemical Cycles 22: GB1003.

Rinne J, Ruitta T, Pihlatie M, Aurela M, Haapanala S, Tuovinen J-P, Tuittila E-S, Vesala T. 2007. Annual cycle of methane emission from a boreal fen measured by the eddy covariance technique. Tellus B 59:449–57.

Schrier-Uijl AP, Kroon PS, Leffelaar PA, Huissteden JC, Berendse F, Veenendaal EM. 2010a. Methane emissions in two drained peat agro-ecosystems with high and low agricultural intensity. Plant and Soil 329: 509–20.

Schrier-Uijl AP, Kroon PS, Hensen A, Leffelaar PA, Berendse F, Veenendaal EM. 2010b. Agricultural and Forest Meteorology. Agricultural and Forest Meteorology 150: 825–31.

Shorter JH, Mcmanus JB, Kolb CE, Allwine EJ, Lamb BK, Mosher BW, Harriss RC, Partchatka U, Fischer H, Harris GW. 1996. Methane emission measurements in urban areas in eastern Germany. Journal of Atmospheric Chemistry 24: 121–40.

Soussana JF, Tallec T, Blanfort V. 2010. Mitigating the greenhouse gas balance of ruminant production systems through carbon sequestration in grasslands. Animal 4: 334–50.

Swain HM, Boughton EH, Bohlen PJ, Lollis LO. 2013. Trade-offs among ecosystem services and disservices on a Florida ranch. Rangelands 35: 75–87.

Teh YA, Silver WL, Sonnentag O, Detto M, Kelly M, Baldocchi DD. 2011. Large greenhouse gas emissions from a temperate peatland pasture. Ecosystems 14: 311–25.

United States Environmental Protection Agency. 2012. Global anthropogenic non-CO_2 greenhouse gas emissions: 1990-2030. EPA 430-R-12-006 Washington, DC: p1-176.

Vickers D, Mahrt L. 1997. Quality control and flux sampling problems for tower and aircraft data. Journal of Atmospheric and Oceanic Technology 14: 512–26.

Wang JM, Murphy JG, Geddes JA, Winsborough CL, Basiliko N, Thomas SC. 2012. Methane fluxes measured by eddy covariance and static chamber techniques at a temperate forest in central Ontario, Canada. Biogeosciences Discussions 9: 17743–74.

Webb EK, Pearman GI, Leuning R. 1980. Correction of flux measurements for density effects due to heat and water vapour transfer. Quarterly Journal of the Royal Meteorological Society 106: 85–100.

Whiting GJ, Chanton JP, Bartlett DS, Happell JD. 1991. Relationships between CH_4 emission, biomass, and CO_2 exchange in a subtropical grassland. Journal of Geophysical Research: Atmospheres 96: 13067–71.

Yu K, Faulkner SP, Baldwin MJ. 2008. Effect of hydrological conditions on nitrous oxide, methane, and carbon dioxide dynamics in a bottomland hardwood forest and its implication for soil carbon sequestration. Global Change Biology 14: 798–812.

CHAPTER 2

INFLUENCE OF TRANSIENT FLOODING ON METHANE FLUXES FROM SUBTROPICAL PASTURES

Published as:

Chamberlain SD, Gomez-Casanovas N, Walter TM, Boughton EH, Bernacchi CJ, DeLucia EH, Groffman PM, Keel EW, Sparks JP. 2016. Influence of transient flooding on methane fluxes from subtropical pastures. *Journal of Geophysical Research – Biogeosciences*

ABSTRACT

Seasonally flooded subtropical pastures are major methane (CH_4) sources, where transient flooding drives episodic and high magnitude emissions from the underlying landscape. Understanding the mechanisms that drive these patterns is needed to better understand pasture CH_4 emissions and their response to global change. We investigated belowground CH_4 dynamics in relation to surface fluxes using laboratory water table manipulations and compared these results to field-based eddy covariance measurements to link within-soil CH_4 dynamics to ecosystem fluxes. Ecosystem CH_4 fluxes lag flooding events, and this dynamic was replicated in laboratory experiments. In both cases, peak emissions were observed during water table recession. Flooding of surface organic soils and precipitation driven oxygen pulses best explained the observed time lags. Precipitation oxygen pulses likely delay CH_4 emissions until groundwater dissolved oxygen is consumed, and emissions were temporally linked to CH_4 production in surface soil horizons. Methane accumulating in deep soils did not contribute to surface fluxes and is likely oxidized within the soil profile. Methane production rates in surface organic soils were also orders of magnitude higher than in deep mineral soils, suggesting that over longer flooding regimes CH_4 produced in deep horizons is not a significant component of surface emissions. Our results demonstrate that distinct CH_4 dynamics may be stratified by depth and flooding of surface organic soils drives CH_4 fluxes from subtropical pastures. These results suggest that small changes in pasture water table dynamics can drive large changes in CH_4 emissions if surface soils remain saturated over longer time scales.

INTRODUCTION

Methane (CH_4) is a globally important greenhouse gas, with a radiative forcing ~25 times higher than CO_2 in the atmosphere, and global CH_4 concentrations have increased 2.5 fold since the preindustrial era (Stocker et al., 2013). Emissions from wetlands and flooded ecosystems are the largest global source of CH_4, however the magnitudes and controls of these fluxes remain poorly quantified. Much of this uncertainty stems from a poor resolution of flooded area, a lack of measurements across varied wetland ecosystems, and few measurements of the belowground microbial and transport processes mediating surface fluxes (Riley et al., 2011; Bridgham et al., 2013; Kirschke et al., 2013). Emission estimates are particularly uncertain for seasonally flooded ecosystems where transient flooding drives large and variable CH_4 emissions that are difficult to quantify using traditional *in situ* chamber measurements (Melack et al., 2004; Chamberlain et al., 2015). A better understanding of fluxes from these ecosystems is needed to improve our estimates of ecosystem CH_4 emissions and their response to environmental change.

Methane fluxes from flooded ecosystems are the product of CH_4 production, consumption, and transport within soils and water. Here, CH_4 is produced exclusively by Archaea (methanogens) that convert end products of fermentation, most notably acetate or CO_2 and H_2, to CH_4 for energy. Methanogens are most active in anaerobic and highly reduced environments, and their activity is generally limited by high oxygen (O_2) concentrations, substrate (C) availability, and the presence of alternative electron acceptors used for respiration (Conrad, 2007). In contrast, CH_4 consuming bacteria (methanotrophs) oxidize CH_4 for energy in the presence of O_2. Methanotrophs are primarily aerobic and their activity is often limited by low O_2 and CH_4 concentrations (Conrad, 2007). Methanotrophic bacteria are

an important moderator of surface emissions and consume significant amounts of soil-produced CH_4 before it reaches the atmosphere (Oremland and Culbertson, 1992; Le Mer and Roger, 2001; Teh et al., 2006). Methane production and consumption in soils is often stratified by water table position and oxygen status (King et al., 1990; Roulet et al., 1993; Conrad et al., 1999), however both processes can co-occur in well-drained soils that maintain anoxic microsites (Silver et al., 1999; Teh et al., 2005; Hall et al., 2013).

We can better understand the mechanisms controlling ecosystem fluxes by examining flux patterns relative to environmental drivers. In seasonally flooded subtropical pastures, transient flooding produces large and variable CH_4 fluxes that consistently lag flooding events (Chamberlain et al., 2015). Lagged CH_4 fluxes are commonly observed under fluctuating water table conditions, where maximum fluxes occur during water table recession. In temperate peatlands, it is hypothesized that these patterns are driven by the flooding of a 'critical zone' within the soil profile where CH_4 production is maximized (due to favorable redox conditions and substrate availability) or by outgassing of CH_4 produced and stored in deep horizons of the soil profile (Moore and Dalva, 1993; Moore and Roulet, 1993; Brown et al., 2014). Subtropical pastures are quite different than temperate peatlands and are characterized by well-drained precipitation recharged mineral soils. Here, oxic conditions may persist below the water table due to large inputs of oxygenated rainwater (Datry et al., 2004; Schilling and Jacobson, 2014). Under these conditions, consumption of oxygen may be incomplete and redox and hydrologic status can become decoupled, allowing anoxic (methanogenesis) and oxic (methanotrophy) processes to co-occur (Hall et al., 2013). Common observations of flux lags across such contrasting ecosystems suggests that similar

mechanisms may drive CH_4 flux dynamics under fluctuating water tables, but these mechanisms have not been evaluated in seasonally flooded subtropical ecosystems.

The goals of this work were to 1) examine patterns in ecosystem CH_4 fluxes under transient flooding events, and 2) determine the mechanisms that influence flux time lags. We measured CH_4 fluxes from seasonally flooded subtropical pastures for three years using eddy covariance to examine flux patterns relative to hydrologic drivers. To link these ecosystem-scale observations to mechanistic processes, we conducted experimental water table manipulations on intact soil columns to evaluate belowground CH_4 consumption, production, and transport in relation to net surface fluxes. We also conducted an incubation experiment to determine variation in CH_4 production rates throughout the soil profile. These three approaches were used to describe ecosystem flux patterns across transient flooding events and to characterize the mechanistic processes that produce these patterns.

METHODS

Study Site

Flux measurements and soils were collected within a fenced improved pasture (92.1 ha) located at the MacArthur Agro-ecology Research Center in Lake Placid, Florida, USA (N 27.1632004, W 81.187302). The MacArthur Agro-ecology Research Center is a 4290 ha beef cattle ranch that operates as an ecological field station and division of Archbold Biological Station. The pasture is planted with *Paspalum notatum* and is rotationally grazed at a density of ~1.6 cow ha^{-1}. Herbicide and fertilizers have not been applied to the pasture since August 2006 and April 2007, respectively. The pastures receive an average of 1300 mm of rain per year, 75% of which falls during the summer wet season (Gathumbi et al., 2005). Pastures are

developed on Immokalee fine sand spodosols, which are characterized by near-surface organic horizons (0-0.15 m depth) and sandy mineral horizons at depth (0.15 – 0.50 m depth; Table 2.1). Within these soils, a spodic horizon is also found at depths greater than 0.5 m below surface. Extensive networks of ditches throughout the pasture drain these soils, though flooding occurs during heavy rain periods. Mean annual temperature throughout the measurement period was 23.03 °C, with a temperature maximum of 35.7 °C and minimum of -2.6 °C. By area, the study pasture is 74.2% pasture grassland, 10.9% depressional wetland, 9.2% cabbage palm (*Sabal palmetto*) hammock, 4.0% drainage ditch, and 1.7% drainage canal (Chamberlain et al., 2015). All soil samples were collected from pasture grassland, the primary land cover.

Table 2.1 Percent carbon (C) and nitrogen (N) throughout the pasture soil profile (n = 3 for all depths). Standard errors are reported for all percent C and N values, and letters indicate significant differences between soil horizons for each element (Tukey's HSD, $P < 0.05$). Depth column indicated the depth range for bulked samples and, in parentheses, the designation used in incubations and mesocosm treatments.

Depth (m)	%C	%N
0.0 – 0.05 (0)	8.48 ± 0.92 *a*	0.49 ± 0.07 *a*
0.05 – 0.15 (0.1)	3.57 ± 1.58 *a*	0.20 ± 0.10 *b*
0.15 – 0.25 (0.2)	0.63 ± 0.19 *b*	0.03 ± 0.01 *b*
0.25 – 0.35 (0.3)	0.20 ± 0.02 *b*	0.09 ± 0.08 *b*
0.35 – 0.45 (0.4)	0.09 ± 0.01 *b*	0.03 ± 0.02 *b*

Eddy Covariance and Environmental Measurements

Methane fluxes were measured continuously from May 2013 to November 2015 with an eddy covariance tower installed in the pasture center (N 27.1632004, W 81.187302). Wind speed and direction were measured with a three-dimensional sonic anemometer (CSAT3, Campbell Scientific Inc., Logan, UT, USA) and CH_4, CO_2, and H_2O concentrations were measured with open-path infrared gas analyzers (LI-7700; LI-7500A, Licor Inc., Lincoln, NE, USA). These

instruments were installed 2.6 m above the pasture surface and interfaced with a LI-7550 datalogger (Licor Inc., Lincoln, NE, USA). Data were collected at 10 Hz and transferred by modem for processing. Water table depth (WTD; m below surface) was measured at the tower site with a pressure transducer (CS451, Campbell Scientific Inc., Logan, UT, USA), volumetric water content (VWC) was measured at 5, 10, and 20 cm depths with water content reflectometers (CS-616, Campbell Scientific Inc., Logan, UT, USA), and groundwater dissolved oxygen (DO; mg/L) was measured with an optical DO probe installed within the water table well (Aquistar DO2, INW USA, Kent, WA, USA). All auxiliary measures were collected as 30 min averages and logged to a CR3000 datalogger (Campbell Scientific Inc., Logan, UT, USA) time synchronized to the LI-7550. Rainfall was measured at 30 min intervals with a tipping bucket gauge (TB4, Hydrologic Services America, Lake Worth, FL, USA) at a weather station 1.7 km southwest of the tower (N 27.150475, W 81.198568). Groundwater DO measurements began in July 2015, and the optical DO probe was installed 0.95 m below the land surface. DO measurements were rejected from analysis if the water table was 0.90 m below surface or deeper. This method has been used in previous studies to continuously monitor groundwater DO concentrations (Datry et al., 2004; Foulquier et al., 2010; Schilling and Jacobson, 2014; 2015).

Methane fluxes were calculated from the covariance of vertical wind speed and CH_4 concentration over 30 min intervals. Raw data were screened for spikes, drop-outs, amplitude resolution, absolute value limits, and skewness and kurtosis as described in Vickers and Mahrt (1997) and designated default in commercial software (Eddy Pro 4.2, Licor Inc., Lincoln, NE, USA). We used double-rotation tilt corrections to align the anemometer with mean wind streamlines and block averaging to calculate mean wind speed and CH_4 concentration over the

30 min interval. Time lags were corrected with the covariance maximization method. Webb, Pearl, and Leuning corrections for density fluctuations were applied according to Webb et al. (1980) and fully analytic spectral corrections were applied according to Moncrieff et al. (1997). All of the above corrections and processing were conducted using commercial software (Eddy Pro 4.2, Licor Inc., Lincoln, NE, USA). We also rejected all fluxes when the open-path CH_4 analyzer was blocked, when CH_4 concentrations were below 1.74 ppm or above 5 ppm, and when fluxes were above 1500 nmol m^{-2} s^{-1} or below -500 nmol m^{-2} s^{-1}, as extreme fluxes and unrealistic concentrations are observed when CH_4 sensor signal quality is low (Dengel et al., 2011; Baldocchi et al., 2012).

Data quality were flagged according to Foken et al. (2005) using commercial software (Eddy Pro 4.2, Licor Inc., Lincoln, NE, USA). Quality flags range from 1 (best) to 9 (worst). All fluxes with flags greater than 6 were rejected from time series analysis (see *Time Series and Diffusive Flux Analysis*), and all fluxes with quality flags greater than 3 were rejected when regressing CH_4 fluxes to environmental variables. Overall, 37% of all half-hour fluxes were removed from the time series analysis dataset, and 64% of fluxes were removed from the regression analysis dataset. For time series analysis, we calculated median daily fluxes and omitted days from analysis with coverage less than 33% as outlined in Chamberlain et al. (2015). Linear regression was used to determine significant relationships between environmental variables and log-transformed daily CH_4 fluxes using only high quality measured data (quality flags 3 or lower, non-gap filled, 33% or higher daily coverage). We calculated daily-integrated fluxes as medians because episodic CH_4 emissions from grazing cattle amplified daily mean fluxes.

Water Table Manipulations

We conducted laboratory water table manipulations on five intact soil columns. Intact columns were used in this experiment to preserve the pasture soil structure and avoid inaccuracies introduced by slurry-based experiments (Teh and Silver, 2006). Soil columns with live *Paspalum notatum* cover were collected randomly in 0.15 x 0.60 m PVC sleeves from pasture within the flux tower footprint in January 2015. PVC sleeves were driven 0.55 m into the ground and the top 0.05 m was left aboveground to allow surface flux measurements during manipulations. Columns were removed and immediately driven back to Cornell University where water table manipulations were conducted. In all five columns, soil gas and pore water sampling ports were installed at 0, 0.1, 0.2, 0.3, 0.4, and 0.5 m depths with Luer lock fittings. All columns were placed in separate 0.52 x 0.66 m mesocosms, and water was directly added to or removed from the mesocosms to adjust the water table depth. The columns base was left open, allowing water to enter or exit during water table adjustments and equilibrate to the mesocosm water level.

The water table in five replicate mesocosms was increased by 0.1 m increments every 24 hours from 0.55 m to 0 m below the surface (7 levels; 0.55, 0.45, 0.35, 0.25, 0.15, 0.05, 0 m below surface). The water table was left at the surface for 48 hours, and then decreased at 24-hour intervals until mesocosms were dry. The total experiment length was 14 days. While precipitation recharge events in the field are often characterized by sharp jumps in the water table (Figure 2.1), we chose to simulate a water table recharge and recession event with even tails to fully examine potential hysteresis in the recharge and recession phases. Oxygenated water was introduced to the columns to simulate precipitation recharge groundwater dynamics observed in these pastures (Figure 2.1). All mesocosms were placed under artificial light

(Sunlight Supply, Vancouver, WA) with a 12-hour photoperiod, and air temperature was maintained at 22 °C.

We measured CH_4 surface fluxes in addition to profile CH_4 concentration and isotopic composition ($\delta^{13}C\text{-}CH_4$) in three of five experimental mesocosms (trace gas mesocosms). Only soil gas O_2 and pore water DO were measured in the remaining two mesocosms (oxygen mesocosms). We measured trace gases and oxygen from separate mesocosms to minimize the total volume of soil gas or pore water removed from each column at each time point. By segregating trace gas and oxygen measurements to separate mesocosms, we never evacuated more than 6% of total column soil pore space.

In the trace gas mesocosms, 30 ml of soil gas was removed by syringe from unsaturated soil horizons to measure CH_4 concentrations and $\delta^{13}C\text{-}CH_4$. In saturated horizons, 10 ml of pore water was removed by syringe, and dissolved CH_4 was measured by equilibrating pore water with a pure N_2 headspace within the syringe at a 3:1 N_2 to water equilibration ratio (Jahangir et al., 2012). Equilibrating syringes were placed on an orbital shaker for 10 minutes and vigorously shaken by hand prior to headspace measurements. All soil and headspace equilibrated gas samples were analyzed for CH_4 concentration and $\delta^{13}C\text{-}CH_4$ on a wavelength-scanned cavity ringdown spectrometer (G2201-*i*, Picarro Inc., Sunnyvale, CA, USA) equipped with a SSIM2 Small Sample Isotope Module (Picarro Inc., Sunnyvale, CA, USA). Gas concentrations in pore water were calculated from headspace concentrations using Henry's law and Bunsen coefficients. Surface fluxes were measured from trace gas mesocosms using a closed dynamic PVC chamber attached to the column surface. The chamber was a closed flow-through design, which circulated the chamber headspace through the spectrometer (G2201-*i*; flow rate 300 ml min^{-1}). When measuring

fluxes, the PVC chamber was attached to each column for 5 minutes, enclosing a 2.55 L volume, and fluxes were calculated by applying a linear regression to concentration increases over the total enclosure period. Concentration and $\delta^{13}C\text{-}CH_4$ measurements were precise to within 0.05 ppm CH_4 and 0.8‰. The spectrometer and SSIM2 were calibrated with known concentration and isotope standards of CH_4 in air (Air Liquide, Philadelphia, PA; Isometric Instruments, Victoria, BC, USA). In the two oxygen mesocosms, 30 ml of soil gas was removed from unsaturated horizons by syringe and soil gas O_2 concentrations were measured with a modified flow-through oxygen sensor (SO-210; Apogee Instruments Inc., Logan, UT, USA). In saturated horizons, 20 ml of pore water was removed and DO was immediately measured using an optical DO sensor (YSI ProDO, Xylem Inc., Rye Brook, NY, USA). Linear regression was used to determine significant relationships between surface CH_4 fluxes and concentration dynamics at different depths within the mesocosms. All mesocosm CH_4 fluxes and concentration measurements were log-transformed to meet assumptions of normality.

Soil Incubations

To compliment the water table manipulations, we also conducted laboratory incubations to assess CH_4 production rates and $\delta^{13}C\text{-}CH_4$ of production throughout the soil profile. We removed three intact 0.1 x 0.55 m cores randomly from the eddy tower footprint in July 2015 following methods described above. In the field, each core was divided into 0-0.5, 0.5-0.15, 0.15-0.25, 0.25-0.35, and 0.35-0.45 m depth sections, homogenized by depth, and stored in ziplock bags; these depths correspond to the mesocosm experiment measurements ports (0, 0.1, 0.2, 0.3, and 0.4 depth). Soils were immediately shipped to Cornell University for

incubations. Incubation results are reported relative to column measurement ports (0, 0.1, 0.2, 0.3, and 0.4 depth).

For all incubations (15 total), 50 grams of homogenized soil and 100 ml of degassed deionized water were added to 473 ml airtight mason jars fitted with thick butyl rubber stoppers (Geo-Microbial Technologies Inc., Ochleata, OK, USA). All incubation jars were gently swirled by hand to ensure mixing of soils and water. Connection points were further sealed with silicone adhesive. The jar headspace was then purged with 100% N_2 gas for 10 minutes (flow rate; 500 ml min^{-1}) to create an anaerobic environment. We conducted a 14-day pre-incubation phase to ensure depletion of O_2 and alternative electron acceptors prior to the measured incubation phase. At the end of pre-incubation, jars were once again flushed with N_2 for 10 minutes and measurements began immediately following headspace flushing. Jars were incubated for 21 days in the dark at 22 °C and headspace gases were sampled every 3-4 days. An equivalent volume of 100% N_2 was added when samples were taken to maintain the internal air volume. All gas samples were analyzed for CH_4 concentration and $\delta^{13}C$-CH_4 on the spectrometer (G2201-*i*) equipped with a SSIM2 Small Sample Isotope Module (Picarro Inc., Sunnyvale, CA, USA). An additional jar filled with 10 ppmv CH_4 in air was sampled in tandem with incubations to track potential leakage from jars. No leakage was observed from the 10 ppmv CH_4 jar throughout the 21-day sampling period. After incubations, soils were dried and weighed to allow for calculation of production rates per g of dry soil (nmol CH_4 g $soil^{-1}$ d^{-1}). Soil CH_4 production rates were then calculated by applying a linear regression to concentration increases across the entire 21-day incubation period (for all regressions; $r^2 > 0.85$; $P < 0.05$).

We compared mesocosm pore water and anaerobic incubation $\delta^{13}C\text{-}CH_4$ values to assess potential fractionation of CH_4 by aerobic oxidation within the mesocosm experiment. The rationale behind this comparison was that aerobic methanotrophic bacteria require oxygen for metabolism (Conrad, 2007), and CH_4 produced in anaerobic incubations will not experience aerobic methanotrophic fractionation effects. We also quantified percent carbon (C) and nitrogen (N) for soils collected in the incubation experiment. Homogenized soils were dried for 24 hours at 40 °C, sieved to 2 mm, and were then analyzed for percent C and N using a LECO C/N analyzer (TruMac, LECO Corporation, St. Joseph, MI, USA).

Time Series and Diffusive Flux Analysis

We used cross-correlation analyses to quantify the time lag between CH_4 fluxes and water table fluctuations for 184 days for the 2013 and 2014 wet seasons (May 1 to October 31). Cross-correlation analyses were only conducted for wet season periods because the water table did not fluctuate or approach the land surface during other parts of the year. In 2015, cross-correlation analysis was conducted for the active flooding period only (August 1 to October 31). Cross-correlations were computed between daily eddy covariance CH_4 fluxes (median; nmol CH_4 m^{-2} s^{-1}) and water table depth. We rejected daily CH_4 fluxes from cross-correlation analysis when less than 33% of CH_4 flux measurements were available. Such periods occurred during July-August of 2013 and 2014 when CH_4 concentration data were not available due to power dropouts and sensor blockage.

We estimated diffusive gas flux rates following Striegl (1993) to better understand CH_4 fluxes observed in mesocosms relative to physical properties during water table recession. We estimated diffusive fluxes rates based on three observed mesocosm conditions

when 1) soils were flooded and emissions were low, 2) water tables were recessing and emission peaked, and 3) water tables were lowest, emissions were zero, yet deep horizon CH_4 concentrations peaked. Here, we estimated diffusive gas fluxes according to the equation:

$$q = -D_{AB}\theta_D\tau\frac{dC_a}{dz}$$

where q = surface flux (nmol m^{-2} d^{-1}), D_{AB} = effective diffusion constant for CH_4 (1.69 m^2 d^{-1} at STP), θ_D = gas-filled porosity, τ = tortuosity, dC_a/dz = CH_4 concentration gradient across depth. τ was assumed to be $\theta_D^{1/3}$ following Striegl (1993). For calculations 1 and 2, we held the concentration gradient constant to quantify the influence of changing gas-filled porosity during water table recession. Here, we calculated the gradient using mean atmospheric (0.075 μM CH_4) and 0.1 m depth (0.478 μM) concentrations from days 6 to 9 of the mesocosm experiment. For 3, we calculated q based on the observed concentration gradient on the final day of the mesocosm treatment between atmospheric (0.075 μM CH_4) and 0.4 m depth (32.85 μM CH_4). θ_D values used in all estimates were calculated as the difference between soil effective porosity and a range of VWC values measured at the eddy tower site during representative pasture conditions (VWC at WTD >= 0 for scenario 1, 0.15 > WTD > 0.1 for scenario 2, and 0.5 > WTD > 0.4 for scenario 3). Here, effective porosity was assumed to be 0.424, equal to the maximum soil VWC (5 cm depth) measured when pastures were fully flooded. θ_D values used in diffusive flux calculations ranged from 0.000-0.054 for (1), 0.014 – 0.067 for (2), and 0.020 – 0.155 for (3). In all calculations, we estimated θ_D from field data because we did not measure VWC in mesocosms; these calculations are meant to be relative rather than precise.

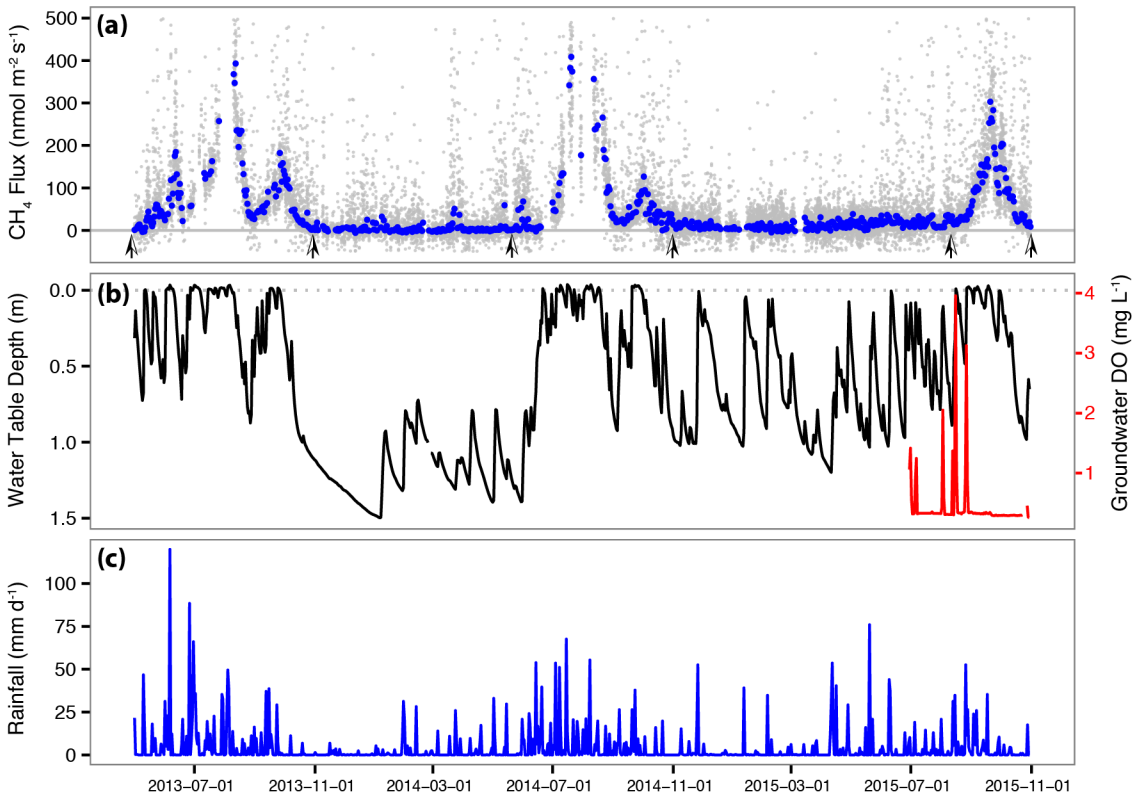

Figure 2.1 Time series of daily CH_4 fluxes (a; blue points), half-hourly CH_4 fluxes (a; grey points), water table depth (b), daily mean groundwater DO concentration (b; red line), and cumulative rainfall (c). Long periods without flux measurements in July-August 2013 and 2014 correspond to periods of instrument signal dropout. Arrows on (a) mark the beginning and end of flooding periods used in cross-correlation analyses.

RESULTS

Pasture CH_4 emissions were highest during summer wet seasons (Figure 2.1a), and CH_4 fluxes positively correlated to water table fluctuations ($r^2 = 0.49$, $P < 0.0001$). Transient flooding events were common in these pastures and were characterized by a rapid increase in the water table followed by a more gradual recession following flooding (Figure 2.1b). Flooding events were most frequent during the wet season and coincided with large and/or frequent precipitation events (Figure 2.1c). Large and extended ecosystem CH_4 emissions were observed during periods when the water table reached the land surface for more than one day. These events were observed throughout the 2013, 2014, and late 2015 wet seasons (Figure

2.1). In contrast, appreciable CH_4 emissions were rarely observed during short duration (less than 1 day) or incomplete flooding events that did not reach the land surface. These observations were common from November 2014 through July 2015, when many recharge events occurred, but the water table never reached the land surface for more than a day and no appreciable emissions occurred (Figure 2.1).

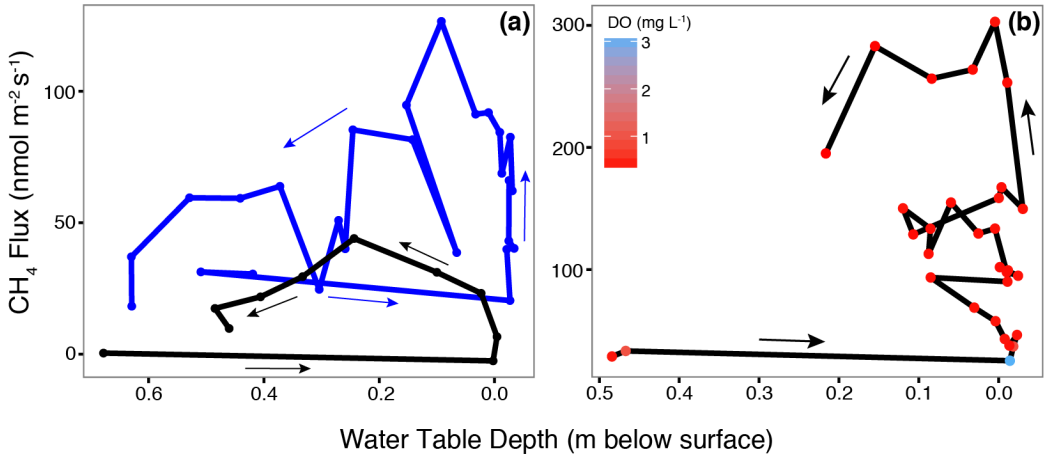

Figure 2.2 Daily CH_4 fluxes (nmol m^{-2} s^{-1}) across flooding events in 2013 (a; black line), 2014 (a; blue line), and 2015 (b). Events vary in length, year, and emission magnitude. The 2013 event was 9 days (May 10 – May 19, 2013), the 2014 event was 26 days (Sept. 18 – Oct. 14, 2014), and the 2015 event was 30 days (Aug. 25 – Sept. 24, 2015). In 2015, daily mean groundwater dissolved oxygen concentrations (DO; mg L^{-1}) are included as a point heat map. Arrows show directionality of each time series.

We observed a delay between ecosystem CH_4 fluxes and pasture flooding events, where peak emissions generally occurred during water table recession (Figure 2.2). This was particularly evident during May-June 2013 when multiple flooding events drove lagged surface fluxes (Figure 2.2a), and during September-October of 2013, 2014, and 2015 when late season flooding events drove similar lags (Figure 2.2a – 2014 only; Figure 2.2b - 2015 only). These dynamics were observed across year, flooding duration, and emission magnitude (Figure 2.2). Lags were less evident at the height of the wet season due to periods of sensor

dropout when the water table was near the surface for extended periods, however CH_4 emissions were sustained and lagged the decreasing water table in August of 2013 and 2014 (Figure 2.1). Correlations between CH_4 fluxes and water table depth were maximized at three to four-day lags. In 2013, correlations were maximized at a four-day lag (cross-correlation = 0.59), in 2014 at a three-day lag (cross-correlation = 0.56), and in 2015 at a three-day lag (cross-correlation = 0.59). These analyses suggest maximum CH_4 fluxes occur three to four days after peak flooding.

Pasture groundwater DO concentrations exhibited pulse dynamics that coincided with periods of pasture flooding and heavy precipitation (Figure 2.1). During precipitation recharge events that flooded pastures, DO concentrations in groundwater spiked to nearly 30 times background levels (range 0.29 – 8.08 mg L^{-1}). Following these DO pulses, groundwater DO rapidly reduced to background levels during water table recession (Figures 2.1). Connections between CH_4 flux lags and DO were most marked in August 2015 when groundwater DO rapidly increased with flooding (3.96 mg L^{-1}) and then returned to anoxic levels within one day (< 1.0 mg L^{-1}). Here, CH_4 emissions were minimized when DO was high and then rapidly increased when DO concentrations decreased (Figure 2.2b). After the initial flood event, subsequent flooding did not increase groundwater DO concentrations and CH_4 fluxes continued to increase (Figure 2.2b).

Dissolved oxygen dynamics were reproduced in the mesocosm experiment (Figure 2.3), and the overall range of DO concentrations in mesocosms were similar to those measured in the field (0.77-7.13 mg L^{-1} in mesocosm; 0.29 – 8.08 mg L^{-1} in field). Dissolved oxygen concentrations were elevated during water table recharge (days 1-6), rapidly de-oxygenated during the flooded phase (days 7-8), and remained reduced during recession (days

9-14; Figure 2.3). In the unsaturated soils, oxygen concentrations were 20.7% (range 19.9 - 21%) during water table recharge and 19.6% (range 18.5 – 20.4%) during recession. During recession, soil horizons above the water table adjustment height remained saturated, likely due to capillary action within the soil columns (Figure 2.3).

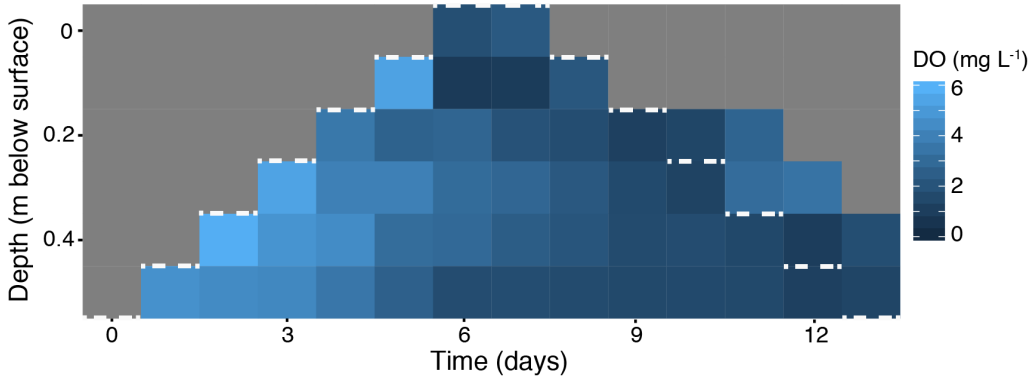

Figure 2.3 Pore water dissolved oxygen concentrations (DO; mg L^{-1}) throughout water table manipulations. Dissolved oxygen concentrations represent the mean from two replicate mesocosms. The dashed white line represents the location of the water table level outside of the column each day. Grey area represents the unsaturated zone within the soil profile.

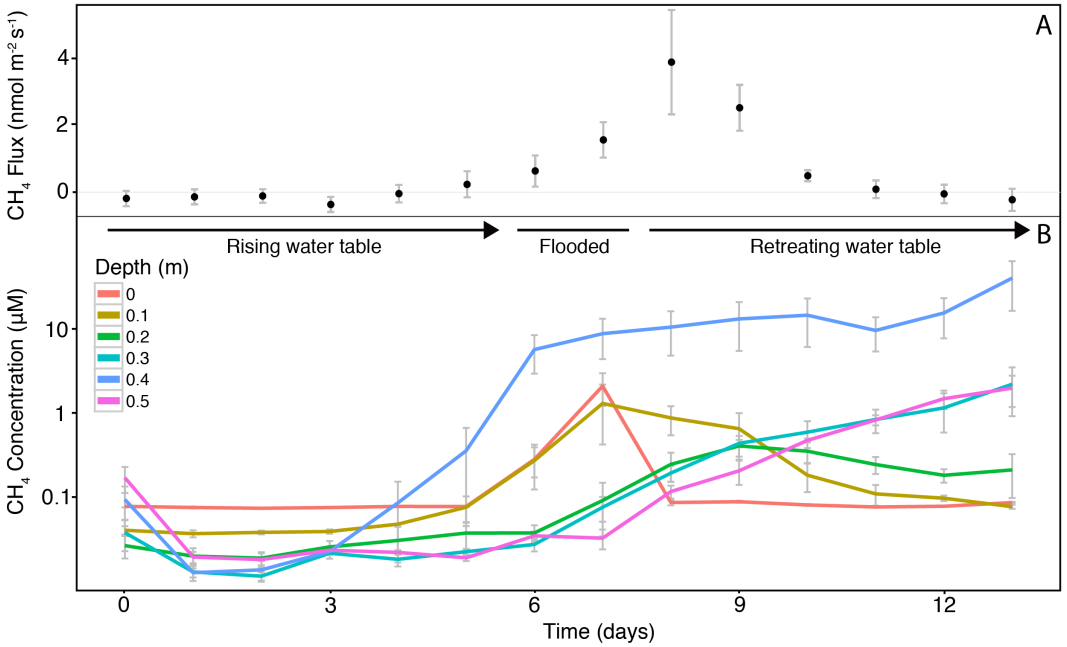

Figure 2.5 Surface fluxes (a; nmol CH_4 m^{-2} s^{-1} ± SE) and soil gas and pore water CH_4 concentrations (b; µM ± SE) throughout mesocosm water table manipulations. During the rising water table, water table depth was increased by 0.1 m per day until the soil surface was flooded, and water levels were reduced by the same interval during the retreating water table.

Lags were reproduced in the mesocosm experiment (Figure 2.4), however fluxes in mesocosms were lower than those observed in the field. This difference is likely due to lower levels of C substrate in laboratory water and the relatively short flooding duration (2 days in mesocosm treatments). In mesocosms, near-zero emissions were observed during the recharge phase, emissions began or increased when columns were flooded, and peaked then tapered back to zero during recession (Figure 2.4a). Emissions peaked when the water table was 0.05 m below surface during recession (one day after peak flooding), and fluxes did not return to zero until the water table was 0.35 m below surface, four days after peak flooding (Figure 2.4a). Our diffusive flux estimates generally follow these trends; diffusive fluxes were low during flooding (0.00-1.59 nmol CH_4 m^{-2} s^{-1} at 0-0.054 θ_D) and increased as soil gas-filled porosity increased during water table recession (0.26-2.12 nmol CH_4 m^{-2} s^{-1} at 0.014 – 0.067 θ_D). According to these calculations, diffusive surface fluxes should be high on the final day of the mesocosm treatment (8.60-131.86 nmol CH_4 m^{-2} s^{-1} at 0.020 – 0.155 θ_D), however we observed zero emissions when water tables were lowest and CH_4 concentrations at depth were highest (Figure 2.4). On the final day, we observed a strong CH_4 concentration gradient from 0.4 m to the surface, and $\delta^{13}C$-CH_4 values enriched toward the surface up to 0.2 m depth. $\delta^{13}C$-CH_4 values at 0.1 m were similar to ambient atmospheric values (Figure 2.5).

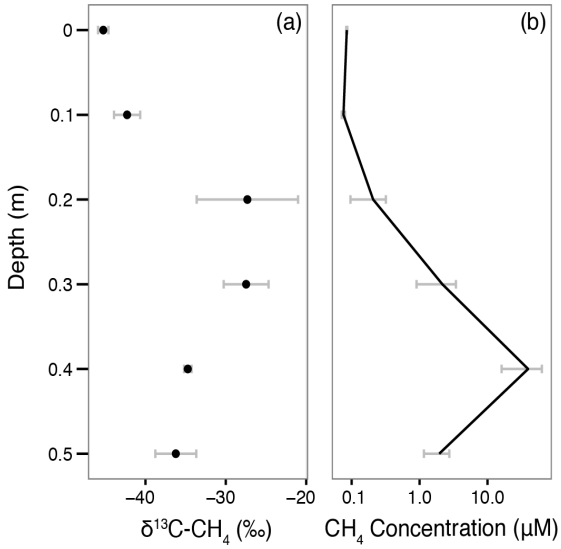

Figure 2.5 Mean $\delta^{13}C$-CH_4 (‰ ± SD; a) and concentration (μM ± SE; b) values throughout the soil profile when water table was 0.55 m below surface on the final day of mesocosm manipulations.

Distinct CH_4 dynamics were observed between surface organic (0 – 0.1 m) and deep mineral soils (Table 2.1; Figure 2.4b). Within the surface horizons, CH_4 concentrations increased above ambient at the point of surface flooding then peaked and tapered off over the course of the receding phase (0 and 0.1 m; Figure 2.4b). Within deep mineral horizons, CH_4 concentrations increased above ambient well after initial flooding and continued to rise until complete dry down (0.2 – 0.5 m depth; Figure 2.4b). The exception to this was the 0.4 m horizon where elevated concentrations were observed during the recharge phase when the water table was 0.25 m below surface and continued to rise throughout the experiment (Figure 2.4b). Methane dynamics in surface organic horizons followed emission patterns (Figure 2.4). Surface fluxes were correlated to CH_4 concentration changes in the 0.1 m horizon ($r^2 = 0.42$; $P < 0.0001$), and poorly correlated to concentration dynamics in all other horizons ($r^2 < 0.18$).

The largest increases in pore water CH_4 concentrations were observed in the 0.4 m horizon, where concentrations were an order of magnitude higher than those observed in any other horizon (Figure 2.4b). However, this pattern is likely a product of experimental design that caused deeper soils to be flooded for longer durations than surface soils (Figure 2.3). To isolate the effect of flooded time in the mesocosm experiment, we conducted anaerobic incubations to assess CH_4 production rates of each soil horizon. Anaerobic incubations showed that CH_4 production rates varied by depth (Kruskall-Wallis, $P = 0.02$; Figure 2.6). Methane production rates were highest in surface organic soils (0-0.05 m; 646.21 ± 507.18 nmol CH_4 g dry $soil^{-1}$ d^{-1}), intermediate in near-surface organic soils (0.05-0.15 m; 9.48 ± 6.27 nmol CH_4 g dry $soil^{-1}$ d^{-1}), and low in deep mineral soils (0.39 ± 0.15, 0.21 ± 0.10, and 1.02 ± 0.56 nmol CH_4 g dry $soil^{-1}$ d^{-1} for horizons 0.15-0.25, 0.25-0.35, and 0.45-0.55 m depth, respectively). Percent C and N data through the soil profile also follow these trends, with the

highest percent C and N levels in surface soils (Table 2.1; Kruskall-Wallis, $P < 0.05$). Percent C content ranged from 8.48 ± 0.92% in surface horizons to 0.09 ± 0.01% in deep horizons (Table 2.1).

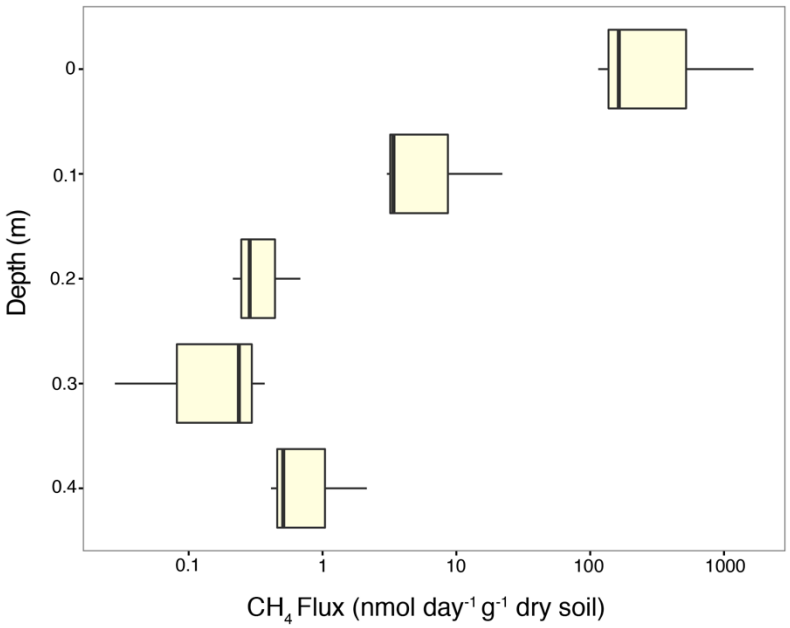

Figure 2.6 Methane production rates (nmol CH_4 g dry $soil^{-1}$ d^{-1}) by depth in subtropical pasture soils (n = 3 per depth). Solid lines are medians, boxes are interquartile ranges (IQR), and whiskers are ± IQR.

Pore water $\delta^{13}C$-CH_4 values also suggest distinct dynamics between surface and deep soil horizons. $\delta^{13}C$-CH_4 values of pore water varied through the depth profile (ANOVA, $P < 0.0001$), and were enriched in deep mineral soils relative to surface organic soils (Figure 2.7). In general, CH_4 isotope values in deep horizons (0.2-0.5 m) varied little during the flooding treatment, however $\delta^{13}C$-CH_4 in surface soils (0-0.1 m) exhibited higher levels of variability throughout the treatment. Pore water and incubation $\delta^{13}C$-CH_4 were similar in surface organic horizons (Figure 2.7). In deep horizons, $\delta^{13}C$-CH_4 in anaerobic incubations were somewhat deplete relative to CH_4 observed in pore water, although the range of measured isotope values overlapped in all deep soil horizons (Figure 2.7).

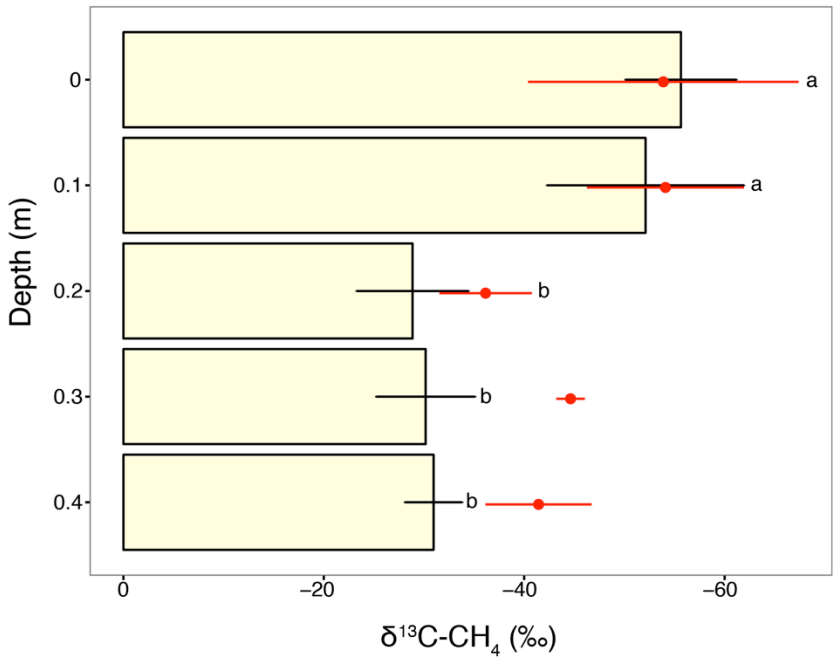

Figure 2.7 Mean $\delta^{13}C\text{-}CH_4$ (‰ ± SD) by depth of pore water samples in mesocosm treatments (bars) and anaerobic incubations (points, n = 3 per depth). Letters denote significant differences between pore water $\delta^{13}C\text{-}CH_4$ by depth in mesocosms (Tukey's HSD, $P < 0.05$).

DISCUSSION

In this study, transient precipitation recharge events exerted a major influence on CH_4 emissions from subtropical grassland pastures. Flooding of surface organic soils had the largest influence on emissions, and precipitation recharge DO dynamics appeared to delay the onset of emissions. Complete flooding for one day or more was necessary to sustain pasture CH_4 emissions suggesting that surface flooding duration controls the magnitude of emissions. The dynamics described here are potentially relevant to similar ecosystems globally because rainfall is a major driver of inundation in the tropics and subtropics (Prigent et al., 2007), and annual emission estimates from these pastures are similar to other flooded ecosystems in these climates (Chamberlain et al., 2015). Generalizability of CH_4 emission estimates are highly

desirable for the tropics and subtropics due to a poor representation of flooding and CH_4 dynamics for these regions in global models (Kirschke et al., 2013).

We consistently observed peak CH_4 emissions during periods of water table recession (Figure 2.2). These patterns are well described in temperate peatlands (Brown et al., 2014; Goodrich et al., 2015), and perhaps suggests common controls to CH_4 fluxes in the two ecosystems. Outgassing of CH_4 stored at depth and flooding of a belowground 'critical zone' of production have both been suggested as potential explanations for observed lags in temperate wetlands (Moore and Dalva, 1993; Moore and Roulet, 1993; Brown et al., 2014). Our basic diffusive flux modeling suggests that changes in surface soil porosity can induce some outgassing and increased surface emissions, but the gas-filled porosity of these soils remains low when the water table drops in the field (1.4 – 6.7% gas-filled space when VWC = 35.6-41% at WTD 0.1-0.15 m below surface). Based on the small changes we observe in gas-filled porosity during recession, it is unlikely that this factor alone drives emission lags. Additionally, our mesocosm results do not support the hypothesis that the outgassing of CH_4 stored at depth drives lags. Diffusive flux modeling suggests that we should observe the highest fluxes on the final day of the mesocosm experiment when gas-filled pore space (2-16%) and deep CH_4 concentrations are high, however we observe no surface emission on this day (Figure 2.4). Instead, it appears that oxidation in upper unsaturated soils may be consuming all deep-produced CH_4 before it reaches the land surface. This can be clearly seen on the final day of the experiment when there is a strong concentration gradient and $\delta^{13}C\text{-}CH_4$ enrichment toward the surface (Figure 2.5). It appears that most of this deep-produced CH_4 is consumed by 0.2 m depth, as $\delta^{13}C\text{-}CH_4$ values at 0.1 m are more similar to atmospheric values (Figure 2.5a). In agreement with temperate observations, our data suggests that flooding of a

near-surface organic 'critical zone' is needed for substantial emissions. However, in these subtropical pastures, groundwater DO dynamics appear to control when and if surface fluxes occur.

The influx of oxygenated groundwater to pasture soils likely modulated the onset of fluxes and may explain the observed lags. Here, the influx of oxygenated water may delay CH_4 production until groundwater DO is consumed (Figure 2.2b), and once favorable conditions are in place (i.e., when DO pools are depleted), emissions can be sustained if surface soil horizons remain deoxygenated (Figures 2.2b, 2.3 and 2.4). These effects are most clearly seen in the mesocosm study, where mostly sub-ambient CH_4 concentrations and near-zero emissions were observed during water table recharge with oxygenated groundwater, but emissions and elevated concentrations were observed during recession when groundwater was deoxygenated (Figures 2.3 and 2.4). In this example, DO presence likely dampens potential CH_4 production during water table recharge, though reduced rates of production can still occur in the presence of DO (Teh et al., 2005). Similar DO dynamics relative to emissions were observed over the course of a 2015 flooding event, though we did not observe additional DO influx during subsequent smaller recharge events (Figure 2.2b). This may result from our probe being unable to capture surface DO influx due to the depth of installation (0.95 m) or from the dilution of oxygenated rainwater into a larger volume of deoxygenated groundwater. Regardless, it appears that DO delays CH_4 emissions during initial groundwater recharge events, though it is unclear whether subsequent rain events dampen CH_4 emissions. Our results do demonstrate that methanogens within these soils respond rapidly to fluctuating redox conditions, in contrast to other wetland systems where CH_4 production lags anoxia from days to weeks (Cadillo-Quiroz et al., 2006).

Further research is warranted to better understand the response of microbial communities and CH_4 dynamics of transient DO influx and fluctuating redox conditions, as our work here is primarily observational. However, our work demonstrates that groundwater DO dynamics should be taken into account when assessing greenhouse gas emissions from landscapes experiencing precipitation recharge. Groundwater DO monitoring is uncommon, and these measurements are generally reported in hydrologic studies that do not account for greenhouse gas fluxes (Datry et al., 2004; Foulquier et al., 2010; Schilling and Jacobson, 2015). Studies of CH_4 fluxes in precipitation-recharged soils could benefit from additional measurements of groundwater DO. As demonstrated here, these measurements provide an additional mechanism influencing CH_4 emission patterns in ecosystems flooded by wet season rains.

Field and laboratory results both suggest that flooding of surface organic soils influences emission lags. Complete flooding was needed to stimulate emissions from pastures (Figure 2.1), and peak emissions occurred when the water table retreated through surface horizons (Figure 2.2). The largest emissions likely occur post-flooding because the water table retreats at a slower rate than it rises, and organic horizons are saturated for longer time periods during recession (Figure 2.1b). These observations are consistent with laboratory results, where CH_4 dynamics in surface soils exerted the strongest influence on emissions (Figure 2.4), and CH_4 production rates were orders of magnitude higher in surface soils than in mineral soils below 0.15 m depth (Figure 2.6). Emissions correlated to CH_4 concentration dynamics in surface soils, while CH_4 in deep mineral soils did not appear to influence emissions (Figure 2.4). This is particularly apparent on the final day of the mesocosm study, where CH_4 concentrations in deep horizons (0.3-0.5 m) were maximized but surface fluxes

were zero (Figure 2.4). It appears that most of this deep horizon CH_4 is consumed before reaching the surface (Figure 2.5), however, the orders of magnitude difference of CH_4 production rates between surface organic and deep mineral soil horizons suggests that CH_4 produced at depth is unlikely to be an important component of surface fluxes even if soils are flooded over longer periods (Figure 2.6).

Large differences in pore water $\delta^{13}C$-CH_4 values between surface (0-0.1 m) and deep horizons (0.2-0.4 m) further points to distinct CH_4 dynamics stratified through the soil profile. Pore water $\delta^{13}C$-CH_4 in surface soils were within the range of values expected for biogenic CH_4 production, however deep horizon values were heavier than expected and outside the accepted range of biogenic CH_4 (Figure 2.7; (Whiticar et al., 1986)). Enriched biogenic $\delta^{13}C$-CH_4 values are commonly observed when methanotrophs oxidize CH_4, however studies more commonly observe $\delta^{13}C$-CH_4 enrichment toward the land-surface, as methanotrophs are active in aerobic surface soils (Liptay et al., 1998; Conrad et al., 1999; Teh et al., 2006).

Four mechanisms may explain our observation of unexpectedly high pore water $\delta^{13}C$-CH_4 values at depth. First, methanotrophs may be active in deep horizons causing CH_4 oxidation and $\delta^{13}C$-CH_4 enrichment at depth. It is unlikely that aerobic oxidation is responsible for observed fractionation because anaerobic incubation $\delta^{13}C$-CH_4 values were similar to those observed in mesocosms (Figure 2.7), however anaerobic oxidation, which is known to be important in freshwater wetland environments is also a viable explanation for this observation (Segarra et al., 2015). We do see clear signs of aerobic oxidation on the final day of the mesocosm experiment when soil gas $\delta^{13}C$-CH_4 enriched in unsaturated horizons toward the surface (Figure 2.5a).

Second, diffusive fractionation can lead to an enrichment of $\delta^{13}C\text{-}CH_4$ values at depth as $^{12}CH_4$ diffuses through the soil profile more rapidly than $^{13}CH_4$ (De Visscher et al., 2004). This effect likely plays a role in our observations at depth, but $\delta^{13}C\text{-}CH_4$ values measured from our incubation jars were similarly enriched relative to surface soils (Figure 2.7). Incubation jars were well mixed and headspace was sampled, minimizing the effect of diffusive fractionation and ruling out diffusion as the sole driver of enrichment at depth within mesocosm pore water.

Third, substrate pool size may influence potential methanogenic fractionation if C substrates are limited in deep mineral horizons. Our results suggest that methanogenic substrates may be limiting in deep horizons, as the C content in these soils was at least 5 times lower than in organic horizons (Table 2.1), and CH_4 production rates were orders of magnitude lower than organic horizons (Figure 2.6). The impact of substrate pool limitation on potential fractionation is well described for photosynthetic uptake of CO_2 (Farquhar and Ehleringer, 1989), but further incubation studies would be needed to determine if pool effects are driving high $\delta^{13}C\text{-}CH_4$ observations in soil pore water.

Finally, distinct methanogenic communities may be stratified by depth within the soil profile. It is known that the two main functional types of methanogens (acetate fermenting vs. CO_2 reducing) fractionate CH_4 to varying degrees (Chanton et al., 2004), and methanogenic communities vary across environmental gradients. This community variation is often described through changes in the $\delta^{13}C$ of pore water CH_4 and methanogenic fractionation factors (Hodgkins et al., 2014; Holmes et al., 2014; McCalley et al., 2014). We observed clear differences in $\delta^{13}C\text{-}CH_4$ between surface and deep soils (Figure 2.7), which suggests that community composition may vary between organic and mineral soil horizons. In the nearby

Everglades, methanogen communities shift across nutrient gradients (Holmes et al., 2014), suggesting that similar mechanisms may be important at our site. Further research is needed to determine methanogen community compositions between soil horizons and disentangle these complex isotope effects.

Pasture CH_4 emissions were largely driven by transient flooding of surface organic soils with high CH_4 production rates. This suggests that changes in pasture flooding could cause large changes in net CH_4 emissions if surface organic soils remain saturated over longer time scales. These results are global significant because pastures are a major land use in subtropical and tropical regions worldwide. Pastures cover 31.4%, 22.7%, and 30.1% of total land area in Central America, tropical South America, and tropical Africa, respectively (Ramankutty et al., 2008), so our findings are likely generalizable to regions that experience wet season flooding. Regionally, pasture is the most common land use in the northern Everglades region and covers 35% of total land area (Hiscock et al., 2003). Our results are particularly relevant to the northern Everglades region where water retention practices are implemented to hold floodwater on pastures to reduce nutrient inputs into downstream Everglades ecosystems (Bohlen and Villapando, 2011). These practices are widely implemented across South Florida (Bohlen et al., 2009), and the potential impacts to greenhouse gas emissions have not been assessed. Further research is needed to assess potential emissions resulting from these practices, as our research documents high magnitude CH_4 emissions from these systems during periods of transient flooding.

ACKNOWLEDGEMENTS

We thank Hilary Swain, Julia Maki, and the rest of the staff at the MacArthur Agro-ecology Research Center for site access, lodging, transportation, and continued support in the field, and thank Suzanne Pierre for help excavating and transporting soil columns. We also thank Mark Conrad for input to analysis and experimental design. This research was supported by the Cornell University's Cross-scale Biogeochemistry and Climate Program, Atkinson Center for a Sustainable Future, Department of Ecology and Evolutionary Biology, Andrew W. Mellon Foundation, Cornell Sigma Xi, and University of Illinois USDA ARS.

REFERENCES

Baldocchi D, Detto M, Sonnentag O, Verfaillie J, Teh YA, Silver W, Kelly NM. 2012. The challenges of measuring methane fluxes and concentrations over a peatland pasture, Agr. Forest Meteorol., 153: 177–187.

Bohlen PJ, Villapando OR. 2011. Controlling runoff from subtropical pastures has differential effects on nitrogen and phosphorus loads, J. Environ. Qual., 40: 989–998,

Bohlen PJ, Lynch S, Shabman L, Clark M, Shukla S, Swain H. 2009. Paying for environmental services from agricultural lands: an example from the northern Everglades, Front. Ecol. Environ., 7: 46–55.

Bridgham SD, Cadillo-Quiroz H, Keller JK, Zhuang Q. 2013. Methane emissions from wetlands: biogeochemical, microbial, and modeling perspectives from local to global scales, Glob. Change Biol., 19: 1325–1346.

Brown MG, Humphreys ER, Moore TR, Roulet NT, Lafleur PM. 2014. Evidence for a nonmonotonic relationship between ecosystem-scale peatland methane emissions and water table depth, J. Geophys. Res., 119: 826-835.

Cadillo-Quiroz H, Brauer S, Yashiro E, Sun C, Yavitt J, Zinder S. 2006. Vertical profiles of methanogenesis and methanogens in two contrasting acidic peatlands in central New York State, USA, Environ. Microbiol., 1428-1440.

Chamberlain SD, Boughton EH, Sparks JP. 2015. Underlying ecosystem emissions exceed cattle-emitted methane from subtropical lowland pastures, Ecosystems, 8: 933–945.

Chanton J, Chaser L, Glasser P. 2004. Carbon and hydrogen isotopic effects in microbial methane from terrestrial environments, in Stable isotopes and biosphere-atmosphere interactions, pp. 85-105, Elsevier, Atlanta, GA.

Conrad ME, Templeton AS, Daley PF, Alvarez-Cohen L. 1999. Seasonally-induced fluctuations in microbial production and consumption of methane during bioremediation of aged subsurface refinery contamination, Environ. Sci. Technol., 33: 4061–4068,

Conrad R. 2007. Microbial Ecology of Methanogens and Methanotrophs, in Advances in agronomy, vol. 96, pp. 1–63, Elsevier, Atlanta, GA.

Datry T, Malard F, Gibert J. 2004. Dynamics of solutes and dissolved oxygen in shallow urban groundwater below a stormwater infiltration basin, Sci. Total Environ., 329: 215–229.

De Visscher A, De Pourcq I, Chanton J. 2004. Isotope fractionation effects by diffusion and methane oxidation in landfill cover soils. J. Geophys. Res. 109(D18111).

Dengel S, Levy PE, Grace J, Jones SK, Skiba UM. 2011. Methane emissions from sheep pasture, measured with an open-path eddy covariance system, Glob. Change Biol., 17: 3524–3533.

Farquhar GD, Ehleringer JR. 1989. Carbon isotope discrimination and photosynthesis, Ann. Rev. Plant. Physiol. Mol. Biol., 40: 503–537.

Foken T, Göockede M, Mauder M, Mahrt L, Amiro B, Munger W. 2005. Post-field data quality control, in Handbook of micrometeorology, edited by Lee X, Massman WJ, Law BE, pp. 181–208, Kulwer Academic Publishers, Dordrecht.

Foulquier A, Malard F, Mermillod-Blondin F, Datry T. 2010. Vertical change in dissolved organic carbon and oxygen at the water table region of an aquifer recharged with stormwater: biological uptake or mixing? Biogeochemistry, 99: 31-47.

Gathumbi SM, Bohlen PJ, Graetz DA. 2005. Nutrient enrichment of wetland vegetation and sediments in subtropical pastures, Soil Sci. Soc. Am. J., 69: 539–548.

Goodrich JP, Campbell DI, Roulet NT. 2015. Overriding control of methane flux temporal variability by water table dynamics in a Southern Hemisphere, raised bog, J. Geophys. Res.

Hall SJ, McDowell WH, Silver WL. 2013. When wet gets wetter: decoupling of moisture, redox biogeochemistry, and greenhouse gas fluxes in a humid tropical forest soil, Ecosystems, 16: 576-589.

Hiscock JG, Thourot CS, Zhang J. 2003. Phosphorus budget-land use relationships for the northern Lake Okeechobee watershed, Florida, Ecol. Eng., 21: 63-74.

Hodgkins SB, Tfaily MM, McCalley CK, Logan TA, Crill PM, Saleska SR, Rich VI, Chanton JP. 2014. Changes in peat chemistry associated with permafrost thaw increase greenhouse gas production, Proc. Natl. Acad. Sci. U.S.A., 111: 5819–5824.

Holmes ME, Chanton JP, Bae HS. 2014. Effect of nutrient enrichment on $\delta^{13}CH_4$ and the methane production pathway in the Florida Everglades, J. Geophys. Res., 119:1267-1280.

Jahangir MMR, Johnston P, Khalil MI, Grant J, Somers C, Richards KG. 2012. Evaluation of headspace equilibration methods for quantifying greenhouse gases in groundwater, J. Environ. Manage., 111: 208–212.

King GM, Roslev P, Skovgaard H. 1990. Distribution and rate of methane oxidation in sediments of the Florida Everglades, Applied and Environmental Microbiology, 56: 2902–2911.

Kirschke S, Bousquet P, Ciais P, Saunois M, Canadell JG, Dlugokencky EJ, Bergamaschi P, Bergmann D, Blake DR, Bruhwiler L. 2013. Three decades of global methane sources and sinks, Nature Geoscience, 6: 813–823.

Le Mer, J, Roger P. 2001. Production, oxidation, emission and consumption of methane by soils: a review, European Journal of Soil Biology, 37: 25–50.

Liptay K, Chanton J, Czepiel P, Mosher B. 1998. Use of stable isotopes to determine methane oxidation in landfill cover soils, J. Geophys. Res. Atmos., 103: 8243–8250.

McCalley CK et al. 2014. Methane dynamics regulated by microbial community response to permafrost thaw, Nature, 514: 478–481.

Melack JM, Hess LL, Gastil M, Forsberg BR, Hamilton SK, Lima IB, Novo EM. 2004. Regionalization of methane emissions in the Amazon Basin with microwave remote sensing, Glob. Change Biol., 10: 530–544.

Moncrieff JB, Massheder JM, De Bruin H, Elbers J, Friborg T, Heusinkveld B, Kabat P, Scott S, Søgaard H, Verhoef A. 1997. A system to measure surface fluxes of momentum, sensible heat, water vapour and carbon dioxide, J. Hydrol., 188: 589–611.

Moore TR, Dalva M. 1993. The influence of temperature and water table position on carbon dioxide and methane emissions from laboratory columns of peatland soils, J. Soil Sci., 44: 651–664.

Moore TR, Roulet NT. 1993. Methane flux: water table relations in northern wetlands, Geophys. Res. Lett., 20: 587–590.

Oremland RS, Culbertson CW. 1992. Importance of methane-oxidizing bacteria in the methane budget as revealed by the use of a specific inhibitor, Nature, 356: 421-423.

Prigent C, Papa F, Aires F, Rossow WB. 2007. Global inundation dynamics inferred from multiple satellite observations, 1993–2000, J. Geophys. Res., 112(D12).

R Core Team. 2015. R: A language and environment for statistical computing. R Foundation for Statistical Computing, Vienna, Austria. http://www.R-project.org/.

Ramankutty N, Evan AT, Monfreda C, Foley JA. 2008. Farming the planet: 1. Geographic distribution of global agricultural lands in the year 2000, Global Biogeochem. Cycles, 22(GB1003).

Riley WJ, Subin ZM, Lawrence DM, Swenson SC, Torn MS, Meng L, Mahowald NM, Hess P. 2011. Barriers to predicting changes in global terrestrial methane fluxes: analyses using CLM4Me, a methane biogeochemistry model integrated in CESM, Biogeosciences Discuss., 8: 1733–1807.

Roulet NT, Ash R, Quinton W, Moore T. 1993. Methane flux from drained northern peatlands: effect of a persistent water table lowering on flux, Global Biogeochem. Cycles, 7: 749–769.

Schilling KE, Jacobson PJ. 2014. Temporal variations in dissolved oxygen concentrations observed in a shallow floodplain aquifer, River Res. Appl.

Schilling KE, Jacobson PJ. 2015. Field observation of diurnal dissolved oxygen fluctuations in shallow groundwater, Ground Water, 53: 493–497.

Segarra KEA, Schubotz F, Samarkin V, Yoshinaga MY, Hinrichs KU, Joye SB. 2015. High rates of anaerobic methane oxidation in freshwater wetlands reduce potential atmospheric methane emissions, Nat. Commun., 6: 7477.

Striegl RG. 1993. Diffusional limits to the consumption of atmospheric methane by soils, Chemosphere, 26: 715-720.

Silver WL, Lugo AE, Keller M. 1999. Soil oxygen availability and biogeochemistry along rainfall and topographic gradients in upland wet tropical forest soils, Biogeochemistry, 44: 301-328.

Stocker TF et al. 2013. Technical Summary, in Climate Change 2013: The Physical Science Basis. Contribution of Working Group I to the Fifth Assessment Report of the Intergovernmental Panel on Climate Change, edited by Stocker TF, Qin D, Plattner GK, Tignor M, Allen SK, Boschung J, Nauels A, Xia Y, Bex V, Midgley PM, Cambridge University Press, New York, NY.

Teh YA, Silver WL, Conrad ME. 2005. Oxygen effects on methane production and oxidation in humid tropical forest soils, Glob. Change Biol. 11: 1283-1297.

Teh YA, Silver WL. 2006. Effects of soil structure destruction on methane production and carbon partitioning between methanogenic pathways in tropical rain forest soils, J. Geophys. Res.

Teh YA, Silver WL, Conrad ME, Borglin SE, Carlson CM. 2006. Carbon isotope fractionation by methane-oxidizing bacteria in tropical rain forest soils, J. Geophys. Res., 111(G2).

Vickers D, Mahrt L. 1997. Quality control and flux sampling problems for tower and aircraft data, J. Atmos. Ocean. Tech., 14: 512–526.

Webb EK, Pearman GI, Leuning R. 1980. Correction of flux measurements for density effects due to heat and water vapour transfer, Q. J. Roy. Meteor. Soc., 106: 85–100.

Whiticar MJ, Faber E, Schoell M. 1986. Biogenic methane formation in marine and freshwater environments: CO_2 reduction vs. acetate fermentation—isotope evidence, Geochim. Cosmochim. Ac., 693–709.

CHAPTER 3

THE IMPACT OF WATER MANAGEMENT PRACTICES ON METHANE EMISSIONS AND SUBTROPICAL PASTURE GREENHOUSE GAS BUDGETS

ABSTRACT

Pastures are an extensive land cover type, however patterns in pasture greenhouse gas (GHG) exchange vary widely depending on climate and land management. Understanding this variation is important, as pastures may be a net GHG source or sink depending on these factors. We quantified carbon dioxide (CO_2) and methane (CH_4) fluxes from subtropical pastures in south Florida for three years using eddy covariance, and estimated annual budgets of CO_2, CH_4, and GHG equivalent emissions. We also estimated the impact of water retention practices on pasture and regional GHG emissions. The pastures were net CO_2 sinks sequestering up to 163.01 ± 53.56 g CO_2-C m^{-2} yr^{-1}, but were also strong CH_4 sources emitting up to 23.36 ± 1.48 g CH_4-C m^{-2} yr^{-1}. Accounting for the increased global warming potential of CH_4, the pastures were strong GHG sources emitting up to 513.82 ± 73.10 g CO_2 eq. m^{-2} yr^{-1}, and all CO_2 uptake was offset by wet season CH_4 emissions from the flooded landscape. Our analysis suggests increased flooding from water management practices is a small component of the pasture GHG budget, and water retention likely contributes 2-11.5% of pasture GHG emissions. Water retention is likely responsible for 29.36 ± 18.74 Mg CH_4-C yr^{-1} of emissions within the Northern Everglades region, equivalent to 1-7% of annual CH_4 emissions from cattle in this county of Florida alone. Our results demonstrate that subtropical pastures are strong GHG sources when accounting for CH_4 emissions from cattle and the flooded landscape, and water retention practices aimed at reducing nutrient loading to the Everglades are likely only responsible for a minor increase in regional GHG emissions.

INTRODUCTION

Pastures cover ~22% of Earth's ice-free surface (Ramankutty et al., 2008), and play an important role in global carbon (C) exchange by removing ~0.2 Pg C from the atmosphere annually. Policies are implemented internationally to promote C sequestration and reduce greenhouse gas (GHG) emissions from pastures (Follett and Reed, 2010). However, pastures are developed on all inhabited continents across a diversity of biomes (Ramankutty et al., 2008), so their GHG budgets are likely variable across climate and soil types. Dominant controls of pasture GHG exchange include net ecosystem exchange (NEE) of carbon dioxide (CO_2) by grasslands and methane (CH_4) emissions from grazing livestock.

The proliferation of eddy covariance towers over the past decade has given us a better understanding of how GHG exchange varies across ecosystem and climate types (Baldocchi, 2008). Pasture NEE and CH_4 fluxes vary widely depending on climate and the ecosystems upon which they are developed. For example, pastures developed on drained peatlands are major sources of CO_2 as highly organic soils oxidize when exposed to the atmosphere (Hatala et al., 2012; Knox et al., 2015; Nieveen et al., 2005; Teh et al., 2011), whereas upland pastures tend to be net sinks of CO_2 (Dengel et al., 2011; Mudge et al., 2011; Soussana et al., 2007). Methane emissions from grazing livestock often offset grassland GHG sinks (Allard et al., 2007; Dengel et al., 2011; Soussana et al., 2007), as CH_4 has a global warming potential 25 times greater than CO_2 over a 100-year time horizon (Forster et al., 2007). Methane and nitrous oxide (N_2O, another potent GHG) emissions from the underlying landscape are particularly important in regions that experience flooding (Chamberlain et al., 2015; Teh et al., 2011), as is common throughout the tropics and subtropics. Due to the variety of factors

influencing pasture GHG exchange, there is great uncertainty about the GHG forcing associated with pastures and how this forcing varies with climate and management.

Land management is known to impact ecosystem GHG fluxes, however these interactions can be complex and have received little research attention (Baldocchi, 2014). For instance, increased grazing pressure and fertilization increase CH_4 and N_2O emissions, respectively, and can reduce pasture GHG sinks up to 89% (Allard et al., 2007). The restoration of peatland pastures to wetlands changes these systems from strong GHG sources to sinks due to the balance between CO_2 and CH_4 fluxes (Knox et al., 2015). Water management practices may exert a particularly large influence on CH_4 emissions, as soil microbes produce CH_4 under flooded or anoxic conditions (Conrad, 2007). Water is often heavily managed in wet regions, such as south Florida where this study was conducted, yet the influence of water management practices on GHG fluxes is rarely evaluated. Runoff from cattle pastures is a major source of nutrient loading to the Everglades, an important wetland complex in this region, and water retention and storage programs have been implemented to reduce nutrient runoff by reducing pasture drainage. While these programs effectively reduce nutrient loads to downstream ecosystems (Bohlen and Villapando, 2011; Bohlen et al., 2009), their impact on pasture GHG emissions is unknown. Understanding the influence of water retention practices on pasture GHG emissions is important given the high CH_4 production and emission rates observed from south Florida pasture soils (Chamberlain et al., 2016).

The objectives of this study were to 1) quantify the environmental controls of pasture NEE and CH_4 fluxes across multiple years, 2) estimate annual pasture NEE, CH_4, and GHG budgets, and 3) estimate the impact of water retention practices on pasture GHG budgets. We measured ecosystem-scale CO_2 and CH_4 fluxes for three years using eddy covariance, and

used these data to estimate annual budgets and determine environmental controls of fluxes. Annual N_2O emissions were also calculated using IPCC Tier 2 guidelines for manure deposition on pastures (IPCC, 2006). We then explored the influence of water retention on pasture GHG budgets by combining water table data from pasture water retention treatments with CH_4 flux data from our eddy covariance tower. This work advances out understanding of pasture GHG emissions and helps to develop a context for evaluating trade-offs between water quality and climate regulating ecosystem services from a globally dominant land use.

METHODS

Study Site

We measured CO_2 and CH_4 fluxes from a fenced pasture (92.1 ha; N 27.1632004, W 81.187302) that was rotationally grazed throughout the measurement period at a capacity of ~1.4 cows ha^{-1}. The pasture is located within a 4290 ha commercial cattle ranch, the MacArthur Agro-ecology Research Center (MAERC), which operates as a division of Archbold Biological Station. The pastures are planted with an introduced forage grass, *Paspalum notatum,* and have not received herbicide or fertilizer since 2006 and 2007, respectively. Roughly 30 hectares of the pasture was intentionally burned in January 2013. The region experiences heavy rainfall and flooding during the summer wet season, and pastures are drained through a network of ditches and canals throughout the landscape. The study pasture is 74.2% *Paspalum notatum* pasture, 10.9% depressional wetland, 9.2% *Sabal palmetto* hammock, 4.0% drainage ditch, and 1.7% drainage canal by area (Chamberlain et al., 2015).

Eddy Covariance Measurements

We measured ecosystem-scale fluxes of CO_2, CH_4, H_2O, and sensible heat using an eddy covariance tower installed within the center of the pasture described above from May 2013 to November 2015. At a height of 2.6 m and a 10 Hz interval, we measured three-dimensional wind speed and direction with a sonic anemometer (CSAT3, Campbell Scientific Inc., Logan, UT, USA) and CO_2, H_2O, and CH_4 concentrations with open-path infrared gas analyzers (LI-7500A and LI-7700, Licor Inc., Lincoln, NE, USA). All instruments interfaced with a datalogger (LI-7550, Licor Inc., Lincoln, NE, USA) and data were transmitted by modem for processing. We also made ancillary atmospheric and hydrologic measurements at 30 min averaging intervals and logged these data to an additional logger (CR3000, Campbell Scientific Inc., Logan, UT, USA) time synchronized to the eddy covariance logger. Ancillary measures at the tower site included air temperature and relative humidity (HMP115, Viasala, Helsinki, Finland), incoming radiation with a net radiometer (NR Lite2, Kipp & Zonen Inc., Bohemia, NY, USA), water table depth with a pressure transducer (CS451, Campbell Scientific Inc., Logan, UT, USA), and volumetric water content at 5, 10, and 20 cm depths with water content reflectometers (CS616, Campbell Scientific Inc., Logan, UT, USA). Rainfall was also measured at 30 min intervals with a tipping bucket gauge (TB4, Hydrologic Services America, Lake Worth, FL, USA) located 1.7 km southwest of the tower (N 27.150475, W 81.198568).

Fluxes were calculated from the covariance of vertical wind speed and scalars ($[CO_2]$, $[CH_4]$, $[H_2O]$, heat) over 30 min intervals. Raw data were screened for spikes, drop-outs, amplitude resolution, absolute limits, skewness, and kurtosis as described in Vickers and Mahrt (1997) and designated default in commercial software (EddyPro 4.2, Licor Inc.,

Lincoln, NE, USA). We aligned the anemometer with mean wind streamlines using double-rotation corrections, used block averaging to calculate mean wind speeds and concentrations over the 30 min interval, and corrected for time lags between wind and gas concentration measurements by covariance maximization. We corrected for air density fluctuations using the Webb-Pearl-Leuning correction (Webb et al., 1980) and applied analytic spectral corrections according to Moncrieff et al. (1997). Quality of fluxes were then flagged according to Foken et al. (2005), where quality flags range from 1 (best) to 9 (worst) depending on atmospheric turbulence, flux stationarity, and flow distortions by the tower structure. All of the above processing and corrections were conducted using commercial software (EddyPro 4.2, Licor Inc., Lincoln, NE, USA). Processed fluxes were rejected when atmospheric conditions were poor (quality flags > 4 for CO_2; quality flags > 6 for CH_4), and additional CH_4 fluxes were rejected when the CH_4 sensor path was blocked, CH_4 concentrations were below 1.74 ppm or above 5.00 ppm, and when fluxes were above 1500 nmol m^{-2} s^{-1} or below -500 nmol m^{-2} s^{-1} (Baldocchi et al., 2012; Dengel et al., 2011). We relaxed the quality flag criteria for CH_4 to reduce the number of CH_4 fluxes removed, and to include periods when cattle grazed the footprint, which may induce non-stationary CH_4 fluxes over half-hourly intervals. Overall, 42% of all CH_4 fluxes and 36% of all CO_2 fluxes were removed from analysis. In this study, negative fluxes represent ecosystem uptake and positive fluxes represent ecosystem emissions. The daytime 90% tower footprint was 290 m across the entire measurement period. This area is largely grassland pasture with intersecting drainage ditches, and two depressional wetlands are located at the outer reaches of the flux footprint (Chamberlain et al., 2015).

Gap Filling, NEE Partitioning, and Annual Budgets

We filled gaps in the NEE half-hourly time series using the Marginal Distribution Sampling method described in Reichstein et al. (2005). Here, NEE fluxes are grouped according to incoming radiation, air temperature, and vapor pressure deficit conditions and mean values are used to fill missing data during similar conditions. When meteorological data are not available, NEE fluxes are filled based on measured fluxes occurring at similar times of day. The filled NEE time series was partitioned into gross ecosystem productivity (GEP) and ecosystem respiration (R_{eco}) using the method described in Reichstein et al. (2005). Here, the relationship between T_{air} and nighttime NEE (when GEP is zero) is described using the Lloyd and Taylor (1994) model, and this relationship is then used to estimate R_{eco} in all periods using the modelled temperature relationship. GEP is then estimated as the difference between NEE and R_{eco}. A complete description of both methods can be found in Reichstein et al. (2005). All NEE gap filling and partitioning was conducted in R 3.2.0 using the 'REddyProc' package (R Core Team, 2015).

We filled gaps in the CH_4 times series by linear interpolation for gaps of up to 2.5 hours and longer gaps were filled using the Mean Diurnal Variation method (Dengel et al., 2011), where gaps are filled based on mean fluxes observed in the same half-hour period on adjacent days. We sampled adjacent half-hourly periods using a moving window of seven days and calculated error estimates for gap-filled values based on the standard deviation of measured fluxes used in the moving window average. Separate moving window averages were used for periods with and without cattle present in the pasture.

Annual NEE, CH_4, and GHG budgets were calculated by integrating daily sums from the gap-filled time series over two annual cycles (April 1, 2013 to March 31, 2014; April 1,

2014 to March 31, 2015). Both annual cycles begin at the onset of the pastures growing/wet season. We calculated the GHG budget by adding daily NEE and CH_4 budgets in terms of CO_2 equivalent emissions, where 1 g CH_4 is equivalent to 25 g CO_2 in the atmosphere based on the CH_4 global warming potential over the 100-yr time horizon (Forster et al., 2007). The GHG budgets presented here include measured fluxes only (NEE + CH_4). Uncertainty in annual NEE and CH_4 budgets were integrated from half-hourly flux random errors and gap-filled estimate errors. Uncertainty in the GHG budget was estimated from the additive variance of the NEE and CH_4 budgets. All relationships between fluxes and environmental variables were described using regression analyses, and CH_4 fluxes were log-transformed to meet assumptions of normality. All regressions between half-hourly fluxes and environmental variables were conducted using non-gap-filled half-hourly data (quality flag 3 or less).

We estimated annual manure N_2O budgets using IPCC Tier 2 guidelines and daily stocking data for the pasture at MAERC containing the eddy covariance tower. Daily N_2O emissions from deposited manure were calculated using the following equation (IPCC, 2006):

$$N_2O_m = N \cdot \frac{Nex}{365} \cdot EF_{N2O}$$

where N_2O_m is the total amount of N_2O produced from manure on the pasture (kg N_2O-N d^{-1}), EF_{N2O} is the N_2O emission factor for 'pasture range and paddock' deposited manure [0.02 (0.005-0.03) kg N_2O-N per kg N excreted], Nex is the N excretion rate per non-dairy North American cattle (70 kg N cow^{-1} yr^{-1}), and N is the daily cattle population within the fenced pasture. EF_{N2O} and N_{ex} values are from the IPCC (2006). Total N_2O emissions from manure were then converted to comparable units (g N_2O-N m^{-2} yr^{-1}) by dividing annual emissions by

the total pasture area (92.1 ha). We did not calculate fertilizer N_2O emissions because fertilizer has not been applied to these pastures since 2007.

Water Retention Analysis

To assess the influence of water retention on CH_4 fluxes, we analyzed existing water table data from eight side-by-side experimental pastures broken into two treatments. Within these pastures, water flow was reduced on one block of four pastures (water control treatment) and water flow was left unobstructed on the other block of four pastures (control). These data were initially published in Bohlen and Villapando (2011), and were used to track the efficacy of water control structures for increasing pasture water and nutrient retention. Raw water table data from these pastures were provided by MAERC. In this study, water table depth was measured at 20-min intervals for four years from all eight pastures (January 2005 to January 2009). These experimental pastures are also part of MAERC and are located 1.5 km southeast (N 27.144434, W 81.177001) of the eddy covariance tower location. The experimental pastures and the separate pasture containing the eddy covariance tower are all planted with *Paspalum notatum*, established on fine sand spodosol soils, drained by ditch networks, and rotationally grazed by cattle (Bohlen and Villapando, 2011).

We estimated the influence of water retention practices on net CH_4 emission and annual GHG budgets by 1) estimating the influence of water retention practices on surface soil flooding, and then 2) estimating the influence of extended surface soil flooding on CH_4 emissions. We first estimated the influence of water retention on soil flooding by calculating daily mean water table depths in retention and non-retention pastures (2005-2009), and then calculating the difference in flooding duration of the surface organic horizon (0-15 cm below

surface) between treatments. We were interested in how long this soil horizon is flooded because, in this region, flooding of the top 15 cm of soil controls ecosystem CH_4 emissions (Chamberlain et al., 2016). We then estimated increases in CH_4 emission by multiplying the yearly difference in surface flooding duration by the mean CH_4 emission rate when the water table was within the 0 – 15 cm surface horizon, as estimated from our eddy covariance data and accounting for CH_4 flux uncertainty. We estimated the regional impact of water retention on CH_4 emissions by extrapolating these finding across the areal extent of water retention pastures in the Northern Everglades region presented in Bohlen et al. (2009). All data processing, analysis, and visualization was conducted in R 3.2.0 using the 'dplyr', 'ggplot2', and 'zoo' packages (R Core Team, 2015).

RESULTS

Climate and Weather

Pasture meteorological and hydrological conditions were characteristic of the humid subtropics, where temperature (°C), incoming radiation (MJ m^{-2} d^{-1}), precipitation (mm d^{-1}), and water table depth (m below surface) all displayed strong seasonality (Figure 3.1). Air temperature was highest in summer (May through September) and decreased in winter (October through April). In general, daily air temperature was more variable during the winter, occasionally dropping below 0 °C during January and February both years (Figure 3.1a). Daily incoming radiation also peaked in summer, but was highly variable on a day-to-day basis due to changing cloud cover (Figure 3.1b). The frequency and intensity of rainfall events increased during summer months, with the most rainfall occurring between May and September each year. The summers of 2013 and 2014 exhibited clearly defined wet seasons

where most rainfall events occurred during the summer and were separated by an extended dry period (Figure 3.1c). Large rainfall events were more dispersed throughout 2015 causing a less clear delineation between dry and wet seasons (Figure 3.1c). The frequency and duration of summer rain events had a clear influence on pasture water table dynamics. In both the 2013 and 2014 wet seasons, extended periods of surface flooding occurred during heavy rainfall periods and both seasons were separated by a period of pasture dry down (Figure 3.1d). In contrast, in 2015, independent rain events drove many water table recharge events throughout the year but did not cause extended flooding until September 2015 when rainfall frequency increased (Figure 3.1d).

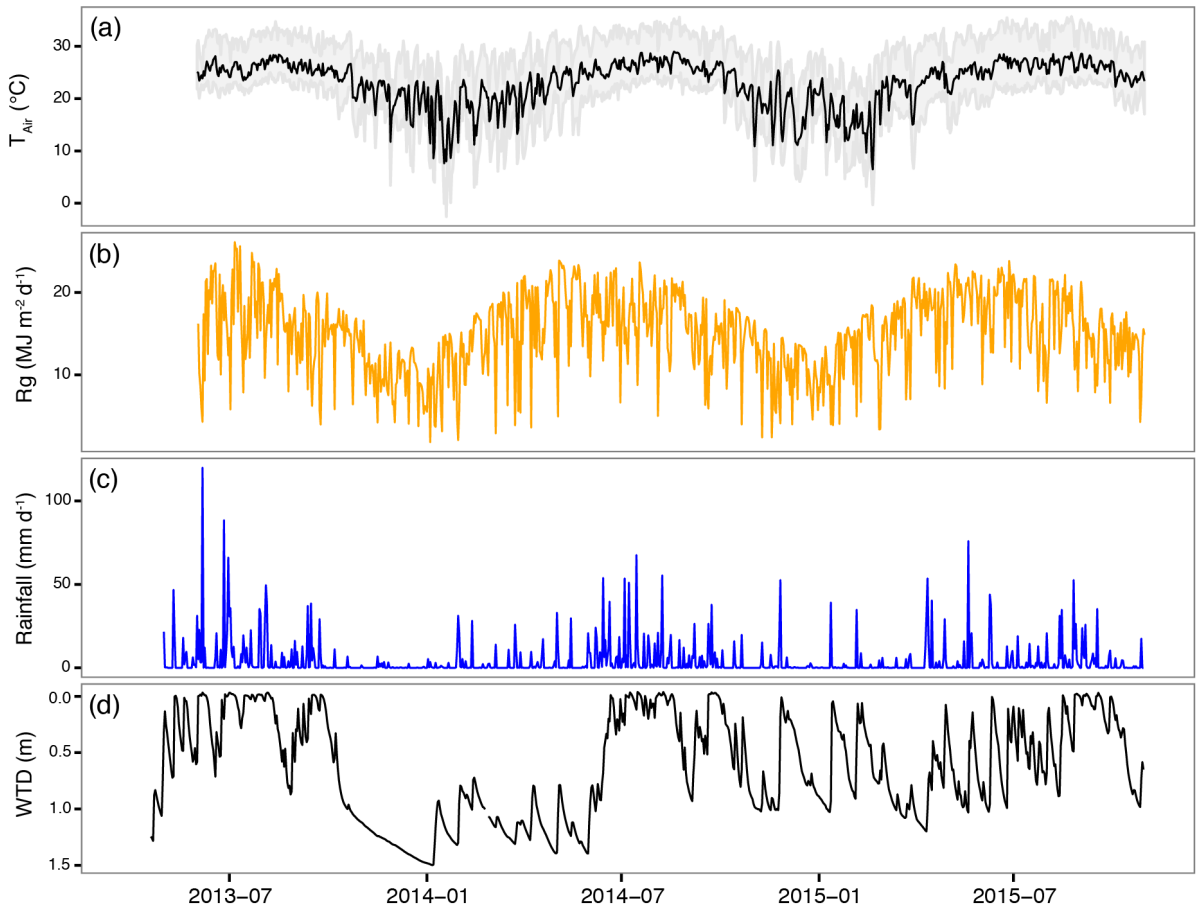

Figure 3.1 Pasture daily mean air temperature (T_{air}; a), incoming radiation (Rg; b), rainfall (c), and water table depth (d). Shaded area on (a) bounds daily minimum and maximum air temperature.

Seasonal Cycles of CH_4, NEE, Partitioned Fluxes (GEP, R_{eco}), and Annual Budgets

Pasture CH_4 emissions were driven primarily by landscape flooding as described in detail in Chamberlain et al. (2015; 2016). Ecosystem CH_4 emissions peaked in the wet season during periods of extended pasture flooding, and appreciable emissions were not observed when the water table reached the surface for one day or less (Figure 3.2a). We observed a weak correlation between GEP and CH_4 fluxes at the daily time scale when the water table was within 5 cm of the land surface ($r^2 = 0.15$, $P = 0.0014$), however these relationships were not observed when pasture water table was lower than 5 cm depth or in the half-hourly time

series. Across both years, the pastures were sources of CH_4, emitting 23.36 ± 1.48 g CH_4-C m^{-2} yr^{-1} in 2013 and 23.54 ± 2.11 g CH_4-C m^{-2} yr^{-1} in 2014 (Table 3.1).

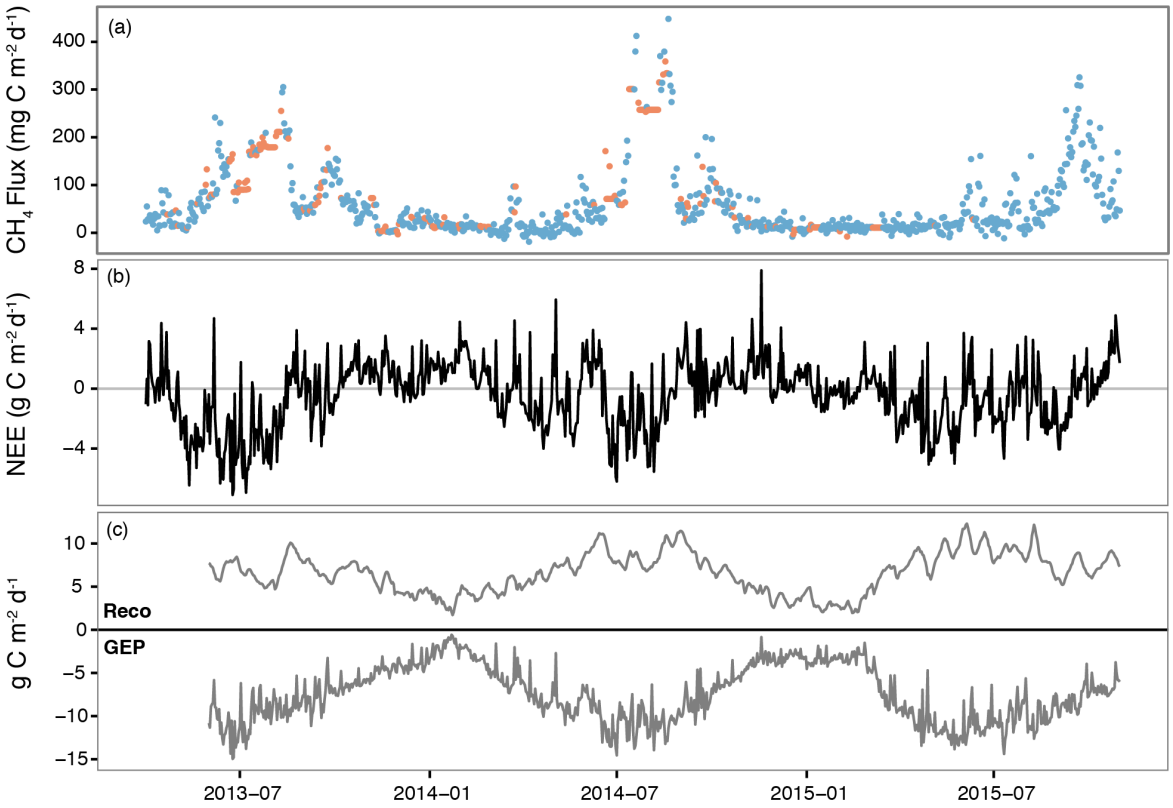

Figure 3.2 Daily pasture CH_4 fluxes (a), net ecosystem exchange (NEE; b), and partitioned NEE fluxes (c). In (c) NEE is partitioned into ecosystem respiration (R_{eco}) and gross ecosystem productivity (GEP). Red dots in (a) represent days when more than 66% of the half-hourly fluxes were gap-filled.

Net ecosystem exchange followed similar seasonal cycles, where daily net C uptake was observed during the wet season and net C loss was observed during the dry season (Figure 3.2b). Daily C uptake was highly variable, and many periods of C loss were observed during the growing season, often adjacent to periods of C uptake (Figure 3.2b). Much of this daily variability was driven by variability in pasture GEP, which exhibited high variability compared to R_{eco} (Figure 3.2c). Variability in GEP was likely driven by the variability in

pasture incoming radiation, as we observed a strong correlation between daily GEP estimates and incoming radiation ($r^2 = 0.47$, $P < 0.0001$). Our observations of daily C uptake correlate well to incoming radiation ($r^2 = 0.41$, $P < 0.0001$; Figure 3.3), and do not correlate well to daily temperature ($r^2 = 0.07$, $P < 0.0001$), suggesting that light availability controlled pasture C uptake independent of season. Pastures were a CO_2 sink, sequestering 163.01 ± 53.56 g CO_2-C m^{-2} yr^{-1} in 2013 and 74.65 ± 50.66 g CO_2-C m^{-2} yr^{-1} in 2014 (Table 3.1). The reduced CO_2 sink strength in 2014 was likely driven by an extended period of C loss in June 2014 when GEP decreased and R_{eco} increased (Figure 3.2c). This event occurred during a particularly dry early summer when the water table was not recharged until late June 2014 (Figure 3.1), at which point C uptake resumed (Figure 3.2b).

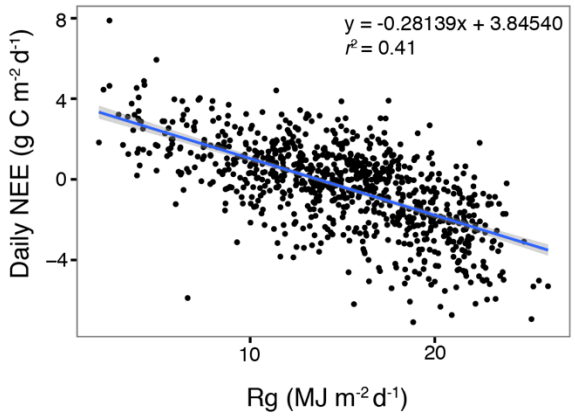

Figure 3.3 Relationship between daily NEE and incoming radiation (Rg) across the entire measurement period. Line and shaded area reflects linear relationship between variables and 95% confidence interval of fit.

When we express pasture CH_4 emissions in terms of CO_2 equivalents, the pastures become a strong GHG gas source (Figure 3.4). After accounting for the global warming potential of CH_4, the pastures produced 420.94 ± 65.06 g CO_2 eq. m^{-2} yr^{-1} in 2013 and 513.82

± 73.10 g CO_2 eq. m^{-2} yr^{-1} in 2014 (Table 3.1). Here, the differences in annual GHG budgets were due to differences in annual NEE, as the pastures produced similar amounts of CH_4 each year (Table 3.1; Figure 3.4). In both years, the pastures were initial GHG sinks until CH_4 emissions began at the onset of the wet season, and once CH_4 emissions began, the pastures remained strong GHG sources for rest of the year (Figure 3.4). Pastures were sources of N_2O in both years, producing 0.17 (0.04-0.26) g N_2O-N m^{-2} yr^{-1} in 2013, and 0.15 (0.04-0.23) g N_2O-N m^{-2} yr^{-1} in 2014. These manure-based emissions correspond to 51.93 (12.98-77.89) g CO_2 eq. m^{-2} yr^{-1} in 2013, and 44.87 (11.22-67.30) g CO_2 eq. m^{-2} yr^{-1} in 2014, where 1 g N_2O is equivalent to 298 g CO_2 in the atmosphere based on the N_2O global warming potential over the 100-yr time horizon (Forster et al., 2007).

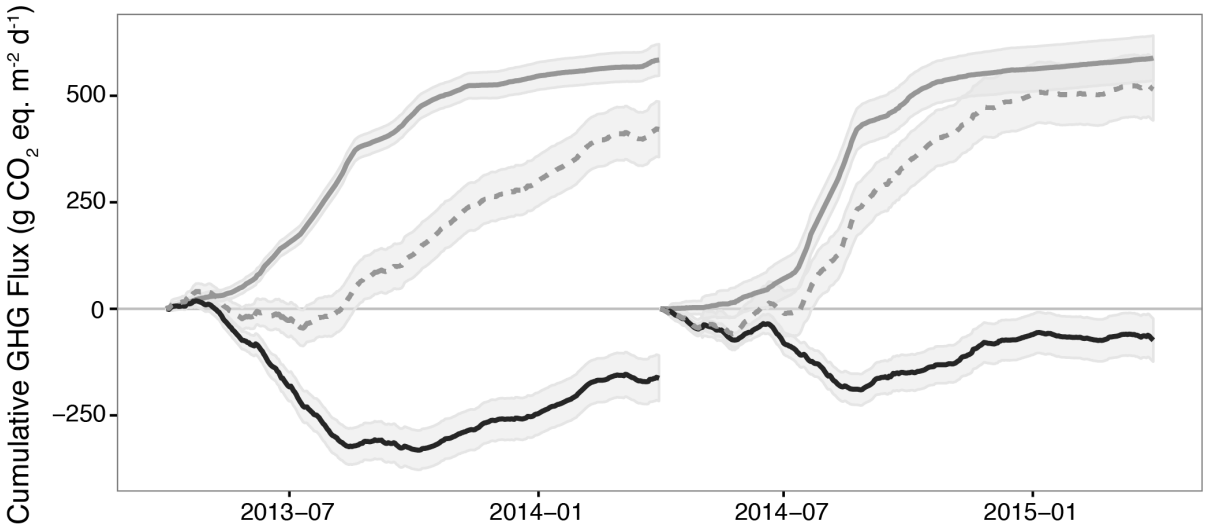

Figure 3.4 Cumulative NEE (black line), CH_4 flux (gray line), and CO_2 equivalent emissions (dotted line; NEE + CH_4). Gray shaded areas surrounding each line represents the 95% confidence interval of cumulative flux and gap-filled value uncertainty.

Water Retention Impacts

On average, water retention structures caused the water table to remain within the surface soil horizon (0 - 15 cm) for an additional 10.75 days per year. There was great variability in this increase in retention; in one pasture the surface soil horizon was flooded for an additional 31 days per year compared to control pastures, and on the other extreme, the surface soil horizon was flooded for 2 days less than control pastures. A more detailed description of flooding dynamics in these experimental pastures can be found in Bohlen and Villapando (2011). We estimated the average and maximum influence of water retention on pasture CH_4 emissions using both the average (10.75 d yr^{-1}) and maximum (31 d yr^{-1}) flooding increases caused by water retention structures.

From 2013 to 2015, eddy covariance-measured CH_4 fluxes were 109.82 ± 70.10 mg CH_4 m^{-2} d^{-1} (median ± IQR; n = 119 days) when the water table was within the surface soil horizon (0 – 15 cm) and 21.50 ± 21.12 mg CH_4 m^{-2} d^{-1}; n = 615 days when the water table was not within this horizon (Mann-Whitney; $P < 0.0001$). There was no difference in ecosystem CH_4 fluxes when the water table was within 5 cm of surface (131.25 ± 60.61 mg CH_4 m^{-2} d^{-1}; n = 69 days) compared to the entire 0 – 15 cm soil horizon (Mann-Whitney; $P = 0.30$).

If we assume that water retention within the tower footprint creates 10.75 days of additional surface soil (0-15 cm) flooding per year (water retention structures are currently installed within the pasture), this effect accounts for 1.18 ± 0.75 g CH_4-C m^{-2} yr^{-1} of net CH_4 emissions. This is attributable to 7.0 ± 4.5% and 5.7 ± 3.7% of the total pasture GHG budget in 2013 and 2014, respectively (Table 3.1). All water retention pastures within the Florida Ranchlands Environmental Services Project (FRESP) cover 2487 ha of land (Bohlen et al., 2009). Regionally, water retention could be responsible for 29.36 ± 18.74 Mg CH_4-C yr^{-1}

assuming retention increases flooding by 10.75 d yr^{-1} across all FRESP retention pastures. Emissions could be as high as 84.67 ± 54.04 Mg CH_4-C yr^{-1} if retention increases surface flooding by 31 d yr^{-1}, as we observed in one experimental pasture.

Table 3.1 Pasture NEE, CH_4, and GHG equivalent emissions (NEE + CH_4) for two years. Water retention impact is estimated potential CH_4 emissions due to increased water table via retention practices. Measured fluxes only are included in GHG budget (N_2O estimates omitted).

Year	**NEE** (g CO_2-C m^{-2} yr^{-1})	**CH_4** (g CH_4-C m^{-2} yr^{-1})	**GHG** (g CO_2 eq. m^{-2} yr^{-1})	**Water retention** (% of GHG budget)
2013-2014	-163.01 ± 53.56	23.36 ± 1.48	420.94 ± 65.06	7.0 ± 4.5%
2014-2015	-74.65 ± 50.66	23.54 ± 2.11	513.82 ± 73.10	5.7 ± 3.7%

DISCUSSION

Our results demonstrate that subtropical Florida pastures, despite being net sinks of CO_2, are strong GHG sources when accounting for CH_4 emissions (Figure 3.4). Methane emissions offset CO_2 uptake almost immediately, as the peak seasons of CH_4 emission and CO_2 uptake coincide during the wet season (Figure 3.2). Further, our analyses show that water retention interventions to improve water quality do not have a large impact on pasture GHG emissions. Increases in water retention associated with these interventions account for 2-11.5% of annual pasture GHG emissions. Total GHG emissions appear to be relatively insensitive to water retention practices because the increases caused by the practices are small compared to natural landscape and cattle CH_4 emissions. The water retention structures used in these treatments are the same used in regional water management projects, so the responses observed in these pastures is likely representative of the region (Bohlen and Villapando, 2011).

Our analysis also showed that N_2O emissions associated with manure deposition are also modest relative to CH_4 emissions. Accounting for manure N_2O fluxes increased pasture

GHG emissions by 12.3% (3.1-18.5%) in 2013, and 8.7% (2.2-13.1%) in 2014. These increases are similar in magnitude to the contribution of water retention to GHG budgets (Table 3.1), suggesting that the GHG burden of water retention is similar to N_2O emissions from grazing cattle manure. Direct studies of N_2O emissions from these pastures are warranted, particularly since our IPCC-based estimates do not account for N_2O fluxes from flooded land. It may also be important to account for fertilizer-based N_2O emissions in some cases, but these pastures have not received fertilizer applications since 2007. In general, it appears that N_2O emissions may impact pasture GHG budgets, but their influence is likely small compared to the contribution of CH_4 emissions.

Assuming the average flooding effect of water control structures (10.75 d yr^{-1}), water retention practices could increase regional emissions by 29.36 ± 18.74 Mg CH_4-C yr^{-1}, and the maximum flooding effect (31 d yr^{-1}) could increase emissions by 84.67 ± 54.04 Mg CH_4-C yr^{-1}.To put these values in perspective, the average cow in the region emits 58.9 kg CH_4-C yr^{-1} (Chamberlain et al., 2015). Water retention practices are therefore equivalent to ranging an additional 180–817 cattle (average scenario), up to 520–2355 cattle (maximum scenario), in the Northern Everglades region. The MacArthur Agro-ecology Research Center, where this study took place, grazes ~3000 cattle at any given time (MacArthur Agro-ecology Research Center, 2015), and Highlands county alone, where MAERC is located, has a population of 125,000 cattle (USDA NASS Southern Region, 2015). This suggests that any impact of water retention on CH_4 emissions is small compared to the CH_4 emitted by the regional cattle population.

Pilot water retention projects, FRESP, ran from 2005-2011, and the regional CH_4 estimates presented here include all pastures within the FRESP project. Since then, the project

has been continued through the South Florida Water Management District under a new Dispersed Water Management-Northern Everglades Payment for Environmental Services (NE-PES) program. NE-PES continues to compensate ranches and is involving additional ranches through over $7 million in additional funding (Shabman and Lynch, 2013). It is worth noting that flood water is not only stored on pastures, but is also stored within pasture wetlands and impoundments (Bohlen et al., 2009; Shabman and Lynch, 2013) that likely exhibited different GHG dynamics. Further research is needed to assess the GHG budgets of these other managed systems located throughout south Florida. Regardless, this study demonstrates that subtropical pastures are strong GHG sources when accounting for CH_4 fluxes, and water retention practices do not explain the majority of pasture CH_4 emissions. This suggests that water retention practices provide the ecosystem services of reduced nutrient loading at a minor climate consequence.

ACKNOWLEDGEMENTS

We thank Hilary Swain, Earl Keel, and the rest of the staff at the MacArthur Agro-ecology Research Center for site access, lodging, transportation, and continued support in the field. We also thank Carl Bernacchi, Evan DeLucia, and Nuria Casanovas-Gomez for help with eddy covariance tower maintenance, data transfer, and sharing gap-filling procedures and meteorological data. This research was funded by Cornell University's Cross-scale Biogeochemistry and Climate Program, Atkinson Center for a Sustainable Future, Department of Ecology and Evolutionary Biology, Andrew W. Mellon Foundation, Cornell Sigma Xi, and University of Illinois USDA ARS.

REFERENCES

Allard V, Soussana JF, Falcimagne R, Berbigier P, Bonnefond JM, Ceschia E, D'hour P, Hénault C, Laville P, Martin C, Pinarès-Patino C. 2007. The role of grazing management for the net biome productivity and greenhouse gas budget (CO_2, N_2O and CH_4) of semi-natural grassland. Agriculture, Ecosystems and Environment 121:47–58.

Baldocchi D, Detto M, Sonnentag O, Verfaillie J, Teh YA, Silver W, Kelly NM. 2012. The challenges of measuring methane fluxes and concentrations over a peatland pasture. Agricultural and Forest Meteorology 153:177–87.

Baldocchi D. 2014. Biogeochemistry: Managing land and climate. Nature Climate Change 4:330–1.

Baldocchi DD. 2008. 'Breathing'of the terrestrial biosphere: lessons learned from a global network of carbon dioxide flux measurement systems. Australian Journal of Botany 56:1–26.

Bohlen PJ, Lynch S, Shabman L, Clark M, Shukla S, Swain H. 2009. Paying for environmental services from agricultural lands: An example from the northern Everglades. Frontiers in Ecology and the Environment 7:46–55.

Bohlen PJ, Villapando OR. 2011. Controlling runoff from subtropical pastures has differential effects on nitrogen and phosphorus loads. Journal of Environmental Quality 40:989–98.

Chamberlain SD, Boughton EH, Sparks JP. 2015. Underlying ecosystem emissions exceed cattle-emitted methane from subtropical lowland pastures. Ecosystems 18:933–45.

Chamberlain SD, Gomez-Casanovas N, Walter MT, Boughton EH, Bernacchi CJ, DeLucia EH, Groffman PM, Keel EW, Sparks JP. 2016. Influence of transient flooding on methane fluxes from subtropical pastures. Journal of Geophysical Research: Biogeosciences.

Conrad R. 2007. Microbial Ecology of Methanogens and Methanotrophs. In: Advances in Agronomy. Vol. 96. Elsevier. pp 1–63.

Dengel S, Levy PE, Grace J, Jones SK, Skiba UM. 2011. Methane emissions from sheep pasture, measured with an open-path eddy covariance system. Global Change Biology 17:3524–33.

Foken T, Gockede M, Mauder M, Mahrt L, Amiro B, Munger W. 2004. Post-field data quality control. In: Lee X, Massman WJ, Law BE, editors. Handbook of Micrometeorology. Vol. 29. Dordrecht: Kulwer Academic Publishers. pp 181–208.

Follett RF, Reed DA. 2010. Soil carbon sequestration in grazing lands: Societal benefits and policy implications. Rangeland Ecology & Management 63:4–15.

Forster P, Ramaswamy V, Artaxo P, et al. 2007. Changes in Atmospheric Constituents and in Radiative Forcing. In: Solomon S, Qin D, Manning M, Chen Z, Marquis M, Averyt KB, Tignor M, Miller HL, editors. Climate Change 2007: The Physical Science Basis. Contribution of Working Group I to the Fourth Assessment Report of the Intergovernmental Panel on Climate Change. New York, NY, USA: Cambridge

University Press

Hatala JA, Detto M, Sonnentag O, Deverel SJ, Verfaillie J, Baldocchi DD. 2012. Greenhouse gas (CO_2, CH_4, H_2O) fluxes from drained and flooded agricultural peatlands in the Sacramento-San Joaquin Delta. Agriculture, Ecosystems and Environment 150:1–18.

IPCC. 2006. Emissions from livestock and manure management. In: Eggleston H, Buendia L, Miwa K, Ngara T, Tanabe K, editors. IPCC Guidelines for National Greenhouse Gas Inventories, Prepared by the National Greenhouse Gas Inventories Programme. Japan: IGES

Knox SH, Sturtevant C, Matthes JH, Koteen L, Verfaillie J, Baldocchi D. 2015. Agricultural peatland restoration: Effects of land-use change on greenhouse gas (CO_2 and CH_4) fluxes in the Sacramento-San Joaquin Delta. Global Change Biology 21:750–65.

Lloyd JJ, Taylor JA. 1994. On the temperature dependence of soil respiration. Functional Ecology 8:315–23.

MacArthur Agro-ecology Research Center. 2015. Cattle Management. http://www.maerc.org/html/operations/cattle

Moncrieff JB, Massheder JM, De Bruin H, Elbers J, Friborg T, Heusinkveld B, Kabat P, Scott S, Soegaard H, Verhoef A. 1997. A system to measure surface fluxes of momentum, sensible heat, water vapour and carbon dioxide. Journal of Hydrology 188-189:589–611.

Mudge PL, Wallace DF, Rutledge S, Campbell DI, Schipper LA, Hosking CL. 2011. Carbon balance of an intensively grazed temperate pasture in two climatically contrasting years. Agriculture, Ecosystems and Environment 144:271–80.

Nieveen JP, Campell DI, Schipper LA, Blair IJ. 2005. Carbon exchange of grazed pasture on drained peat soil. Global Change Biology 11:607–18.

R Core Team. 2015. R: A Language and Environment for Statistical Computing. Vienna, Austria: R Foundation for Statistical Computing http://www.r-project.org/

Ramankutty N, Evan AT, Monfreda C, Foley JA. 2008. Farming the planet: 1. Geographic distribution of global agricultural lands in the year 2000. Global Biogeochemical Cycles 22:1–19.

Reichstein M, Falge E, Baldocchi D, Papale D, Aubinet M, Berbigier P, Bernhofer C, Buchmann N, Gilmanov T, Granier A, Grunwald T, Havrankova K, Ilvesniemi H, Janous D, Knohl A, Laurila T, Lohila A, Loustau D, Matteucci G, Meyers T, Miglietta F, Ourcival JM, Pumpanen J, Rambal S, Rotenberg E, Sanz M, Tenhunen J, Seufert G, Vaccari F, Vesala T, Yakir D, Valentini R. 2005. On the separation of net ecosystem exchange into assimilation and ecosystem respiration: Review and improved algorithm. Global Change Biology 11:1424–39.

Shabman L, Lynch S. 2013. Moving from concept to implementation: The emergence of the Northern Everglades Payment for Environmental Services Program. Resources for the Future Discussion Paper:13–27.

Shoemaker JK, Keenan TF, Hollinger DY, Richardson AD. 2014. Forest ecosystem changes from annual methane source to sink depending on late summer water balance.

Geophysical Research Letters 41:673–9.

Soussana JF, Allard V, Pilegaard K, Ambus P, Amman C, Campbell C, Ceschia E, Clifton-Brown J, Czobel S, Domingues R, Flechard C, Fuhrer J, Hensen A, Horvath L, Jones M, Kasper G, Martin C, Nagy Z, Neftel A, Raschi A, Baronti S, Rees RM, Skiba U, Stefani P, Manca G, Sutton M, Tuba Z, Valentini R. 2007. Full accounting of the greenhouse gas (CO_2, N_2O, CH_4) budget of nine European grassland sites. Agriculture, Ecosystems and Environment 121:121–34.

Teh YA, Silver WL, Sonnentag O, Detto M, Kelly M, Baldocchi DD. 2011. Large greenhouse gas emissions from a temperate peatland pasture. Ecosystems 14:311–25.

USDA NASS Southern Region. 2015. Florida Cattle County Estimates. http://www.nass.usda.gov/Statistics_by_State/Florida/Publications/County_Estimates/2015/FLCattle15.pdf

Vickers D, Mahrt L. 1997. Quality control and flux sampling problems for tower and aircraft data. Journal of Atmospheric and Oceanic Technology 14:512–26. http://journals.ametsoc.org/doi/abs/10.1175/1520-0426(1997)014%3C0512:QCAFSP%3E2.0.CO

Webb, EK, Pearman GI, Leuning R. 1980. Correction of flux measurements for density effects due to heat and water vapour transfer. Quarterly Journal of the Royal Meteorological Society 106:85–100.

CHAPTER 4

SOURCING METHANE AND CARBON DIOXIDE EMISSIONS FROM A SMALL CITY: INFLUENCE OF NATURAL GAS LEAKAGE AND COMBUSTION

ABSTRACT

Natural gas leakage and combustion are major sources of carbon dioxide (CO_2) and methane (CH_4), however our understanding of emissions from cities is limited. We mapped pipeline leakage using a mobile CH_4 detection system, and continuously monitored atmospheric CO_2 and CH_4 concentrations and carbon isotopes ($\delta^{13}C$-CO_2 and $\delta^{13}C$-CH_4) for one-year above Ithaca, New York. Pipeline leakage rates were low (< 0.39 leaks $mile^{-1}$), likely due to the small extent of cast iron and bare steel within the pipeline system (2.6%). Our atmospheric monitoring demonstrated that the isotopic composition of locally emitted CO_2 approached the $\delta^{13}C$ range of natural gas combustion in winter, correlating to natural gas power generation patterns at Cornell's Combined Heat and Power Plant located 600 m southeast of the monitoring site. Atmospheric CH_4 plumes were primarily of natural gas origin, were observed intermittently throughout the year, and were most frequent in winter and spring. No correlations between the timing of atmospheric natural gas plumes and Cornell Plant operations could be drawn. However, elevated CH_4 and CO_2 concentrations were observed coincident with high winds from the southeast, and the plant is the only major emission source in that wind sector. Natural gas use at centralized facilities is growing, and our results suggest that these facilities may be an important source of urban and suburban emissions.

INTRODUCTION

Carbon dioxide (CO_2) and methane (CH_4) emissions are responsible for 50% and 29% of positive anthropogenic radiative forcing to the atmosphere, respectively (Stocker et al., 2013). Between 30 to 40 percent of all anthropogenic greenhouse gas emissions originate from cities, however these estimates are highly uncertain (Satterthwaite, 2008). Cities are generally defined as having populations greater than 20,000 residents (Satterthwaite, 2008), however cities vary widely in terms of density and development, making it difficult to scale emission estimates. Within the United States, studies to date have focused on quantifying emissions from major urban areas (population > 1,000,000) such as Boston (Phillips et al., 2013; McKain et al., 2015), Washington DC (Jackson et al., 2014), Salt Lake City (Pataki et al., 2003a), Indianapolis (Mays et al., 2009; Cambaliza et al., 2015), and Los Angeles (Turnbull et al., 2011; Wennberg et al., 2012), whereas little research has focused on sourcing greenhouse gas emissions from small cities. Today, roughly 46% of the global urban population lives in cities smaller than 500,000 (United Nations, 2014), so data are needed from this major and growing land use. Small cities are commonly made up of low-density suburban landscapes, and while these landscapes are predominant across North America (Gordon and Janzen, 2013) they have received less research attention.

Energy generation for electricity, heating, and industry is a major driver of urban emissions, and within the United States, roughly one quarter of the total energy supply is generated from the combustion of natural gas (EPA, 2015). Natural gas combustion facilities are the leading sector of electricity generation in the United States, recently exceeding net electricity generation from coal (EIA, 2015). Natural gas usage emits greenhouse gases through direct leakage of CH_4 and combustion of CH_4 to CO_2. The US Environmental

Protection Agency estimates that the natural gas and energy supply chains are the largest emission source of CH_4 in the United States, and dominant source of CO_2 equivalent emissions in residential, commercial, and industrial sectors (EPA, 2015). These estimates are highly uncertain and heavily debated.

Much of the controversy stems from a poor accounting of fugitive CH_4 emissions, and independent and industry studies have produced a wide range of leak rate estimates (Howarth et al., 2011; Cathles et al., 2012; Wennberg et al., 2012; Gallagher et al., 2015; Lamb et al., 2015; McKain et al., 2015; EPA 2015). It is necessary to constrain CH_4 leakage rate estimates because at higher leak rates (above ~3%) natural gas usage for electricity generation has a higher greenhouse gas footprint than coal (Howarth et al., 2011). Contemporary studies of major US cities have documented high CH_4 leakage rates from natural gas pipeline infrastructure (Townsend-Small et al., 2012; Phillips et al., 2013; Jackson et al., 2014; Cambaliza et al., 2015; McKain et al., 2015), though leakage rates are significantly reduced in cities that have replaced older cast iron distribution pipelines with less leak prone alternatives (Gallagher et al., 2015). Additionally, continuous concentration and isotope measurements from rooftops have found that natural gas combustion is the dominant driver of urban CO_2 emissions in winter months (Pataki et al., 2003a; Moore and Jacobson, 2015). These patterns have been primarily described in larger urban areas, and small cities and suburban areas are underrepresented in literature. Given the extent of small cities and suburbs and the lack of available data, it is important to better constrain emissions from these systems.

The goals of this work were to better understand temporal and spatial patterns in CH_4 leakage and combustion in the small city of Ithaca, New York, USA. We established a continuous rooftop-monitoring site and generated a 12-month record of CO_2 and CH_4

concentration and isotope values ($\delta^{13}C\text{-}CO_2$; $\delta^{13}C\text{-}CH_4$) to identify temporal patterns in ecosystem-scale emissions. Here, we used a wavelength-scanned cavity ringdown spectrometer (WS-CRDS) to collect high-resolution (~ 0.5-1 Hz) paired measurements of $\delta^{13}C$ and gas concentrations. To our knowledge, this is the first long-term continuous record of urban CH_4 and CO_2 concentrations and $\delta^{13}C$. We also conducted mobile gas concentration surveys to identify street-level CH_4 leakage from natural gas pipeline infrastructure. We combined these two approaches to describe the extent of CH_4 leakage from local infrastructure, determine the contribution of natural gas leakage and combustion to atmospheric CH_4 and CO_2, and identify potential emission sources observed from our rooftop measurements. Finally, we present a basic data processing, filtering, and quality control framework to guide future studies using rooftop WS-CRDS measurements to identify ecosystem greenhouse gas sources.

METHODS

Description: Ithaca, New York

Ithaca, New York is a small city (population 30,720 in 2014) with a density of 2,151 persons per km^2. The landscape of Ithaca ranges from a more densely populated downtown surrounded by suburban and exurban neighborhoods comprised of mostly single-family homes. The Ithaca metro area also includes the surrounding Town of Ithaca and Cayuga Heights (populations of 19,930 and 3,729, respectively), which are lower density suburban neighborhoods (US Census, 2014). Cornell University is located within Ithaca, and hosts an additional student population of 21,850 students per academic year, many of which live in large dormitories on campus (Cornell, 2013a). Ithaca is located within a continental climate,

and experiences warm humid summers and cold winters with temperatures dropping below O °C (NEWA, 2015). All measurements took place within the Ithaca metro area described above.

Leak Mapping Surveys

We identified individual CH_4 leaks throughout Ithaca, NY, using a custom built mobile leak monitoring system. A WS-CRDS (G2201-*i*, Picarro Inc., Sunnyvale, CA) was installed in an automobile and continuously measured CO_2 and CH_4 concentrations during survey drives. Air was drawn through perforations in a ¼" Teflon sampling tube covered with PTFE membranes mounted on the vehicle front bumper, and a second vacuum pump increased the flow rate through gas sampling lines. Air was drawn from the sampling line into the WS-CRDS at 300 ml min^{-1}. GPS location was recorded at 1-second intervals (GPS18x, Garmin Ltd., Olathe, KS) and merged with WS-CRDS files post-survey. We corrected for time lags between GPS location and CH_4 measurements due to sampling line length (~3.7 m) by measuring the time delay between the injection of gas standards at the front bumper inlet and WS-CRDS response time (~19 seconds). The WS-CRDS was calibrated with known concentration and isotope standards of CH_4 and CO_2 in air. We used 0, 5, and 10 ppm CH_4 standards (Air Liquide, Philadelphia, PA); 301, 510, and 1000 ppm CO_2 standards (Air Liquide, Philadelphia, PA); -44.42 and -3.58‰ $\delta^{13}C$-CO_2 standards (Oztech Trading Corp, Stafford, AZ); and -66.5 and -23.9 ‰ $\delta^{13}C$-CH_4 standards (Isometric Instruments, Victoria, BC) for calibrations. Concentration and $\delta^{13}C$ measurements were precise to within 0.05 ppm CH_4, 0.20 ppm CO_2, 1.15‰ $\delta^{13}C$-CH_4, and 0.16 ‰ $\delta^{13}C$-CO_2. These calibrations and precisions also apply to the *Rooftop Gas Monitoring* section below. The measurement system was powered through a

1000W sine wave inverter attached to a 12 V battery run in parallel with the vehicle's battery system. This mobile system has been used successfully to map CH_4 emission plumes from pasture ecosystems in south Florida (Chamberlain et al., 2015).

In total, 148 miles of road were sampled within the area shown in Figure 4.1 at an average speed of 15.5 mph, which included all major roads and the majority of residential and side roads (Appendix Figure A.1). Surveys were conducted on May 27-28th and June 29-30th, 2015 on days with low wind speed (Appendix Table A.1). Post-survey, all data were compiled and we defined potential leaks as temporally discrete CH_4 concentration peaks that were above the 98% percentile of all measured concentrations (> 1.93 ppmv). Survey time series were de-trended prior to peak identification to control for fluctuations in background CH_4 concentration throughout the day. Leak locations were then identified and mapped using R 3.2.0 and the 'ggmap' package (R Core Team, 2015).

Rooftop Gas Monitoring

In Ithaca, CO_2 and CH_4 isotope concentrations were continuously monitored with a WS-CRDS analyzer (G2201-*i*, Picarro Inc., Sunnyvale, CA) from an air inlet 16 m above the ground from the rooftop of Corson Hall on the Cornell University campus (N 42.447128, W 76.479203). Measurements began in September 2014 and were near continuous through September 2015. The rooftop measurement site is centrally located on Cornell University campus and is surrounded by roads, lawns, and other university office buildings. Ithaca's residential and urban core is located 1.3 km to the west, and Cornell's Combined Heat and Power Plant, which combusts natural gas for heat and electricity, is located ~600 m to the southeast (Figure 4.1).

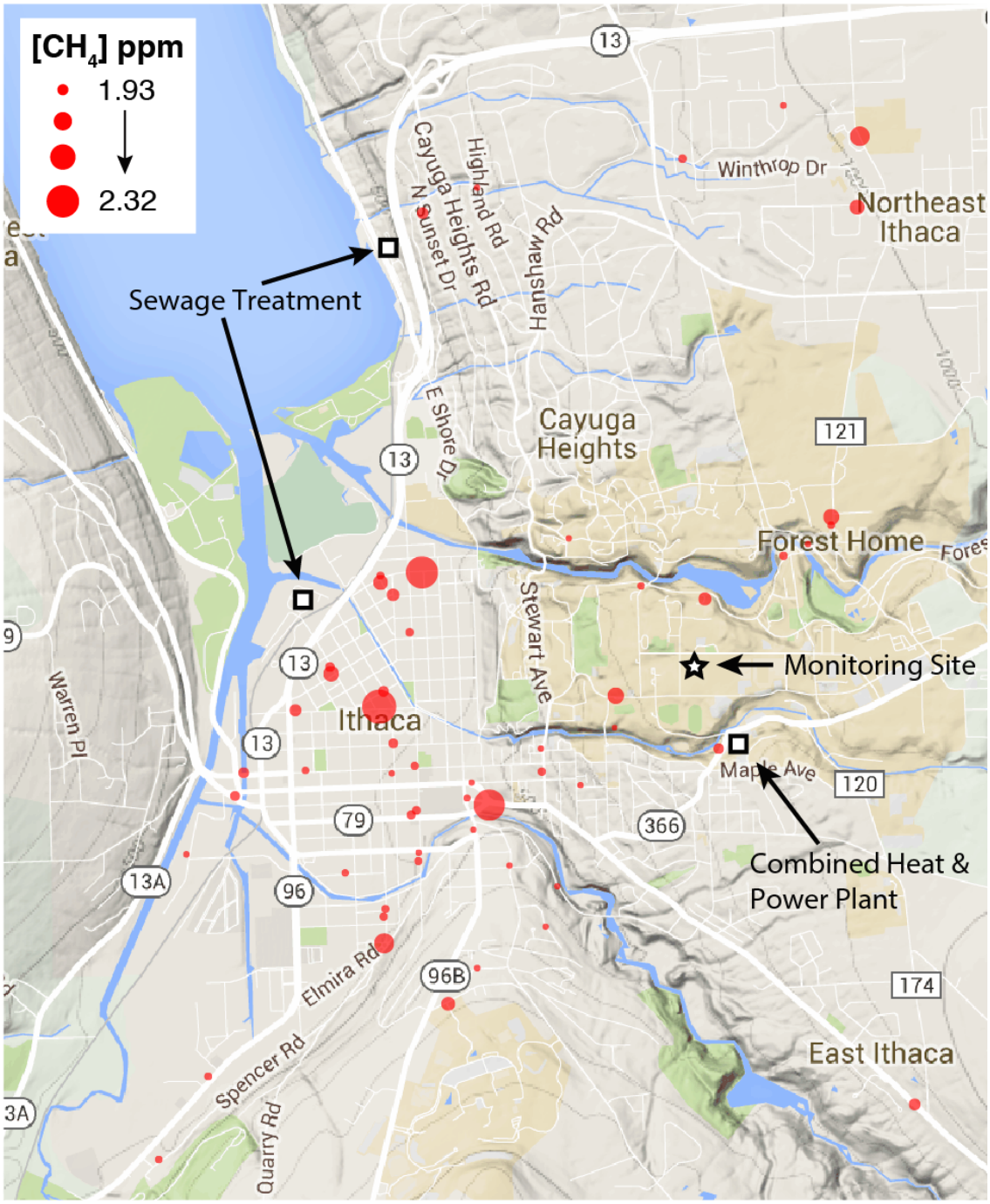

Figure 4.1 Methane leak locations across Ithaca, New York. In total, 57 potential leaks (>1.93 ppmv CH_4; 98% percentile of all measurements) were mapped across 148 miles of road (< 0.39 leaks $mile^{-1}$). Locations of the rooftop-monitoring site and potential CH_4 point sources are also shown on the map.

Air samples were drawn from a monitoring mast installed at the edge of the building roof to avoid possible interference from rooftop infrastructure. The Corson Hall rooftop maintains a working greenhouse with air conditioners, ventilation exhausts, and one sewage vent pipe (> 9 m from the air intake). The sample inlet was connected to an inverted funnel at the top of the mast to prevent water intake to the analyzer. Air samples were drawn though ¼" Teflon tubing with a PTFE membrane filter running from the sample mast to the WS-CRDS using a vacuum pump (sampling rate; 30 ml min^{-1}). The WS-CRDS was housed within a greenhouse storage room and calibrated with known CO_2 and CH_4 concentration and isotope standards in air at the beginning of deployment as described in *Leak Mapping Surveys*. The instrument was checked for drift every 2 weeks using 5 ppm CH_4 and 510 ppm CO_2 standards (Air Liquide, Philadelphia, PA). Observed drifts (1σ) were as high as 0.05 ppm CH_4, 0.58‰ $\delta^{13}C$-CH_4, 1.90 ppm CO_2, and 0.43‰ $\delta^{13}C$-CO_2. Our reported drift range is similar to the range reported in Moore and Jacobson (2015), and is within the maximum drift range reported by the manufacturer (G2201-*i*, Picarro Inc., Sunnyvale, CA). We did not observe any systematic directional drift and therefore did not correct for instrument drift.

Keeling Plot Approach

We used Keeling plots to identify the isotopic source value of urban CO_2 and CH_4 emissions to the atmosphere. Keeling plots have been used to identify local sources of CO_2 in both urban (Pataki et al., 2003a; Townsend-Small et al., 2012; Moore and Jacobson 2015) and natural ecosystems (Bowling et al., 2005, 2009). In this approach, measured gas concentrations (c_m) are decomposed into their background (c_b) and local source components (c_s).

$$c_m = c_b + c_s \qquad \text{(equation 1)}$$

Applying an isotope mass-balance approach, we can then re-write equation 1 to describe isotopes in the atmosphere:

$$\delta^{13}C_m c_m = \delta^{13}C_b c_b + \delta^{13}C_s c_s \qquad \text{(equation 2)}$$

where $\delta^{13}C_m$, $\delta^{13}C_b$, and $\delta^{13}C_s$ are the carbon isotope ratio of measured, background, and local CO_2 or CH_4, respectively. We then rewrite c_s in terms of c_m and c_b, substitute equation 1 into equation 2, and describe measured isotopes ($\delta^{13}C_m$) as follows:

$$\delta^{13}C_m = c_b(\delta^{13}C_b - \delta^{13}C_s)\frac{1}{c_m} + \delta^{13}C_s \qquad \text{(equation 3)}$$

This equation can be used to identify the isotopic composition of locally emitted greenhouse gases ($\delta^{13}C_s$) by regressing measured isotope values ($\delta^{13}C_m$) by the inverse of measured concentration ($1/c_m$) for either CO_2 or CH_4, where $\delta^{13}C_s$ is the calculated y-intercept of the regression. For more details on this approach and derivation see Pataki et al. (2003b) or Zobitz et al. (2006). The Keeling approach has been used successfully to identify local sources of both CH_4 and CO_2 in urban settings (Pataki 2003a; Townsend-Small et al., 2012; Moore and Jacobson 2015).

Data Processing and Analysis

The WS-CRDS measured air samples every 1-2 seconds and collected ~2400 measurements per hour. Raw WS-CRDS data were averaged into half-hour intervals. We constructed Keeling plots and calculated $\delta^{13}C_s$ for both gas species ($\delta^{13}C_s$-CO_2 and $\delta^{13}C_s$-CH_4) at daily intervals using half-hourly nighttime only data. Nighttime only data were used to construct Keeling plots because locally emitted gases accumulate during stable nocturnal conditions and photosynthesis effects can be ignored (Pataki 2003b). We defined nighttime as periods when

incoming solar radiation was 0 W m^{-2} at the Cornell University Game Farm Road weather station (N 42.449181, W 76.449038), located ~2.5 km from the rooftop-monitoring site. Nightly $\delta^{13}C_s$ values for both species were calculated from the y-intercept of ordinary least squares regression (OLS) of $\delta^{13}C_s$ by $1/c_m$ as recommended in Zobitz et al. (2006). We applied three quality control measures to filter low-quality $\delta^{13}C_s$ estimates from both CO_2 and CH_4 datasets. These criteria ensured that, 1) a sufficient concentration range was measured each night, 2) linearity assumptions in the Keeling plot mixing model were met, and 3) highly uncertain $\delta^{13}C_s$ values were removed from analysis. First, we rejected nights from analysis that did not display a sufficient gas concentration range for either gas species ($range_{CO2} < 15$ ppmv; $range_{CH4} < 0.10$ ppmv). At concentration ranges below these thresholds $\delta^{13}C_s$ standard error increased exponentially (Figure 4.2), as has been documented in other studies (Pataki et al., 2003b; Bowling et al., 2005; Zobitz et al., 2006). Second, we assessed linearity in the OLS regression of $\delta^{13}C_s$ and $1/c_m$ using a significance threshold ($P < 0.05$) and r^2 threshold for the fit of each species ($r^2_{CO2} < 0.75$; $r^2_{CH4} < 0.50$). Finally, $\delta^{13}C_s$ values with intercept standard errors larger than 2‰ than were removed from analysis to constrain $\delta^{13}C_s$ uncertainty. The full workflow of data processing, $\delta^{13}C_s$ estimation, and quality control is outlined in Figure 4.3. Overall, 40.2% of all calculated $\delta^{13}C_s$-CO_2 values and 12.0% of all calculated $\delta^{13}C_s$-CH_4 values remained after applying quality control criteria.

The rooftop time series was analyzed in relation to hourly meteorological data (wind speed, wind direction, incoming solar radiation) collected from the Cornell University Game Farm Road weather station located ~2.5 km from the rooftop-monitoring site (NEWA; 2015). Wind speed and direction data were used to assess spatial patterns in gas sources, and solar radiation data were used to define nighttime periods.

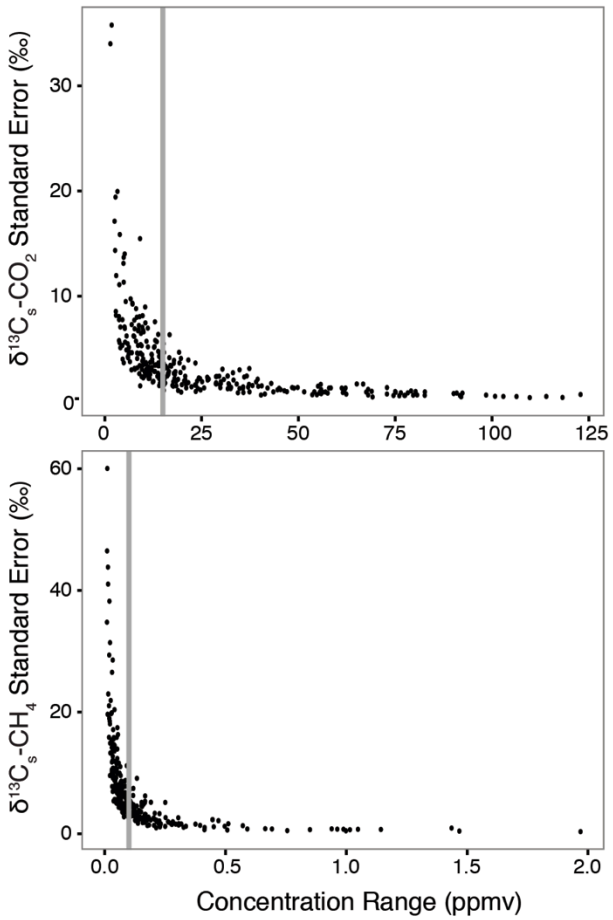

Figure 4.2 Standard error of Keeling plot intercepts ($\delta^{13}C_s$-CO_2 and $\delta^{13}C_s$-CH_4) versus nightly measured concentration ranges. Vertical grey lines correspond to quality thresholds used in this study (see Figure 4.3).

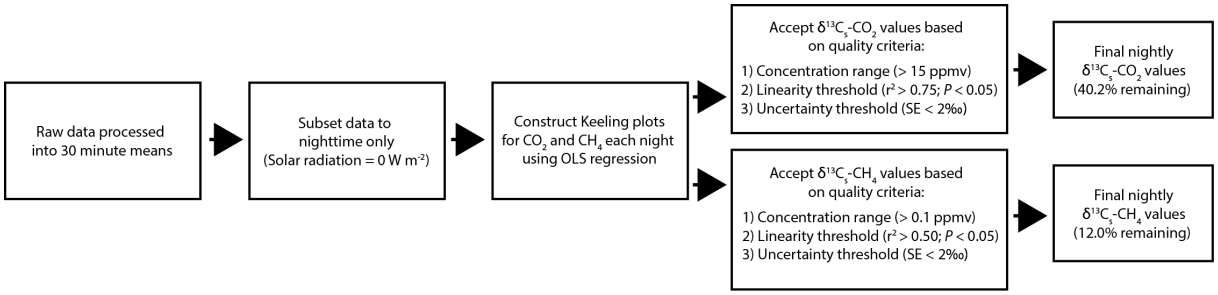

Figure 4.3 Workflow schematic for processing raw WS-CRDS data to final $\delta^{13}C_s$-CO_2 and $\delta^{13}C_s$-CH_4 values with Keeling plots. The same workflow and quality control criteria are used for both gas species, however quality control thresholds differ.

Natural gas turbine combustion data from the Cornell Combined Heat and Power Plant (N 42.442827, W 76.475002) was supplied by Cornell's Facilities Services (2015), and we integrated daily gas turbine combustion power (MW) by adding the two plant turbines' combustion power output and taking a daily mean. Linear regression was used to correlate $\delta^{13}C_s$-CO_2 and combustion power estimates. To assess connections between normal plant operations and atmospheric data, we omitted time points when either turbine was not operational (0 W output). Periods when either turbine was not operational comprised only 5.8% of the Cornell Plant's combustion power dataset. All data processing, analysis, and visualization of rooftop and auxiliary data were done in R 3.2.0 using the 'dplyr', 'gpplot2' 'openair', and 'readr' packages (R Core Team, 2015).

Source $\delta^{13}C$ Identification

We measured $\delta^{13}C$ values from local sewage and natural gas CH_4 sources, natural gas-derived CO_2, and three leaks identified in mapping surveys. The $\delta^{13}C$ value of pipeline natural gas CH_4 was determined from 9 replicate plumes created by a residential gas line, where gas was accumulated in an inverted chamber and the WS-CRDS sampled the chamber headspace. $\delta^{13}C$-CO_2 data were collected for combustion of this natural gas source using the same inverted chamber method, and we additionally measured natural gas combustion CO_2 in free atmosphere surrounding an active basement furnace. Here, the air inlet to the WS-CRDS was placed adjacent (within 10 cm) to the furnace pilot light and combustion area. Sewage $\delta^{13}C$ values were estimated for both CO_2 and CH_4 from a known sewage vent pipe located on the rooftop of Corson Hall. Here, we placed the WS-CRDS inlet tube at least 1 m within the vent pipe and measured air for ~10 min. Direct $\delta^{13}C$ values are reported for natural gas CH_4

measured within the inverted chamber because measured concentrations were at least 100 times higher than background, and the Keeling approach was used to estimate $\delta^{13}C_s$ values for all sources measured in free atmosphere (natural gas combustion CO_2 and sewage pipe). We also collated reported $\delta^{13}C$-CO_2 values for gasoline combustion from Paris, France (Widory and Javoy, 2003), Salt Lake City, Utah (Bush et al., 2007), and Vancouver, Canada (Semmens et al., 2014). Ecosystem respiration $\delta^{13}C$-CO_2 values are reported for temperate forests with similar mean annual precipitation (Pataki et al., 2003b). Source $\delta^{13}C$ values for both gas species are included in Figures 4.4 and 4.6 to aid the discussion of atmospheric $\delta^{13}C_s$ values relative to potential gas sources. All measured and cited source end-member values are reported in Appendix Table A.2.

We also determined the isotopic signature of three leaks identified from our mobile surveys during a re-inspection on foot, two within Ithaca and one on Cornell campus. During these re-inspections, CH_4 leak plumes were identified in the survey vehicle, and when found, the uncovered WS-CRDS sample inlet was placed directly within the emission plume by hand. We used the Keeling approach to estimate $\delta^{13}C_s$-CH_4 values for all leaks measured. We only re-visited a small subset of leaks because our main concern was to place an upper bound on the natural gas leak rate and identify if sewage false positives could occur.

RESULTS AND DISCUSSION

Street-Level CH_4 Leaks

We identified 57 potential street-level CH_4 leaks across 148 road miles within Ithaca at an average rate of < 0.39 leaks per road mile (Figure 4.1). This estimate represents an upper bound of natural gas leaks, as at least one of the potential leaks we identified was a sewage

CH_4 plume (Table 4.1). Regardless of potential sewage false positives, this maximum leak rate is considerably lower than rates observed from cities with extensive cast iron and bare steel pipeline systems (Phillips et al., 2013; Jackson et al., 2014; Gallagher et al., 2015), and is within the range of estimates for cities with active pipeline replacement programs (Gallagher et al., 2015). The main gas service provider for the Ithaca system, NYSEG, has replaced nearly all cast iron and bare steel pipelines, and as of 2014, these pipelines make up 2.6% of the entire system (PHMSA, 2014). Plastic and cathodic protected coated steel pipelines comprise 48.7% and 46.8% of NYSEG's total pipeline system (PHMSA, 2014), respectively. The small extent of cast iron and bare steel within the Ithaca system likely explains the low observed leak rate (Gallagher et al., 2015). Potential leaks were concentrated in the most densely populated areas surrounding the city center, and fewer were identified on Cornell University campus and the suburban neighborhoods in Cayuga Heights and Northeast Ithaca (Figure 4.1).

Table 4.1 Location, description, maximum measured concentration, and isotopic value (± SD) of street-level leaks monitored during follow up surveys. Natural gas and sewage end-member sources had $\delta^{13}C\text{-}CH_4$ values of -35 ± 0.50‰ and -57.58 ± 0.58‰, respectively.

Latitude	Longitude	Leak Description	$[CH_4]$ (ppmv)	$\delta^{13}C\text{-}CH_4$ (‰)
42.451963	-76.498648	pavement crack	27.82	-30.08 ± 6.60
42.451963	-76.498648	sewer manhole	136.98	-43.38 ± 0.22
42.439182	-76.493634	pavement crack	5.73	-33.34 ± 0.33
42.450901	-76.478779	sewer manhole	54.93	-57.94 ± 0.31

The highest leak concentrations observed in our mobile surveys of Ithaca were much lower than those observed in larger cities. For instance, the highest concentration we observed in our mobile survey was 2.32 ppm CH_4, while in studies of Boston and Washington DC the threshold for leak detection was set above 2.5 ppm CH_4, the 95% percentile of all measured concentrations (Phillips et al., 2013; Jackson et al., 2014). Given these differences in leak

detection, we set our detection threshold to a conservative 98% percentile of all measured concentrations (> 1.93 ppm). We measured much higher concentrations from three leaks upon re-inspection on foot, where peak concentrations ranged from 5.73 to 136.98 ppm CH_4 (Table 4.1). Known natural gas and sewage end-members had $\delta^{13}C$-CH_4 values of -35 ± 0.50‰ and -57.58 ± 0.58‰, respectively, and these values suggest that both plumes emitted from pavement cracks were of natural gas origin and the leak on Cornell campus was a sewage plume (Table 4.1). At one leak location in downtown Ithaca, elevated CH_4 concentrations were measured from a pavement crack and within a nearby manhole cover, and $\delta^{13}C$-CH_4 values within the manhole cover (-43.38 ± 0.22‰) suggest mixing between sewage and natural gas sources (Table 4.1). Our finding of one sewage false positive suggests that our mobile survey leak rate is high, but clearly bounds the total leak rate at less than 0.39 leaks per mile, well within the range of cities with similar pipeline infrastructure (Gallagher et al., 2015).

Seasonal Cycle of Urban CO_2 and CH_4 Sources

Natural gas combustion was a major source of CO_2 above Ithaca during winter months. Background CO_2 concentrations were lowest and exhibited high diel variability in summer, demonstrating the strong influence of growing season photosynthesis and respiration, and CO_2 concentrations higher and less variable in winter months during plant senescence (Figure 4.4a). Locally emitted $\delta^{13}C_s$-CO_2 estimates also varied with season, we observed the lowest $\delta^{13}C_s$-CO_2 values during winter and the highest $\delta^{13}C_s$-CO_2 values in summer. Winter $\delta^{13}C_s$-CO_2 values were mostly within the $\delta^{13}C$ range of natural gas combustion, while summer $\delta^{13}C_s$-CO_2 values were highly variable, although they fell between the $\delta^{13}C$ ranges of

ecosystem respiration, gasoline combustion, and natural gas combustion (Figure 4.4b). These data suggest that natural gas combustion is the primary source of CO_2 in winter, while all sources contribute to atmospheric CO_2 in summer. Power generation from natural gas combustion at the Cornell Combined Heat and Power Plant corroborate these findings, where natural gas power generation peaked in winter and was lowest in summer (Figure 4.4c). Nightly $\delta^{13}C_s$-CO_2 estimates originating from the plant's direction (120-180°) decreased as natural gas power generation rates increased ($r^2 = 0.15$, $P = 0.018$; Figure 4.5), indicating an increased contribution of natural gas combustion CO_2 to the atmosphere during periods of heavy natural gas use. Similar seasonal $\delta^{13}C_s$-CO_2 patterns have been observed in major urban areas, and these transitions were attributed to increased CO_2 emissions from natural gas heating in winter (Pataki et al., 2003a; Moore and Jacobson 2015).

Most of the CH_4 plumes measured from rooftop atmospheric monitoring were of natural gas origin (Figure 4.6). Large CH_4 plumes increased in frequency in the spring compared to other seasons (Figure 4.6a). We also observed an increase in natural gas $\delta^{13}C_s$-CH_4 estimates during this period because the increased frequency of large nightly CH_4 plumes allowed for the estimation of accurate Keeling plots. Nightly $\delta^{13}C_s$-CH_4 estimates mostly fell within the $\delta^{13}C$ range of known natural gas sources, however in summer 2015, two $\delta^{13}C_s$-CH_4 estimates were within the range of sewage CH_4 (Figure 4.6b). These data suggest that throughout most of the year natural gas leakage is the major CH_4 emission source from Ithaca, New York, though CH_4 emissions during summer months may also be influenced biogenic CH_4 production. No clear connections were observed between natural gas $\delta^{13}C_s$-CH_4 plume timing and Cornell Plant operations and shutdown events (Figure 4.6).

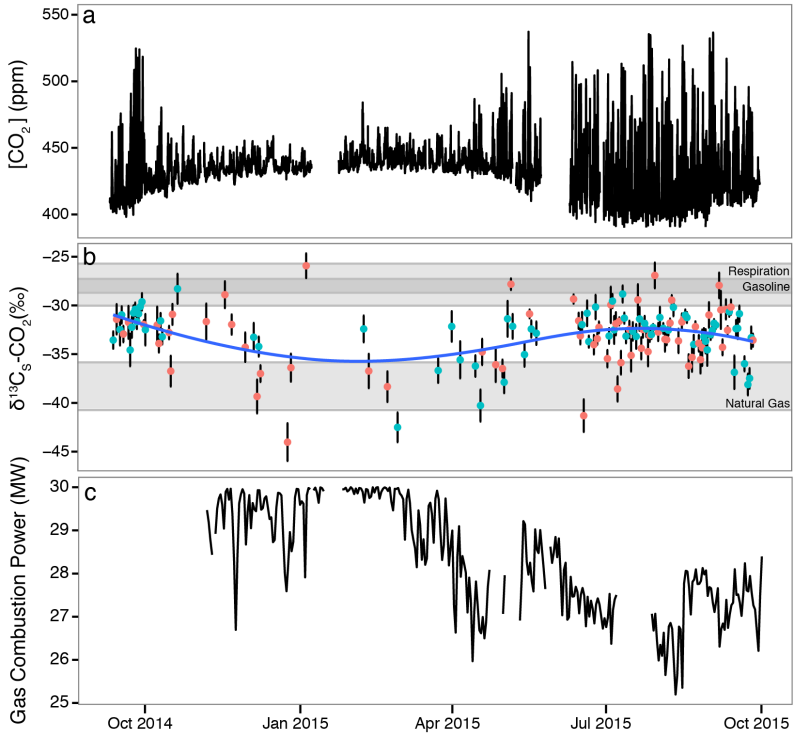

Figure 4.4 Time series of (a) CO_2 concentration (b) and $\delta^{13}C_s$-CO_2 estimates measured from a rooftop-monitoring mast on Corson Hall, Cornell University, Ithaca, New York, and (c) mean daily power produced natural gas combustion at the Cornell Combined Heat and Power Plant. Shaded regions on (b) indicate the range δ^{13}C-CO_2 values for known sources. Red dots for $\delta^{13}C_s$-CO_2 on (b) indicate potential rooftop emission interference (0-120° nightly median wind direction). Solid blue line on (b) is a local polynomial regression fit to $\delta^{13}C_s$-CO_2 values.

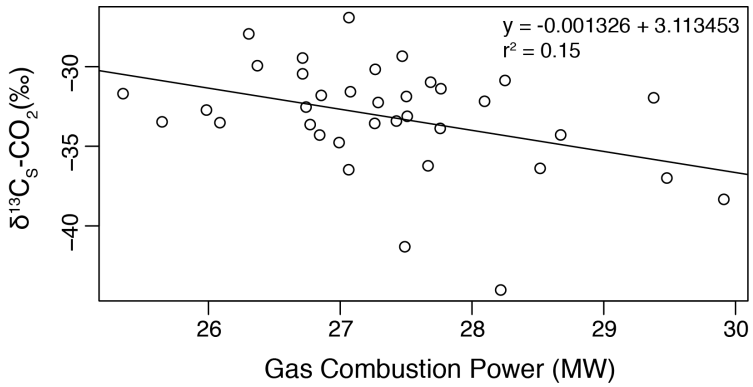

Figure 4.5 Regression of daily Cornell Plant gas combustion power and $\delta^{13}C_s$-CO_2 estimates originating from the plant's direction (120-180° nightly wind direction).

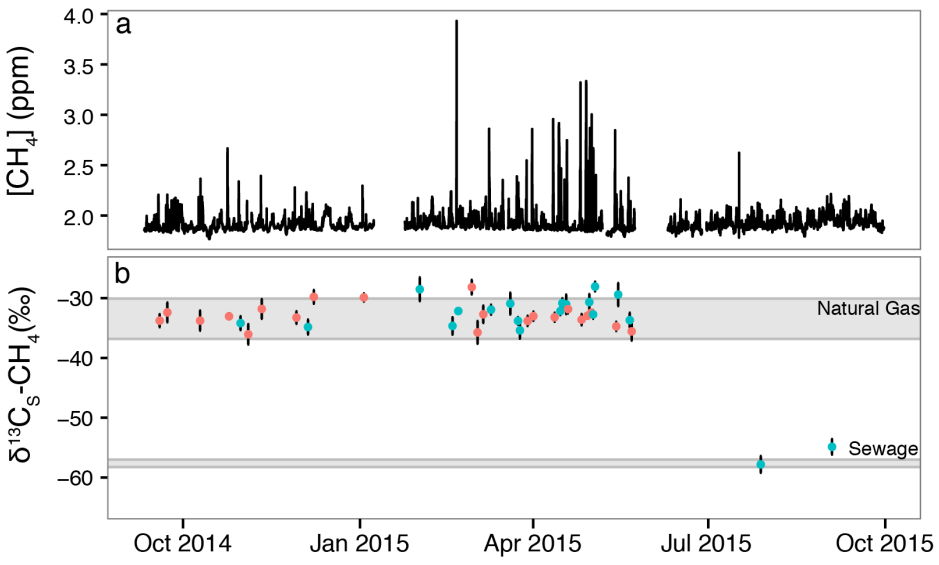

Figure 4.6 Time series of (a) CH_4 concentration and (b) $\delta^{13}C_s$-CH_4 measured from a rooftop-monitoring mast on Corson Hall, Cornell University, Ithaca, New York. Shaded regions on bottom panel indicate the range $\delta^{13}C_s$-CH_4 values for known sewage and natural gas sources. Red dots for $\delta^{13}C_s$-CH_4 on (b) indicate potential rooftop emission interference (0-120° nightly median wind direction).

One intrinsic challenge of using rooftop-based measurements is the influence of the building itself on the concentration and isotopic composition of the gases of interest. Although this source of interference has not been addressed in previous studies (Pataki et al., 2003a; Moore and Jacobson 2015), there is always a risk of simply measuring the metabolism of the building a mast is installed on. We addressed this concern by analyzing spatial emission patterns relative to the rooftop-monitoring site. High nighttime CH_4 and CO_2 concentrations were measured at low wind speeds (< 4 m s^{-1}) with winds from the north to east (Figure 4.7). Winds from these directions (0-110°) pass across the roof of the building, so it is possible that building emissions impacted $\delta^{13}C_s$ values estimated when winds cross the rooftop. To better understand if rooftop interferences were driving observed $\delta^{13}C_s$ patterns, we color coded potential $\delta^{13}C_s$ values that might be impacted by rooftop plumes. Here, $\delta^{13}C_s$ estimates were color coded for 'potential interference' if the nightly median wind direction originated from 0-

120° degrees. A number of our $\delta^{13}C_s$-CO_2 estimates may have been impacted by 'rooftop interference', however these values fell within the general pattern of the greater time series (Figure 4.4b), so it is unlikely that these estimates bias conclusions. In the case of our CH_4 data, it appears that the two summer $\delta^{13}C_s$ values of sewage-origin may have been emitted from Corson Hall (Figure 4.6b). A sewer ventilation pipe is located on the rooftop, and elevated sewage CH_4 concentrations were measured within the vent tube (Appendix Table A.2). For all other seasons, $\delta^{13}C_s$ values exhibiting 'rooftop interference' fell within the general pattern of the $\delta^{13}C_s$-CH_4 time series (Figure 4.6b).

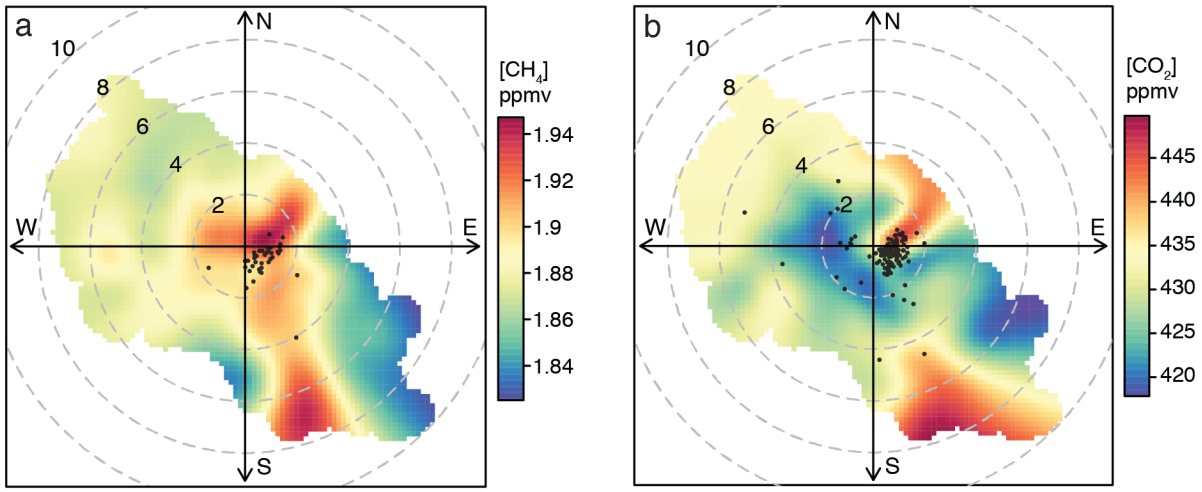

Figure 4.5 Polar plots of nighttime (a) CH_4 concentration and $\delta^{13}C_s$-CH_4, and (b) CO_2 concentration and $\delta^{13}C_s$-CO_2 by wind speed and direction. Pixel colors on (a) and (b) represents the mean gas concentration measured at the respective wind speed (m s^{-1}) and direction over the entire measurement period, and black dots on (a) and (b) mark the nightly mean wind speeds and median wind directions for all $\delta^{13}C_s$ estimates.

Source Identification of Emissions

The most likely sources of natural gas leakage and combustion relative to our rooftop-monitoring site are the major gas combustion turbines at Cornell's Combined Heat and Power Plant, located ~600 m southeast (130-150°; Figure 4.1), and a minor steam boiler located in an adjacent building ~100 m southeast of our monitoring site (130-150°). The vast majority of natural gas use and combustion for the university campus occurs at Cornell's Combined Heat and Power Plant. In 2012, 89.6% of campus-wide fossil fuel combustion took place within this facility, where natural gas is the primary fuel source (Cornell, 2013b). Natural gas combustion at the plant produced 127,490 Mg CO_2-eq and only 314 Mg CO_2-eq from non-natural gas sources in 2012 (Cornell, 2013b). Energy generated from combustion at the facility is then used to produce electricity and heat steam, and steam is distributed through Cornell campus to heat buildings. Corson Hall and the surrounding buildings are all heated by steam supplied from the Cornell Plant, however the building ~100 m to the southeast operates a small natural gas boiler to increase the pressure of steam supplied by the Cornell Plant (Joyce, personal communication). Operations at this boiler may influence our observations as well, however natural gas combustion rates are minor relative to rates at the Cornell Plant and comprise some component of the remaining 10.4% of campus-wide gas combustion (Cornell, 2013b). Daily gas use rates for this boiler were not available.

Our atmospheric observations generally support these conclusions. We observed elevated CH_4 and CO_2 concentrations carried by southeast winds at high speeds (> 6 m s^{-1}), and the vast majority of all $\delta^{13}C_s$ estimates for both gas species originated from the southeast (Figure 4.7). $\delta^{13}C_s$-CH_4 estimates from this direction (120-180°; without building interference) ranged from -36.05 to -28.16‰, all within the range of known natural gas

sources (Figure 4.6b). Additionally, the correlation between $\delta^{13}C_s$-CO_2 values and daily power generation rates corroborates the influence of plant gas combustion on our atmospheric measurements ($r^2 = 0.15$, $P = 0.018$; Figure 4.5). We observe no clear connection between Cornell Plant operations and the timing of natural gas CH_4 plumes observed at the rooftop monitoring location. Small amounts of natural gas are intentionally vented to the atmosphere when the turbines are stopped for maintenance (Joyce, personal communication), however we do not observe any connection between the timing of observed plumes and shutdown events. During our mobile surveys we circled the Cornell Plant and did not observe elevated CH_4 concentrations, however gas facility emissions are known be temporally variable (Zavala-Araiza et al., 2015). Increased CH_4 monitoring at locations closer to the plant is warranted to further assess potential connections, as our monitoring site is likely too distant to clearly capture CH_4 emission events.

Implications for Small City/Suburban Emissions and Energy Usage

This work provides a case study for greenhouse gas emissions from a small city heavily reliant on natural gas with a well-maintained distribution pipeline system and major combined heat and power facility. Within Ithaca, natural gas use comprises 83% of all heating generation (Nicklaus, 2012), and between 2008 and 2012 Cornell's natural gas usage went from 3.6% to 89.6% of total combustion marking a shift from coal to natural gas use (Cornell, 2013b). Our results suggest that combustion from centralized facilities may be a significant greenhouse gas source in such cities, and that pipeline leakage is likely a minor source of CH_4 to the atmosphere. The low pipeline leakage rates presented here are in line with studies that have observed low leakage rates from systems with cast iron and bare steel replacement

programs (Gallagher et al., 2015). Instead, the natural gas-derived CH_4 and CO_2 plumes we observed most likely originated from the combined heat and power facility servicing Cornell University. A nearby boiler may also influence our results, but this combustion source is minor compared to the high levels of gas combustion at the central facility (Cornell, 2013b). Seasonal correlations between natural gas combustion activity at the Cornell Plant and urban $\delta^{13}C_s$-CO_2 values are evident (Figure 4.5), and these finding are supported by observations of elevated CH_4 concentrations carried on winds from the plant's direction (Figure 4.7). Further research is needed to pinpoint the exact origins of these CH_4 plumes. Understanding the natural gas loss rates from combined power generation facilities is important as these are the largest and a growing sector of US electricity generation (EIA, 2015). At the Cornell Plant, venting occurs when the turbines are shutdown and natural gas is emitted from the plant's stacks to relieve gas from the system before turbines can safely be turned back on (Joyce, personal communication), however we did not observe a temporal connection between CH_4 plumes and known shutdown events. If these events are a significant CH_4 source, emissions could potentially be controlled through flaring of lost gas to CO_2 within the stacks, a technique commonly used at landfills and natural gas production sites (EPA, 2015). Further research is needed to better understand CH_4 emission patterns and magnitudes from natural gas combustion facilities.

ACKNOWLEDGEMENTS

This research was funded by the Cornell University's Atkinson Center for a Sustainable Future, Department of Ecology and Evolutionary Biology, Andrew W. Mellon Foundation, and Cornell Sigma Xi. We also thank Robert Bland, Lanny Joyce, and Josh LaPenna of

Cornell University's Facilities Services Energy & Sustainability for their input on plant operations and willingness to share data. The Sparks lab provided useful comments on the manuscript.

REFERENCES

Bowling DR, Burns SP, Conway TJ, Monson RK, White JWC. 2005. Extensive observations of CO_2 carbon isotope content in and above a high-elevation subalpine forest. Global Biogeochemical Cycles 19:1–15.

Bowling DR, Massman WJ, Schaeffer SM, Burns SP, Monson RK, Williams MW. 2009. Biological and physical influences on the carbon isotope content of CO_2 in a subalpine forest snowpack, Niwot Ridge, Colorado. Biogeochemistry 95:37–59.

Bush SE, Pataki DE, Ehleringer JR. 2007. Sources of variation in $\delta^{13}C$ of fossil fuel emissions in Salt Lake City, USA. Applied Geochemistry 22:715–23.

Cambaliza MOL, Shepson PB, Bogner J, Caulton DR, Stirm B, Sweeney C, Montzka S a., Gurney KR, Spokas K, Salmon OE, Lavoie TN, Hendricks A, Mays K, Turnbull J, Miller BR, Lauvaux T, Davis K, Karion, Moser B, Miller C, Obermeyer C, Whetstone J, Prasad K, Miles N, Richardson S. 2015. Quantification and source apportionment of the methane emission flux from the city of Indianapolis. Elementa: 3:000037.

Cathles LM, Brown L, Taam M, Hunter A. 2012. A commentary on 'The greenhouse-gas footprint of natural gas in shale formations' by R.W. Howarth, R. Santoro, and Anthony Ingraffea. Climatic Change 113:525–35.

Chamberlain SD, Boughton EH, Sparks JP. 2015. Underlying ecosystem emissions exceed cattle-emitted methane from subtropical lowland pastures. Ecosystems 18:933–45.

Cornell University. 2013a. University Facts. http://www.cornell.edu/about/facts.cfm

Cornell University. 2013b. Cornell University—Ithaca Greenhouse Gas (GHG) Emissions Inventory Fiscal Year 2012. http://www.sustainablecampus.cornell.edu/initiatives/greenhouse-gas-emissions-inventory

Cornell University Facilities Services. 2015. Real Time Building Utility Use Data: http://portal.emcs.cornell.edu/

Energy Information Agency (EIA). 2015. Electric Power Monthly. http://www.eia.gov/electricity/data/browser/

Gallagher ME, Down A, Ackley RC, Zhao K, Phillips N, Jackson RB. 2015. Natural gas pipeline replacement programs reduce methane leaks and improve consumer safety. Environmental Science and Technology Letters 2:286–91.

Gordon DLA, Janzen M. 2013. Suburban nation? estimating the size of Canada's suburban population. Journal of Architectural and Planning Research 30:197–220.

Howarth RW, Santoro R, Ingraffea A. 2011. Methane and the greenhouse-gas footprint of natural gas from shale formations. Climatic Change 106:679–90.

Jackson RB, Down A, Philips NG, Ackley RC, Cook CW, Plata DL, Zhao K, Phillips NG. 2014. Natural gas pipeline leaks across Washington, DC. Environmental Science & Technology 48:2051–8.

Joyce WS. 2015. Personal communication. Utilities and Energy Management, Cornell University, Ithaca, NY.

Lamb BK, Edburg SL, Ferrara TW, Howard T, Harrison MR, Kolb CE, Townsend-Small A, Dyck W, Possolo A, Whetstone JR. 2015. Direct measurements show decreasing methane emissions from natural gas local distribution systems in the United States. Environmental Science & Technology 49:5161–9.

Mays KL, Shepson PB, Stirm BH, Karion A, Sweeney C, Gurney KR. 2009. Aircraft-based measurements of the carbon footprint of Indianapolis. Environmental Science & Technology 43:7816–23.

McKain K, Down A, Raciti SM, Budney J, Hutyra LR, Floerchinger C, Herndon SC, Nehrkorn T, Zahniser MS, Jackson RB, Phillips N, Wofsy SC. 2015. Methane emissions from natural gas infrastructure and use in the urban region of Boston, Massachusetts. Proceedings of the National Academy of Sciences of the United States of America 112:1941–6.

Moore J, Jacobson AD. 2015. Seasonally varying contributions to urban CO_2 in the Chicago, Illinois, USA region: Insights from a high-resolution CO_2 concentration and $\delta^{13}C$ record. Elementa: 3:000052.

Network for Environmental and Weather Applications (NEWA). 2015. Weather Data. http://newa.cornell.edu/index.php?page=all-weather-data

Nicklaus F. 2012. Energy Supply and Demand Tompkins County , New York. Tompkins County. http://tompkinscountyny.gov/files/planning/energyclimate/documents/EnergySupplyandDemand_fn_Final_5_24_12.pdf

Pataki DE, Bowling DR, Ehleringer JR. 2003a. Seasonal cycle of carbon dioxide and its isotopic composition in an urban atmosphere: Anthropogenic and biogenic effects. Journal of Geophysical Research 108:1–8.

Pataki DE, Ehleringer JR, Flanagan LB, Yakir D, Bowling DR, Still CJ, Buchmann N, Kaplan JO, Berry JA. 2003. The application and interpretation of Keeling plots in terrestrial carbon cycle research. Global Biogeochemical Cycles 17:1022.

Phillips NG, Ackley R, Crosson ER, Down A, Hutyra LR, Brondfield M, Karr JD, Zhao K, Jackson RB. 2013. Mapping urban pipeline leaks: Methane leaks across Boston. Environmental Pollution 173:1–4.

Pipeline and Hazardous Materials Safety Adminstriation (PHMSA). 2014. Annual Data 2010 to present. http://phmsa.dot.gov/pipeline/library/data-stats/distribution-transmission-and-gathering-lng-and-liquid-annual-data.

R Core Team. 2015. R: A language and environment for statistical computing. R Foundation for Statistical Computing, Vienna, Austria. http://www.R-project.org/.

Satterthwaite D. 2008. Cities' contribution to global warming: notes on the allocation of greenhouse gas emissions. Environment and Urbanization 20:539–49.

Stocker TF et al. 2013. Technical Summary, in Climate Change 2013: The Physical Science Basis. Contribution of Working Group I to the Fifth Assessment Report of the Intergovernmental Panel on Climate Change, edited by Stocker TF, Qin D, Plattner GK, Tignor M, Allen SK, Boschung J, Nauels A, Xia Y, Bex V, Midgley PM, Cambridge University Press, New York, NY.

Semmens C, Ketler R, Schwendenmann L, Nesic Z, Christen A. 2014. Isotopic compostion of CO_2 in gasoline, diesel and natural gas combustion exhaust in Vancouver, BC, Canada. University of British Columbia, Vancouver, BC. https://open.library.ubc.ca/cIRcle/collections/facultyresearchandpublications/42387/items/1.0103591

Townsend-Small A, Tyler SC, Pataki DE, Xu X, Christensen LE. 2012. Isotopic measurements of atmospheric methane in Los Angeles, California, USA: Influence of 'fugitive' fossil fuel emissions. Journal of Geophysical Research Atmospheres 117:1–11.

Turnbull JC, Karion A, Fischer ML, Faloona I, Guilderson T, Lehman SJ, Miller BR, Miller JB, Montzka S, Sherwood T, Saripalli S, Sweeney C, Tans PP. 2011. Assessment of fossil fuel carbon dioxide and other anthropogenic trace gas emissions from airborne measurements over Sacramento, California in spring 2009. Atmospheric Chemistry and Physics 11:705–21.

United Nations. 2014. *World Urbanization Prospects: The 2014 Revision*; Highlights (ST/ESA/SER.A/352). http://esa.un.org/unpd/wup/Highlights/WUP2014-Highlights.pdf

United States Census Bureau (US Census). 2014. Ithaca, New York (quickfacts). http://quickfacts.census.gov/qfd/states/36/3638077.html

United States Environmental Protection Agency (EPA). 2015. Inventory of U.S. Greenhouse Gas Emissions and Sinks: 1990 – 2013. Washington, DC, http://www3.epa.gov/climatechange/Downloads/ghgemissions/US-GHG-Inventory-2015-Main-Text.pdf

Wennberg PO, Mui W, Wunch D, Kort EA, Blake DR, Atlas EL, Santoni GW, Wofsy SC, Diskin GS, Jeong S, Fischer ML. 2012. On the sources of methane to the Los Angeles atmosphere. Environmental Science and Technology 46:9282–9. http://pubs.acs.org/doi/abs/10.1021/es301138y

Widory D, Javoy M. 2003. The carbon isotope composition of atmospheric CO_2 in Paris. Earth and Planetary Science Letters 215:289–98.

Zavala-Araiza D, Lyon DR, Alvarez RA, et al. 2015. Reconciling divergent estimates of oil and gas methane emissions. Proceedings of the National Academy of Sciences. 112: 15597-15602.

Zobitz JM, Keener JP, Schnyder H, Bowling DR. 2006. Sensitivity analysis and quantification of uncertainty for isotopic mixing relationships in carbon cycle research. Agricultural and Forest Meteorology. 136: 56–75.

APPENDIX

CHAPTER 1

Enteric Fermentation CH_4 Emission Calculations: IPCC Tier 2

All enteric fermentation emission factors were calculated according to IPCC Tier 2 guidelines (IPCC, 2006). In order to generate emission factors, gross energy intake values were estimated for cattle as follows:

$$GE = \frac{\left(\frac{NE_m + NE_a + NE_l + NE_{work} + NE_p}{REM}\right) + \left(\frac{NE_g}{REG}\right)}{\frac{DE\%}{100}} \quad \text{(A1)}$$

where GE=gross energy (MJ d^{-1}), NE_M=net energy for maintenance (MJ d^{-1}), NE_a=net energy for activity (MJ d^{-1}), NE_l=net energy for lactation (MJ d^{-1}), NE_{work}=net energy for work (MJ d^{-1}), NE_g=net energy for growth (MJ d^{-1}), REM=ratio of net energy available in a diet for maintenance to digestible energy consumed, REG=ratio of net energy available for growth in a diet to digestible energy consumed, and DE%=percent digestible energy.

Emission factors and GE values were generated for two subcategories of cattle: 1) mature non-pregnant cows and 2) mature pregnant cows. We chose these two subcategories because cattle management data obtained from the MacArthur Agro-ecology Research Center (MAERC) documented the total herd size within the pasture and the percent of herd pregnant. We assumed all cattle grazing the pasture were mature (non-growing), non-working, and non-lactating. These assumptions were also made based on the available cattle management data. No data were available on growth and lactation rates of cattle at MAERC, so we assumed cattle were either mature non-pregnant or mature pregnant. These assumptions simplified equation A1 to:

$$GE = \frac{\left(\frac{NE_m + NE_a + NE_p}{REM}\right)}{\frac{DE\%}{100}} \quad \text{(A2)}$$

We then used the following equations to then estimate GE:

$$NE_m = 0.322 \cdot (weight)^{0.75} \quad \text{(A3)}$$

$$NE_a = 0.17 \cdot NE_m \quad \text{(A4)}$$

$$NE_p = 0.10 \cdot NE_m \quad \text{(A5)}$$

$$REM = \left[1.123 - (4.092 \cdot 10^{-3} \bullet DE\%) + \left[1.126 \cdot 10^{-5} \bullet (DE\%)^2\right] - \left(\frac{25.4}{DE\%}\right)\right] \quad \text{(A6)}$$

where weight=average weight of cattle (kg) and the coefficients in A1, A2, and A3 are the Tier 2 suggestions for non-lactating grazing cows, pasture grazed cows, and pregnant cows, respectively (IPCC, 2006). We used a DE% value of 61.38 for Bahia grass (*Paspalum notatum)* as reported by EPA (2014). Bahia grass is the primary forage species planted on improved pastures at MAERC. The average cattle weight of cattle at MAERC was 544 kg and was used in all calculations. Gross energy intake was estimated to be 138.2 MJ d^{-1} for non-pregnant cows and 150.0 MJ d^{-1} for pregnant cows. Enteric fermentation emission factors (EF; kg CH_4 $animal^{-1}$ d^{-1}) were then calculated as follows:

$$EF = \frac{GE \cdot Y_m}{55.65} \quad \text{(A7)}$$

where Y_m is the cattle CH_4 conversion factor, estimated to be 0.065 ± 0.010 (IPCC, 2006). We calculated a non-pregnant cow EF of 58.9 ± 9.1 kg CH_4 $animal^{-1}$ yr^{-1} and a pregnant cow EF of 63.9 ± 9.8 kg CH_4 $animal^{-1}$ yr^{-1}.

Manure CH_4 Emission Calculations: IPCC Tier 2

Emission factors for manure deposited on pastures were developed according to the following equation:

$$EF_m = VS \cdot B_o \cdot 0.67 kg/m^3 \cdot \frac{MCF}{100} \cdot MS \quad \text{(A8)}$$

where EF_m = emission factor for manure (kg CH_4 animal^{-1} d^{-1}, VS = daily volatile solid excreted (kg dry matter animal^{-1} d^{-1}), B_o = maximum CH_4 producing capacity for manure (m^3 CH_4 kg^{-1}), MCF = methane conversion factor for manure management system by climate region (%), and MS = fraction of livestock category using a manure management system. We assumed MS=1 because all cattle were depositing manure within the same pasture system, and used values of B_o = 0.19 ± 0.03 and MCF of 1.5% as suggested in IPCC Tier 2 lookup tables (IPCC, 2006). Finally, VS values were estimated for both livestock categories using the following equation:

$$VS = \left[GE \cdot \left(1 - \frac{DE\%}{100} \right) + (0.04 \cdot GE) \right] \cdot \left(\frac{1 - ASH}{18.45} \right) \quad \text{(A9)}$$

where ASH = the ash content of manure as a fraction of feed intake, which was estimated to be 0.08 (IPCC, 2006). We calculated an EF_m for non-pregnant cows of 2.0 ± 0.3 kg animal^{-1} yr^{-1}, and an EF_m for pregnant cows of 2.2 ± 0.3 kg animal^{-1} yr^{-1}. Manure and enteric fermentation CH_4 budgets were calculated at a daily time scale accounting for herd size and the percentage of pregnant cattle present within the Griffin Park pasture.

CHAPTER 4

Table A.1 Mean meteorological conditions during all mobile survey drives. Conditions include air temperature (°C), relative humidity (RH; %), wind speed (m s^{-1}), and wind direction (°). All conditions are averaged across the survey period from measurements collected from the Cornell Game Farm Road weather station (N 42.449181, W 76.449038).

Date	Duration (EST)	Air Temp	RH	Wind Speed	Wind Direction
2015-05-27	09:41-18:03	25.0	63.1	2.1	220
2015-05-28	10:38-15:37	20.7	63.2	4.2	299
2015-06-29	11:09-12:57	17.6	82.7	2.6	292
2015-06-30	10:26-13:51	17.9	92.0	3.6	131

Table A.2 Measured and cited end-member source descriptions and isotopic values (± SD**)**. Value in parentheses equals the number of replicates for each measured or cited value. Cited values list reference under 'measurement location or citation', all other values are measurements made in this study.

Source	**Measurement location or reference**	**$\delta^{13}C$-CO_2 (‰)**	**$\delta^{13}C$-CH_4 (‰)**
Natural gas	Furnace (free air)	-40.74 ± 0.09 (1)	
Natural gas	Gas line combustion (chamber)	-35.84 ± 0.09 (1)	
Gasoline	Widory and Javoy, 2003	-28.69 ± 0.50 (10)	
Gasoline	Semmens et al. 2014	-27.27 ± 0.93 (22)	
Gasoline	Bush et al. 2007	-28.56 ± 0.35 (20)	
Respiration	Pataki et al. 2003	-25.71 ± 1.35	
Sewage	Rooftop sewage vent pipe	-29.87 ± 0.22 (2)	-57.58 ± 0.58 (2)
Natural gas	Gas line leakage (chamber)		-35.89 ± 0.50 (9)

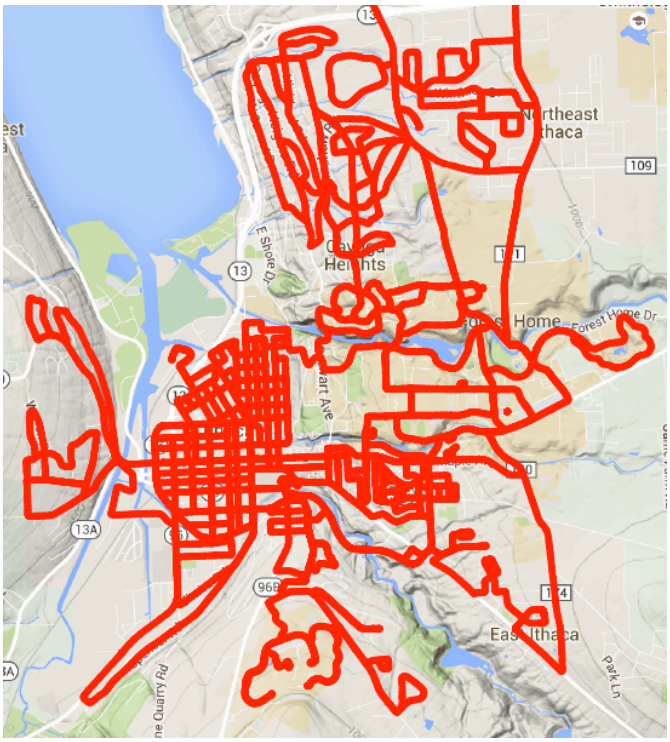

Figure A.1 Roads surveyed during Ithaca mobile CH_4 concentration mapping. All roads were driven during summer 2015 on days of low wind speed.

REFERENCES

Environmental Protection Agency (EPA). 2014. Annex 3. Methodological descriptions for additional source or sink categories. Washington DC. p. A125-A384.

Intergovernmental Panel on Climate Change (IPCC). 2006. Emissions from livestock and manure management. Eggleston HS, Buendia L, Miwa K, Ngara T, Tanabe K, editors. 2006 IPCC guidelines for national greenhouse gas inventories. Vol. 4. Agricultural, forestry and other land uses. IGES, Japan. p. 10.1-10.87.